May 2013

Small-Area Population Estimation: an Integration of Demographic and Geographic Techniques

Chengbin Deng
University of Wisconsin-Milwaukee

SMALL-AREA POPULATION ESTIMATION: AN INTEGRATION OF DEMOGRAPHIC AND GEOGRAPHIC TECHNIQUES

by

Chengbin Deng

A Dissertation Submitted in

Partial Fulfillment of the

Requirements for the Degree of

Doctor of Philosophy

in Geography

at

The University of Wisconsin-Milwaukee

May 2013

ABSTRACT

SMALL-AREA POPULATION ESTIMATION: AN INTEGRATION OF DEMOGRAPHIC AND GEOGRAPHIC TECHNIQUES

by

Chengbin Deng

The University of Wisconsin-Milwaukee, 2013

Under the Supervision of Professor Changshan Wu

Abstract

Knowledge of detailed and accurate population information is essential to analyze and address a wide variety of socio-economic, political, and environmental issues and to support necessary planning practices for both public agencies and the private sector. However, such important data are generally only available once every decade through the National Census. Moreover, populations in some rapidly-developing areas may increase quickly, such that this ten-year frequency does not meet the needs of these areas. Therefore, a cost-effective method for population estimation is necessary. To address this issue, this research integrated geographic,

sociological, and demographic theories and exploited remotely sensed imagery and geographic information system (GIS) datasets to derive better population estimates at the census block level, the finest level of the national census.

Specifically, three new approaches have been proposed in this dissertation to assist in the improvement of small-area population estimation accuracy. First, existing remotely sensed and GIS data have been adopted to estimate two major components of a demographic framework, including the redistribution of newly built dwelling units from the aggregated geographic level to the census block level and the estimation of persons per household (PPH) at such a fine scale. Second, in addition to the use of existing data, new urban environmental indicators were also extracted and employed to improve population estimation. In particular, to implement the automatic enumeration for individual housing units, a new spectral index, biophysical composition index (BCI), has been proposed to derive impervious surface information, a desirable urban environmental parameter. Third, using the extracted high-resolution urban environmental information and GIS data, a new bottom-up method was developed for small-area population estimation at the census block level by incorporating these high-resolution data into the demographic framework.

Analyses of the results suggest three major conclusions. First, existing GIS spatial factors, together with demographic information, can assist in improving the accuracy of small-area population estimation. Second, the BCI has a closer relationship with impervious surface area than do other popular indices. Moreover, it was shown to

be the most effective index of the four evaluated for separating impervious surfaces and bare soil, which consequently might assist in more accurately deriving fractional land cover values. Third, the use of the new environmental indicators extracted from remote sensing imagery and GIS data and the integration of demographic and geographic approaches has significantly improved the estimation accuracy of housing unit (HU) numbers, PPH, and population counts at the census block level.

Therefore, this research contributes to both the remote sensing and applied demography fields. The contribution to the remote sensing field lies in the development of a novel spectral index to characterize urban land for monitoring and analyzing urban environments. This index provided more significant separability between impervious surfaces and bare soil than did other existing indices. Moreover, three major contributions have been made in the field of applied demography: 1) the generation of accurate HU estimates using high-resolution remote sensing and GIS datasets, 2) the development of a model to derive an accurate PPH estimate, and 3) the improvement of small-area population estimation accuracy through the integration of geographic and demographic approaches.

Dedicated to my parents

TABLE OF CONTENTS

LIST OF FIGURES

LIST OF TABLES

ACKNOWLEDGMENTS

I would like to thank my advisor, Professor Changshan Wu. Without his sincere help, I would not become a young scholar in geography.

Special thank also goes to my committee members, Professor Mark Schwartz, Professor Woonsup Choi, Professor Le Wang from SUNY-Buffalo, and Professor Christopher De Sousa from Ryerson University for their valuable suggestions to my dissertation work.

Moreover, I gratefully acknowledge all the people who generously helped me during my graduate study, Professor Hyejin Yoon, Ms. Donna Genzma, Professor Ryan Holifield, Professor Kristin Sziarto, Professor Michael Day, Dr. Patti Day, Professor Zengwang Xu, and Dr. Alison Donnelly. In addition, I am very grateful to my colleagues and friends at UWM, Wei Huang, Rong Yu, Wenliang Li, Miao Li, Hui Xiao, Alarico Fernandes, I-Hui, Lin, Yang Song, Wei Xu, Hong Zhuo, Lingling Liu, Xing Huang, Zhijian Wang, and Zhong Zheng, for their consistent support and help.

Last but not the least, I would like to express my deep gratitude to my parents for their consistent encouragement and support to my study.

CHAPTER 1 INTRODUCTION

1.1 Background

More than half of the world's population currently resides in urbanized areas, and urbanization is projected to continue in both developed and developing regions throughout the world in the coming decades (United Nations, 2010). This rapid population increase contributes to a series of environmental problems and natural resource issues. For example, along with urban development, population growth has been regarded as one of the major reasons for air pollution, including the excessive release of related organic gases, nitrogen oxides, *etc.* (Cramer, 1998), potentially due to congestion, excessive industrialization, and immoderate energy consumption, *etc.* (Mayer, 1999). Second, the rapid population increase leads to increased water contamination and growth in freshwater demand (Vörösmarty *et al.*, 2008). Third, urban population size is found to be positively correlated with the intensity of the urban heat island phenomenon (Cayan and Douglas, 1984; Jauregui *et al.*, 1992; Kukla *et al.*, 1986; Oke, 1973; Nasrallah *et al.*, 1990). Further, a growing population necessitates more food production and living space, therefore resulting in deforestation and habitat destruction as more natural lands have to be transformed to arable and residential lands to meet these demands (Cropper and Griffiths, 1994). Moreover, consistent population growth may have also severe impacts on threatened species, which may result in increasingly greater biodiversity losses (Kirkland and

Ostfeld, 1999; Thompson and Jones, 1999; McKee *et al.*, 2003). In addition, poor sanitary conditions prompt public health concerns that crowded urban environments and the corresponding polluted and degraded environments (*e.g.,* water pollution, atmospheric pollution, food contamination, *etc.*) might also trigger outbreaks of infectious diseases, such as measles and influenza. (Pimentel *et al*., 2007). To avoid and/or mitigate these urban environmental problems that that affect our daily lives, it is necessary to sensibly and effectively allocate limited public resources to encourage sustainable development.

An awareness of population totals and distributions is essential for sustainable public planning, environmental management, and commercial applications (Rees *et al.*, 2004). On the one hand, in public planning, small-area population estimates are a critical component in deriving several diagnostic indicators, such as the mortality rate, morbidity rate and unemployment rate, *etc*. Moreover, small-area population information can be employed as an important input for social, urban and regional studies, including assessments of employment equality, policy impact analysis, land use models, transportation interaction models, infrastructure planning, *etc*. For example, the location and size of a population are important inputs when forecasting travel demands and planning facility locations (Plane and Rogerson, 1994). On the other hand, in commercial applications, small-area population data can be used to calculate *per capita* sales volumes, assess markets and identify potential customer groups based on their economic/ethnic status or living preferences, *etc*.

Currently, population information can be obtained from three major sources: population registers, decennial censuses, and estimates from remote sensing imagery (Rhind, 1991). First, population registers continuously record up-to-date socio-economic information on the resident population, which is more commonly used in the Nordic countries (*e.g*., Denmark, Finland, Norway and Sweden) where advanced technology and complete social systems are present. Second, decennial censuses provide the most widely used and accurate population data in the United States and the United Kingdom. However, decennial census data are only available every ten years following the national census. Conducting a national census is labor-intensive, time-consuming and costly. Estimates of the cost of surveying an individual rose from $4.76 in 1980 to $10.02 in 1990 and to $15.99 in 2000 (Gauthier, 2002). Moreover, in the areas experiencing rapid population growth, the ten-year frequency does not meet the needs of public facility planning. In addition to these two traditional methods, researchers have considered remote sensing techniques for population estimates, particularly in less-developed areas and countries without historical census data or registers. Its major advantage is its low cost and efficiency compared to population registers and national censuses (Lo, 1995). Its accuracy, however, is highly dependent on the estimation methods and may vary substantially. Therefore, to address this mismatch between the substantial demand in a variety of practical applications and limited availability of population information, it is necessary to develop a cost-effective population estimation methodology.

In recognition of the importance of population estimation, researchers have proposed various models based on either demographic theory or remote sensing/geographic information system (GIS)-based techniques. Specifically, demographers have developed the Component Method II (CM-II) method, the Administrative Records (AR) method, the Ratio Correlation (RC) method, and the Housing Unit (HU) population estimation methods (Ghosh and Rao, 1994). In particular, the HU method has played a crucial role in population estimation. This method assumes that homes are a basic human necessity that represents significant identifiers and evidence of the influence of human activity on land cover. Therefore, the population totals in a small area are closely related to the number of housing units in that area. As a result, the U.S. Census Bureau has employed this approach as its method for generating population totals at the sub-county level since the 1990s (U.S. Census Bureau, 1998; Smith and Cody, 2004; U.S. Census Bureau, 2005), including incorporated places (*e.g.,* cities, boroughs, and villages) and minor civil divisions (*e.g.,* towns and townships). In addition, remote sensing/GIS researchers have exploited remote sensing imagery to manually count residential units as the first step of the HU method (Hsu, 1971; Lo, 1986a, 1986b) or estimate population density using spectral reflectance methods or their mathematical transformations (*i.e.,* logarithmic or square root transformations) using regression models (Hsu, 1973; Iisaka and Hegedus, 1982; Lo, 1995; Harvey, 2002, Li and Weng, 2005; Lu *et al.*, 2006; Wu and Murray, 2007).

Although the HU method has been widely employed in the fields of applied demography and remote sensing/GIS to derive small-area population estimates, several issues remain unresolved. The first pertains to the different spatial scales considered in these two fields. In demography, housing unit counts are obtained by disaggregating building permit data or electronic utility data at an aggregated level, such as the county, town, or occasionally, the administrative district, the boundaries of which differ from those of the census unit, instead of at a finer level (such as the census block group and census block levels). In other words, the aggregated data source itself limits the accuracy of small-area population estimates using demographic methods. However, remote sensing researchers are more familiar with image pixels and prefer to use pixel-based population estimation. However, coarse- and medium-resolution remote sensing imagery only characterizes the spectral response of the overall landscape within a pixel, rather than the direct relationship with additional details of a house due to its relatively low spatial resolution. However, such a spatial unit is inconsistent with census boundary frequently used by demographers. The mismatch of spatial scales between the two fields results in independent developments with minimal collaboration. In contrast, high-resolution remote sensing imagery, such as digital aerial photographs, IKONOS, worldview imagery, *etc.*, might remove such limitations. However, most of the current methods using orthophotographs (Hsu, 1971; Watkins, 1984; Watkins and Morrow-Jones, 1985; Lo, 1986a, 1986b) require researchers to be skilled at image interpretation and sufficiently familiar with the study area to manually count the residential units, which is extremely time-consuming and labor-intensive and

not applicable to a large geographic areas. The use of high-resolution, remotely sensed imagery data may allow improved estimates of the number of housing units if an automated acquisition method can be developed, which will accordingly improve small-area population estimates.

The second problem relates to the assumption of constant person per household (PPH) figures in the HU method. In both fields, PPH is consistently assumed to remain identical to PPH figures obtained from the latest decennial census (Starsinic and Zitter, 1968; Smith and Lewis, 1983; U.S. Census Bureau, 2005). Essentially, rather than being a static demographic indicator, PPH changes over time. Several studies have noted that the PPH in the U.S. has exhibited a steep downward trend over the past two centuries, falling from 5.8 in 1790 to 4.8 in 1900 and to 2.6 in 2000 (Kobrin, 1976; U.S. Census Bureau, 2001; Bongaarts, 2001). According to the life-cycle model, there are several reasons for this PPH decline related to the spatial requirements of individuals at needs different ages, including declining fertility and mortality rates and the trend of young people living separately from their parents (Kobrin, 1976; Smith *et al.*, 2002; Sabagh *et al.*, 1969; Speare *et al.*, 1975). As a result, the use of unchanged PPH values results in overestimates of population counts (Starsinic and Zitter, 1968; Smith and Lewis, 1980). While some studies have attempted to obtain better PPH estimates at the county-level (Smith, 1986; Smith *et al.*, 2002), few have explored the estimation of inter-census PPH at a high spatial scale (such as the census block), primarily due to the unavailability of the necessary datasets.

Thus, inter-census, small-area population estimates may be improved if PPH can be estimated with the aid of advanced remote sensing and GIS techniques.

1.2 Population estimation methods: a review

1.2.1 Demographic methods

Among demographic approaches, four methods are widely applied to estimate population totals, including the Ratio-Correlation (RC) method, the Component Method II (CM-II) method, the Administrative Records (AR) method, and the Housing Unit (HU) method (Smith and Mandell, 1984; Ghosh and Rao, 1994).

The RC method assumes that the symptomatic variables (R_1, R_2,..., R_n, representing school enrollment, auto registration, the ratio of resident births/death, *etc*) are correlated with the population totals (Martin and Serow, 1978). The essence of the RC method is regression analysis, although the symptomatic variables are expressed in ratio form. Specifically, they are represented in the form of "ratios of ratios" (Plane and Rogerson, 1994). The RC method can be expressed as a regression model as follows:

$$K_i = a_0 + a_1 R_{i1} + a_2 R_{i2} + \cdots + a_n R_{in} + \varepsilon_i \tag{2.1}$$

$$K_i = \frac{p_i^t / p_{all}^t}{p_i^0 / p_{all}^0} \tag{2.2}$$

$$R_{ij} = \frac{s_{ij}^t / s_{all}^t}{s_{ij}^0 / s_{all}^0} \qquad (2.3)$$

where K_i is change in the share of the total population residing in subregion i; p_i^t and p_i^0 are the population totals in the i_{th} subregion in the most recent census year t and a previous census base year o, respectively; p_{all}^t and p_{all}^0 are the total population counts for the whole region at time t and time o, respectively; R_{ij} represents the percentage change in of a symptomatic variable of type j in subregion i; S_{ij}^t and S_{ij}^0 are the actual values of a symptomatic variable of type j in the i_{th} subregion at time t and time o, respectively; S_{all}^t and S_{all}^0 are the total values of the symptomatic variable of type j for the entire region at time t and time o, respectively; $a_0, a_1, \ldots a_n$ are the regression coefficients.

Using the coefficients obtained from the regression analysis, K_i can be estimated based on different types of symptomatic variables in subregion i in the estimate year e. Accordingly, by rearranging equation (2.2), the population in subregion i can be calculated as follows:

$$p_i^e = \frac{p_i^t}{p_{all}^t} \, p_{all}^e \, K_i \qquad (2.4)$$

where p_i^e is the population of the i_{th} subregion in estimate year e, while p_{all}^e is the total population of the entire region at time e, which can be obtained from other sources (Schmitt and Crosetti, 1954; Goldberg $et\ al.$, 1964; Smith and Mandell, 1984). There are several criticisms of the RC method (Namboodiri, 1972; Plane and

Rogerson, 1994). First, there is a doubt that it is unnecessary for the sum of the coefficients of the RC regression model to be close to one. Second, some question whether it is appropriate to leave the ratio between the population variable K_i and the symptomatic variables Ri unchanged in at an inter-census year o from that of the previous two censuses.

The CM-II method is another important demographic estimation method proposed by the U.S. Census Bureau. This approach considers some major demographic changes between the estimation year and the most recent census year. Under the CM-II method, population totals can be calculated as follows:

$$p_t = p_0 + b - d + m \qquad (2.5)$$

where p_t is the population total in year t, p_o is the population in the last census year o; b and d are the estimated numbers of births and deaths, respectively, both of which can be estimated under the assumption that they are uniformly distributed throughout the year, m is the net migration at all ages, calculated by multiplying the net migration rate by the estimated surviving population between times t and o (Smith and Mandell, 1984).

Similar to the CM-II method, the AR method also accounts for demographic change. However, there is a significant difference between the two: the CM-II method estimates the entire net change, while the AR method estimates two categorical changes. More specifically, the AR method estimates the net migration of the population under 65 years of age using federal income tax forms and employs federal

Medicare enrollment data to estimate the net migration of people 65 and above, while the CM-II method only relates school enrollment data to overall population changes.

Unlike the RC, CM-II, and AR methods that are only available for population estimates at an aggregate level (such as the state- and county-levels), the HU method has been the only method used by the U.S. Census Bureau to generate small-area population estimation for almost two decades. This method is considered the most commonly used, and among the most accurate and cost-effective methods for estimating small-area populations (Smith and Mandell, 1984; U.S. Census Bureau, 1998; Smith and Cody, 2004; U.S. Census Bureau, 2005). Specifically, the numbers of occupied housing units, persons per household and group quarter population are three major components of the HU method. The formula for the HU method can be written as follows:

$$E_t = HU_t \times r_t \times P_t + G_t \tag{2.6}$$

where E_t is the estimated population of a small area in a non-census year t; HU_t is the population estimate at time t; r_t is the occupancy rate at time t; P_t is the number of persons per household at time t; and G_t is the group quarters population (*e.g.*, persons residing in college dormitories, military barracks, nursing homes, prisons, *etc.*) at time t.

1.2.2 Remote sensing and GIS techniques

1.2.2.1 Overview of remote sensing /GIS-based population estimation methods

According to the aforementioned reviews, an apparent limitation of demographic models is the substantial difficulty of updating most of the demographic variables and obtaining the latest socioeconomic data. Therefore, it is impractical to generate timely population estimates. In contrast, as up-to-date remotely sensed and GIS datasets are much easier to acquire, remote sensing and GIS techniques may have the potential to be integrated into demographic methods and thus improve existing small-area population estimation methods.

Lo (1986b) noted that remote sensing/GIS-based population estimation methods can be grouped into four categories: 1) measured land-area-based estimation; 2) land-use-based estimation; 3) dwelling-unit-based estimation; and 4) spectral-radiance-based estimation. In addition to these four categories, the latest developments in remote sensing techniques have produced a fifth category, new indicators-based estimation, which is reviewed in below.

In the first category, remotely sensed data were employed to measure the built-up urban area, and subsequently the empirical relationship between built-up area and population totals were established according to the allometric growth model (Lo and Welch, 1977). The law of allometric growth was originally demonstrated by Huxley (1932) and applied to urban growth and population settlement (Norbeck, 1965; Tobler, 1969). The equation for the first category of estimation techniques can be written as follows:

$$P = aS^b \qquad\qquad (2.7)$$

Further, this formula can also be expressed as:

$$log\ P = log\ a + b\ log\ S \tag{2.8}$$

where P is the estimated population; S is the size of the built-up area obtained from the remotely sensed imagery; and a and b are the model coefficients.

In the second category, remote sensing imagery was used to classify land use, and in particular, to further classify the residential areas into detailed categories, such as single-family residential land use, multi-family residential land use, *etc*. The population totals were then estimated as the sum of the geographical areas allocated of different land use types multiplied by their population densities (Kraus *et al*. 1974). The equation for the second category can be represented as follows:

$$P = \sum_{i=1}^{n}(S_i D_i) \tag{2.9}$$

where P is the estimated population; S_i is the area of the sub-residential land use type obtained from the remotely sensed imagery; and D_i is the corresponding density of the sub-residential land use type.

In essence, the principle of the first category resembles to that of the second because remotely sensed images were similarly used to classify land use types and to calculate their areas. Their major difference lies in the classification: the first category classifies land use into built-up and non-built-up types, while the second category classifies types of residential land use in greater detail (Wu *et al.*, 2005).

In the third category, the dwelling-unit-count approach employs large-scale aerial photographs to identify the various dwelling units and manually count their number belonging to each dwelling type (Watkins 1984, Watkins and Morrow-Jones, 1985, Lo 1986a). Somewhat similar to the second category, the population totals were estimated by multiplying the number of dwellings by the population density of the respective dwelling unit type as follows.

$$P = \sum_{i=1}^{n}(H_i D_i) \tag{2.10}$$

where P is the estimated population; H_i is the number of dwelling units of type i counted in the remote sensing images; and D_i is the corresponding density of dwelling type i.

Hsu (1971) was the first to estimate population totals by multiplying the number of manually counted dwelling units by the average number of persons per household, under assumptions that a household can be represented by an occupied dwelling unit and that there was no considerable change in the average number of persons per household between the estimate year and the census year. Following Hsu's work, Lo and Chan (1980) successfully identified five types of rural dwelling units by visual interpreting the spatial pattern of these housing units in aerial photographs and subsequently estimated the rural population in the New Territories, Hong Kong. However, some unsolved problems were present in their research, such as the overestimation resulting from vacant units and the underestimation due to the occupancy of multiple families/households in multi-storied buildings. Although

relatively high accuracy can be achieved, this approach might be considered extremely time-consuming and labor-intensive due to the need to manually count the number of dwelling units and hence impractical for large-scale applications. To facilitate dwelling unit counts, several automatic approaches have been developed. The results, however, were not as accurate as those obtained from manual counts. Converting aerial photographic data into a raster format, Lo (1989) estimated the number of dwelling units for each grid cell by multiplying the true percentage by the theoretical maximum number of dwelling units and demonstrated the relationship between the actual number of housing units and the number of buildings observed in aerial photographs using a double logarithmic regression model. Similarly, Webster (1996) estimated dwelling unit figures using linear regression models with variables directly obtained from remote sensing images, including mean reflectance values, texture and context measures. Further, Lo (2003) derived the number of housing units using a regression model by considering the relationship between the geographic extent of residential land use and the number of housing units.

In the fourth category, spectral radiance and reflectance values obtained from remote sensing images were directly applied to establish empirical relationships for population estimates. Lo (1995) employed regression analysis to estimate both population density per pixel and dwelling units per pixel using three factors from remote sensing imagery, including mean radiance values of three bands of Système Pour l'Observation de la Terre (SPOT) images, the proportion of high-density residential lands, and the absolute number of high-density residential lands. Chen

(2002) correlated areal census dwelling data with residential densities derived from Landsat TM images at the macro, medium and micro levels. Harvey (2002a, 2002b) established a series of regression models to explore the statistical relationships between the population density of a census collection district (CD) and various spectral indicators, such as the mean CD reflectance, the ratio of different bands, the ratio of difference and sum, *etc*. Li and Weng (2005) utilized stepwise regression analysis to develop population density models for the city of Indianapolis, Indiana and found that the estimation accuracy was substantially improved by a series of remotely sensed data, such as textural indicators, land surface temperature, sub-pixel fraction information, principal spectral radiance, vegetation indices, *etc*.

Due to recent and rapid developments in remote sensing technology, more terrain information can be extracted from remote sensing imagery. Therefore, in addition to the four categories described above, new spectral indicators have also been used in population estimation, which are regarded as the fifth category in this chapter. For example, spatial metrics represent measures of landscape characteristics, including percentage of landscape, the standard deviation of an area, mean size of patches, patch density, *etc*. The spatial metrics extracted from high-resolution remotely sensed imagery (such as IKONOS images), were found to be closely correlated with population density. Furthermore, a logarithmic linear regression was developed to model the relationship between logarithmic population density and different indices of spatial metrics (Liu *et al.* 2006).

In addition to spatial metrics, image texture statistics were also employed to model the relationship between population densities of land used for single-family/multi-family purposes and semi-variances using different lag lengths. The result indicated that the population model based on semi-variogram texture statistics performed better than the traditional land use-based dasymetric method and exhibited better accuracy statistics (Wu *et al.* 2006).

In addition to spatial metrics and texture information, the impervious surface fraction has also recently been used in population estimation. Lu and his colleagues (Lu *et al.* 2006) developed regression models for square root population density based on the percentage of residential area, the average impervious surface value, and the average residential impervious surface value. They found that including the impervious surface fraction and residential land use type can effectively improve the accuracy of the estimation of block group-level population density. Moreover, Wu and Murray (2007) classified population estimation methods into two groups, zonal-based and the pixel-based regression models, and considered environmental indicators including the residential impervious surface fraction, spectral radiance, and land-use classification. The results showed that the impervious surface fraction exhibited competitive performance and consistently outperforms land-use classification. Moreover, traditional zonal approaches had slightly better estimation accuracy than pixel-based models. Finally, in addition to remotely sensed information, existing GIS datasets, such as newly developed transportation network and land use/land cover data, were also used to derive population estimates (Qiu *et al*. 2003).

1.2.2.2 A new population estimation indicator: the impervious surface fraction

1.2.2.2.1 The importance of impervious surfaces

The impervious surface fraction is an important indicator in both physical geography and socio-economics. First, it effectively reflects the trend toward urbanization. Clear evidence of the continuing trend toward urbanization is that, in the 25 years prior to 2007, over 17 million hectares of rural lands had been transformed into developed lands in the United States (U.S. Department of Agriculture 2009). As a result, the change in land cover from undeveloped land to impervious surfaces has accompanied the rapid process of urbanization (Arnold and Gibbons 1996). Due to the different physical characteristics of natural vegetation and man-made materials, these environmental changes could have significant effects on residents and the environment. As they are impenetrable and thus preclude water storage and retention, impervious surfaces change the water balance by altering the direction, routing and flow rates of streams (Bowles 2002). Consequently, close correlations between impervious surfaces and water resource issues, such as stormwater runoff, water quality, stream health and aquatic ecosystem quality have been demonstrated (Brabec *et al.,* 2002, Environmental Protection Agency 1994, Harbor 1994, Lee 2009, Schueler 1991, 1994, Xian *et al.* 2007). Moreover, impervious surfaces absorb solar energy when exposed to the sun and then increase the temperature of the surrounding air (Akbari 2005). Thus, impervious surfaces are associated with the urban heat island (UHI) effect and air pollution problems (Lo and Quattrochi 2003, Rosenfeld *et al.* 1996, Sailor 1995, 2002, Walcek

and Yuan 1995, Yuan and Bauer 2007), which lead to respiratory difficulties, heat cramps, heat exhaustion, heat stroke, and heat rash among sensitive populations (Centers for Disease Control and Prevention 2006).

In addition to its use in physical geography, impervious surface information may also be useful in socio-economic and socio-cultural modeling, including applications such as home values, population segregation, and population estimates. Yu and Wu (2006) modeled home values in Milwaukee using both ordinary least squares regressions and regression tree techniques, with explanatory variables including different structural characteristics of houses and soil-impervious surface fractions extracted from remote sensing imagery. Population segregation, represented by the local segregation index (Duncan and Duncan 1955), was analyzed using both a global regression model and geographically weighted regression model, with explanatory variables including the soil fraction, impervious surface fraction and texture statistics (Yu and Wu 2004). As it is closely associated with anthropogenic impacts such as buildings and transportation infrastructure (Ji and Jensen 1999, Wu and Murray 2007), it is appropriate to estimate population using impervious surface data (Wu and Murray 2007, Lu *et al.* 2006). Therefore, in addition to its importance in hydrological and ecological modeling in planning and resource management, accurate impervious surface information will also be applied to assist in population estimation in this research.

1.2.2.2.2 Development of impervious surface fraction estimation

Ridd (1995) was the first to propose a conceptual urban land composition model, the vegetation-impervious surface-soil (V-I-S) model (figure 1), to characterize urban morphology and ecosystems. The primary motivation for this urban landscape model is that, due to the mixed pixel problem in medium- and coarse-resolution remote sensing imagery, the traditional classification method that uses only one land use/land cover type for each pixel might not be appropriate to characterize urban composition in detail.
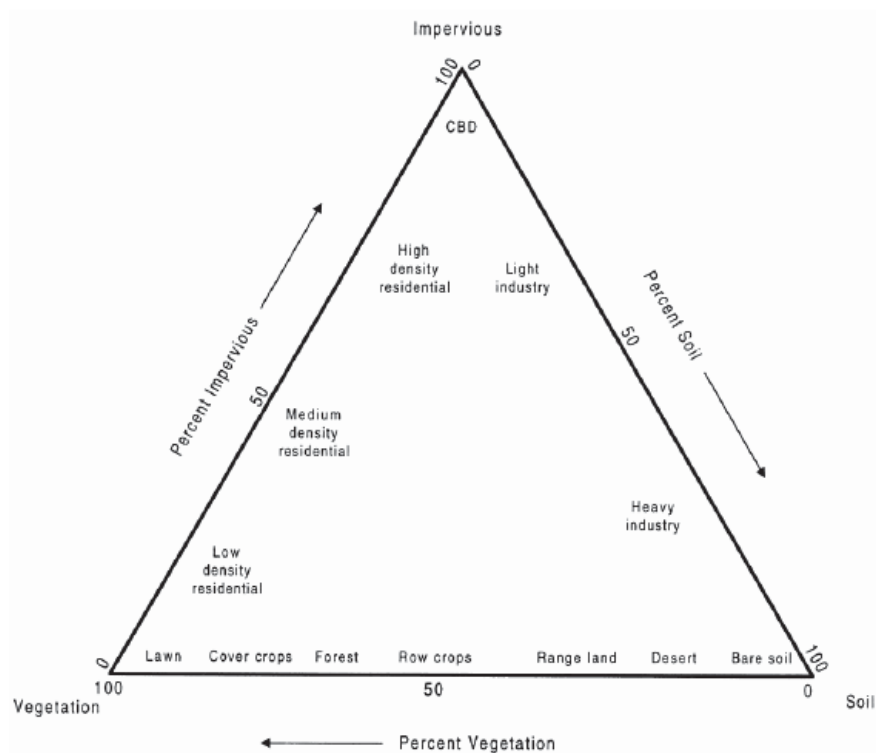
Fig. 1. Vegetation-Impervious Surface-Soil Model (after Ridd 1995)

Since Ridd (1995), several researchers have developed different methods to acquire impervious surface information from remote sensing imagery. Flanagan and

Civco (2001) obtained the subpixel impervious surface fraction using both artificial neural networks and a subpixel classification method for watersheds in Connecticut. Wu and Murray (2003) employed constrained linear spectral mixture analysis (LSMA) to extract the fractions of vegetation, low albedo, high albedo, and soil and then estimated the impervious surface fraction by combining low-albedo and high-albedo endmembers under the assumption that urban impervious surfaces consist of low- and high-albedo materials. Further, Wu (2004) proposed a normalized spectral mixture analysis (NSMA) model to reduce significant brightness differences in each endmember but maintain their original spectral shapes, thereby improving impervious surface estimation accuracy. In addition to Ridd's V-I-S model, Lu and Weng also developed a conceptual model with the assumption that all land cover can be regarded as a linear combination of green vegetation, shade and soil/impervious surfaces (Lu and Weng 2004).

1.2.3 Integration of demographic models and remote sensing/GIS techniques for

small-area population estimation

1.2.3.1 Estimation of the number of housing units

Represented by the result of multiplying the occupancy rate by the number of housing units, the number of households is one of the most important components in the HU population estimation method. The occupancy rate is always taken from the most recent census; thus the number of households is highly dependent on the number of housing units (Smith 1986). Currently, there are three major sources for the number of

housing units in population estimation, *i.e.,* building permits, electric utility customer records and remote sensing imagery.

Building permit data are often combined with demolition data in the estimation process. The change in the number of housing units is calculated as the number of newly constructed housing units less the reported number of demolitions obtained from building permit data (Starsinic and Zitter1968; Smith and Lewis 1980, 1983; Smith 1986). In addition to total change in the number of housing units, Smith (1986) also disaggregated the calculation based on various housing types (*i.e.*, single-family, multi-family and mobile homes). Errors may occur if a single time lag is selected arbitrarily, due to the considerable lag between the date the building permit is issued and the completion date (i.e. 3 to 5 months for single-family units, 10 to 20 months for multi-family units, and no lags for mobile homes) (Smith 1986, Smith and Lewis 1980).

Demographers have also used customer data from electrical companies to derive the number of housing units. Two popular methods, the absolute change method and the ratio method, have been used. The absolute change in the number of housing units was calculated as the difference between residential electricity customer records in the estimation year and the most recent census year (Starsinic and Zitter 1968, Smith 1986). Similarly, in the ratio method the researcher calculates the ratio of the total number of households in the most recent census to the total number of customers reported by the electric utility, and then multiplies the current number of customer

records by this ratio, under the assumption that the ratio has remained unchanged (Smith and Lewis 1980, 1983; Smith 1986). However, methods that employ customer data from electrical utilities have been considered to perform better than those using building permit data due to greater data source quality and availability (Starsinic and Zitter1968; Smith and Lewis 1980, 1983; Smith 1986).

As noted above, the number of housing units has also been derived from remote sensing imagery. For medium-resolution images, such as TM/ETM+ images, the number of housing units has been estimated through regression analysis of the relationship between residential land use area and the number of housing units (Lo 2003). When considering high-resolution imagery, such as aerial photographs, manual counting is a useful but less effective method to obtain the number of housing units, as it requires a relatively high degree of familiarity with the research area (Hsu 1971, Lo and Chan 1980, Watkins 1984, Watkins and Morrow-Jones 1985).

1.2.3.2 Person per household (PPH) estimation

Currently, PPH estimation methods can be divided into three categories. First, PPH can be directly derived from the most recent census by simply assuming the value has remained unchanged since the previous calculation (Starsinic and Zitter 1968). Obviously, this method is only suitable for locations where the PPH trend is stable and when the estimation date is close to the most recent census (Smith 1986).

Second, PPH can be obtained through simple mathematical extrapolation. Linear extrapolation has been employed to estimate inter-census PPH, assuming that

the change from the most recent census year to the estimation year is identical to that between last two censuses (Starsinic and Zitter1968). PPH has also been extrapolated under the assumption of a proportional change, which was estimated by combining the data from the most recent census and annual population surveys (Smith 1980, 1986). However, these methods tend to overestimate PPH when it declines sharply (Smith 1980).

The third category is regression analysis. Smith and his colleagues (Smith *et al*. 2002) were the first to estimate household size at the county-level using four ordinary least squares (OLS) regression models using demographic variables related to births, school enrollees, and Medicare enrollees as the independent variables. At present, there are few in-depth studies on PPH estimation, likely because small sample size could cause significant estimation errors (Ghosh and Rao 1994).

Given the rapid developments in remote sensing and GIS technologies, it is of substantial importance to investigate whether small-area population estimation can benefit from these new technologies. Detailed GIS datasets and remote sensing information extracted from high-resolution imagery might be employed to assist in estimating housing number counts and inter-census PPH at the census block-level to improve small-area population estimates. Therefore, this research focuses on three aspects.

First, this research focuses on the use of existing GIS and remotely sensed datasets for estimating population at the census block level. Specifically, Chapter 2 of

this dissertation explores the applicability of incorporating GIS, remotely sensed and demographic datasets in a demographic model, the housing unit method, to generate small-area population estimates in Grafton, WI. Specifically, the two primary components of the demographic framework, HU counts and PPH, were obtained by modeling their relationships with demographic and geographic variables using a sequence of ordinary least-squares (OLS) regression models.

Second, a new spectral index, the biophysical composition index (BCI), was proposed in Chapter 3 to facilitate the derivation of urban land cover information in practical applications following Ridd's conceptual urban landscape model, the vegetation – impervious surface – soil triangle model (1995), by reexamining the Tasseled Cap (TC) transformation. Moreover, this research examined the applicability of BCI to remote sensing images at three different spatial resolutions. This index was further employed to assist in the derivation of urban impervious surface information, which can provide detailed urban environmental information for the automated enumeration of housing units in a demographic framework.

Finally, Chapter 4 attempted to improve small-area population estimation by combining demographic theory and high-resolution remotely sensed and GIS datasets. Using newly generated environmental indicators, a bottom-up method for population estimation at the finest scale available in national census data was developed by incorporating high-resolution remote sensing imagery/GIS datasets into a demographic housing unit model. HU counts and PPH, two primary factors in the housing unit method, were separately estimated using detailed urban environmental information

extracted from high-resolution remote sensing imagery and GIS data. Accordingly,

population counts for each census block were obtained by adopting the HU model. In

addition, sensitivity analyses were conducted to evaluate the sources of errors in

population estimates obtained via the HU method.

CHAPTER 2 SMALL-AREA POPULATION ESTIMATION USING REMOTE SENSING AND GIS TECHNIQUES[*]

2.1. Introduction

Accurate estimates of small-area population are essential for supporting a wide variety of planning processes. The size and distribution of the population are often key determinants for resource allocation for state and local governments (Smith et al., 2002). Population estimates are critical in decisions about when and where to build public facilities such as schools, libraries, sewage treatment plants, hospitals, and transportation infrastructure. Also, population estimates are often used by private sectors for customer profile analysis, market area delineation, and site location identification (Martin and Williams, 1992; Plane and Rogerson, 1994). In addition, population information is an important input in many urban and regional models, such as land use and transportation interaction models, urban sprawl analysis, environment equity studies, and policy impact analysis (Rees et al., 2004). Clearly, accurate and timely population estimates are of great importance (Smith et al., 2002). Accurate population data, however, is only available for every decade through the national census survey. It is obvious that this frequency does not meet the needs for rapid growth

---

[*] Portions of this chapter have been published in *International Journal of Remote Sensing*, coauthored with Drs. Changshan Wu and Le Wang.

areas where noteworthy local intercensal population changes occur. Thus, appropriate estimation methods for such geographical areas are extremely necessary.

Numerous methods have been proposed for population estimates in demography, such as Component Method II (CM-II), Administrative Records (AR), Ratio Correlation (RC), and Housing Unit (HU) method (Ghosh and Rao, 1994). The CM-II method updates population estimates by accounting for the major components of local demographic change. The population is calculated by starting with the recent census population, adding the estimated number of births, subtracting the number of deaths, then adding net migration and the changes in group quarter population. The AR method, similar to the CM-II method, additionally uses administrative records for estimating net migration for population under age 65. These records include federal income tax returns, Immigration and Naturalization Service records, and military movement records. The RC method relates population changes to the changes in several symptomatic indicators, such as school enrolment, car registration, work force information, and occupied housing units. A regression model is utilized to construct the relationship between population changes and the changes of symptomatic indicators between two census years. In the HU method, population estimates for a small area are calculated as the product of the number of occupied housing units and household size plus the population in group quarters. Among all these methods, the HU method is the most commonly used, and considered one of the most accurate and cost-effective methods for small-area population estimation (U.S. Census Bureau, 1998; Smith and Cody, 2004). In fact, the HU method has been used by U.S. Census

Bureau as the single method for estimating population of subcounty areas (e.g.

incorporated places and minor civil divisions) since 1996 (U.S. Census Bureau, 1998;

Smith and Cody, 2004; U.S. Census Bureau, 2005).

Besides these demographic models, remote sensing and GIS techniques

provide an alternative for small-area population estimation. One early application of

remote sensing technique is the house counting approach. In particular, dwelling units

are manually counted from high resolution aerial photographs, and then these counts

are multiplied by the surveyed household size to derive population estimates (Lo,

1986a, 1986b). This approach, although relatively accurate, requires tremendous

amount of time and labor, and is rarely employed by state and local agencies. To

address this issue, automatic approaches have been proposed for housing unit and

population estimation. With these approaches, either spectral radiance/reflectance or

urban physical parameters are extracted from remote sensing imagery to represent

housing information. With these parameters, regression models are typically applied

to derive population estimates (Lo, 1995; Webster, 1996; Chen, 2002; Harvey, 2002a,

2002b; Li and Weng, 2005; Wu and Murray, 2007). Similarly, existing GIS datasets,

such as transportation network and land use land cover data, were also applied to

derive population estimates (Qiu et al., 2003; Wu et al., 2005).

These demographic models and remote sensing/GIS-based approaches for

population estimation have been developed almost parallelly. Each of them, however,

has its own issues. The HU method, a popularly applied demographic approach, can

only produce population estimates at an aggregated geographical level (e.g. town, city, or county), instead of a finer local level (e.g. census block level). This is mostly due to the problems of data acquisition. Currently, commonly utilized data sources of housing unit information are building permits and electric customer information, most of which can only be obtained at an aggregated geographical level. Although some methods have been developed to derive population and HU estimates at the block group level using simple interpolation and step-down techniques (Perry and Voss, 1996), such estimates, however, are unreliable. These techniques assume that population count in a census block is a linear function of its geographic area, thereby distributing population from an aggregated unit to a block accordingly. Such assumption, however, is problematic due to the heterogeneous population distribution within a geographic area. On the other side, remote sensing/GIS based automatic techniques can reveal detailed spatial information (either radiance/reflectance or physical parameters). This information, however, is not directly associated with housing units, and may produce large errors when applied as the solo data source to estimate housing units or population (Harvey, 2002a, 2002b; Li and Weng, 2005; Wu and Murray, 2007). Therefore, state and local agencies seldom utilized remote sensing/GIS based automatic approaches for producing small-area population estimates.

The other problem of both approaches is that the relationship between population and housing units (or indicative parameters extracted from remote sensing imagery) is always assumed to be unchanged from the most recent decennial census

(U.S. Census Bureau, 2005). Several researches have pointed out that the persons per household (PPH) in the U.S. has a tremendously downward trend during the past two centuries, falling from 5.8 in 1790 to 4.8 in 1900, then to 2.6 in 2000 (Kobrin, 1976; U.S. Census Bureau, 2001; Bongaarts, 2001). This drop is most likely due to declining birth rates and the tendency for adults to head separate households. Acknowledging the problems of using historical PPH values, Starsinic and Zitter (1968) developed PPH estimation methods through extrapolating historical trends. Smith (1986) adjusted the estimated PPH in small areas by examining changes in larger areas (e.g., states) where current PPH estimates are available from other sources. These simple approaches may generate biased results when PPH trends are not stable (Smith et al., 2002). Smith et al. (2002) estimated the county-level PPH by introducing population age structure variables, births, school enrolment, and Medicare enrolment (for age 65 and older). Currently, studies on the PPH estimation are rare, and it is of great necessity to estimate the PPH at the detailed level (e.g. census block).

To address the above issues associated with the HU method and remote sensing/GIS based automatic approaches, we propose to integrate GIS and remote sensing techniques into the HU method for deriving better small-area population estimates. In particular, the first objective of this paper is to redistribute new housing units at an aggregated geographic level (e.g. village or town) to census blocks with the help of remote sensing and GIS information. The second objective is to develop a model for better PPH estimation at the census block level through incorporating

remote sensing, GIS, and demographic data. The remaining of this paper is organized as follows. Next section introduces the study area and data. The third section details model development and accuracy assessment techniques. Analysis of results and accuracy assessment are discussed in section 4, and finally conclusions and future research are given in section 5.

2.2 Study Area and Data

Village and Town of Grafton, Wisconsin, USA (see figure 2.1) is selected as the study area for this research. Located in the north of Milwaukee City, Grafton has a geographic area of 66.1 km^2, including a variety of land use types, such as residential, commercial, transportation, forestry, agricultural, as well as other rural lands. Since 1990, Grafton has been experiencing rapid population growth, with a significant amount of residential and commercial developments. Its population is 13,330 in 1990, and rises to 14,444 in 2000, with an increment of 7.7%.   In addition, the housing unit number rises from 4,827 in 1990 to 5,773 in 2000, with 946 new housing units constructed, or an increment of 16.4%.   Due to the noteworthy population growth in this area, detailed population estimates are essential for supporting urban and rural planning.
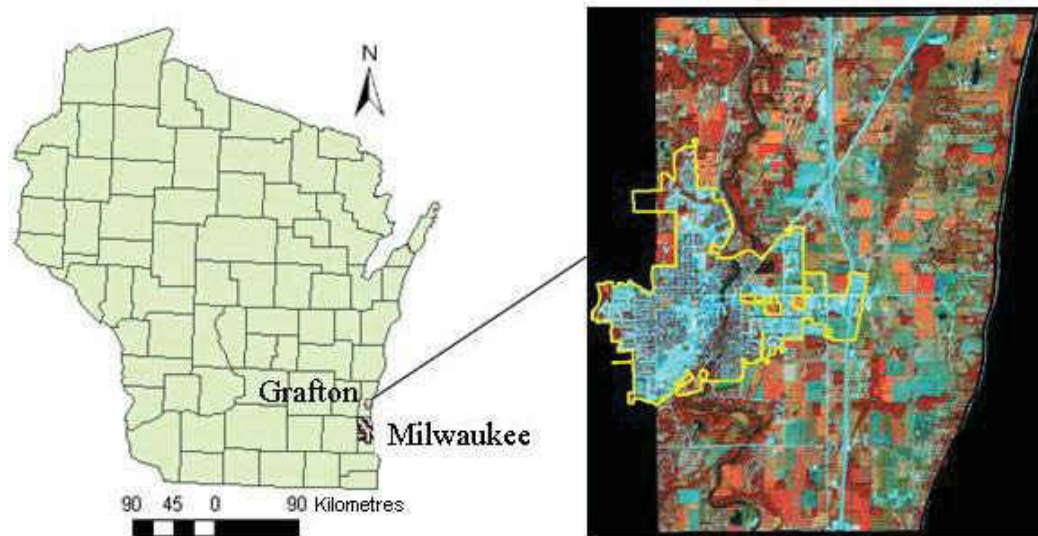
Figure 2.1 Study area as the Town and Village of Grafton, WI, USA

For the study area, population data at the census block level in 1990 and 2000 were acquired from the U.S. Census Bureau. In Grafton, there are 266 blocks in 1990, and 313 blocks in 2000. In fact, a number of census blocks in 1990 have been sub-divided into several small blocks in 2000. Moreover, the boundaries of several census blocks have been modified. To address this data inconsistency problem, an area-weighted spatial interpolation (Goodchild and Lam, 1980) was applied to the 1990 block data, and associated information was transferred to the 2000 block boundary. Besides census data, detailed land use data for 1990 and 2000 (see figure 2.2) were obtained from the Southeast Wisconsin Regional Planning Commission. A Landsat Thematic Mapper (TM) image acquired on August 01, 1989 and a Landsat Enhanced Thematic Mapper Plus (ETM+) image acquired on September 08, 2000 were downloaded from the WisconsinView project website (http://www.wisconsinview.org/). Both images were re-projected to the UTM projection (zone 16, datum WGS84), and a further georeference was conducted to

reduce geometry misregistration. The residual mean square (RMS) of the georeferenced image is within 0.2 pixel. Moreover, atmospheric correction was performed using the algorithm developed by Richter (1996a, 1996b, and 2005). In particular, this method involves two steps, including 1) calculating the reflectance of every pixel based on standard atmospheres, aerosol types, and visibility, and 2) correcting the adjacency effect using weighting functions. More details about this algorithm can be found in Richter (1996a, 2005).These Landsat images will be utilized to extract urban biophysical information for better estimation of housing units and persons per household. In this research, demographic and spatial data in 1990 are employed for model development, and data in 2000 are applied for model calibration and accuracy assessment.
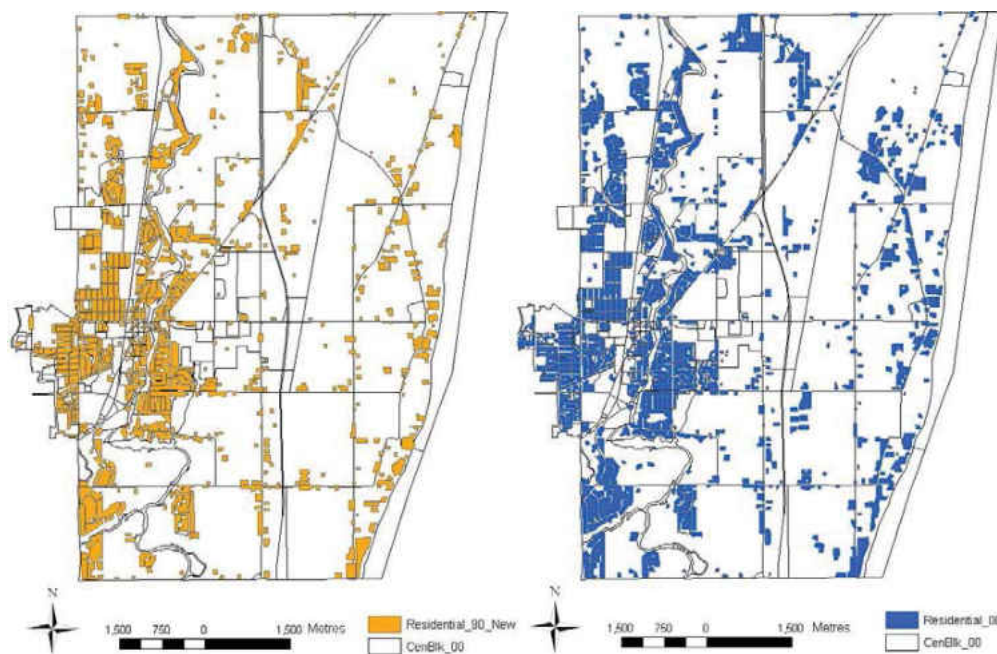
Figure 2.2 Detailed land use data of 1990 (Left) and 2000 (Right) obtained from the

Southeast Wisconsin Regional Planning Commission (Residential land uses are

shown in color)

2.3 Methodology

2.3.1 Housing Unit Estimation

With traditional demographic methods, the number of new housing units is

typically estimated from building permit and electrical customer information. This

information, however, can only be obtained at an aggregated geographical level, and

there is a need to assign these new housing units to individual blocks. In this paper, two

interpolation methods were employed to derive housing unit estimates at the census

block level. This first method is the simple step-down interpolation technique (Perry

and Voss, 1996), with which new housing units at the aggregated level are assigned to

each census block according to the geographical area of that block. The second method

is the dasymetric mapping method developed in this paper. Dasymetric mapping was

created for visualizing population data consistent to land use types to avoid the problem

of ecological fallacy. Dasymetric mapping has been popularly utilized for population

density estimation and areal interpolation (Mennis, 2003; Wu and Murray, 2005;

Mennis and Hultgren, 2006), but not particularly applied for housing unit estimation. In

this paper, a dasymetric mapping method was developed to re-distribute newly

developed housing units to individual census blocks with the help of ancillary remote

sensing and GIS data. In particular, three variables derived from remote sensing and

GIS dataset are utilized. These variables include 1) single-family land use area change,

2) multi-family land use area change, and 3) the change of Normalized Difference

Vegetation Index (NDVI), representing vegetation cover change. It is assumed that the

number of newly developed housing units is positively associated with land use area

changes (e.g. single-family and multi-family) and negative related to vegetation cover

change. In order to quantify the weight for each variable, an ordinary least squares

(OLS) regression analysis model (Equation 2.1) was developed as follows.

$$\Delta HU = \alpha_0 + \alpha_1 \times \Delta R_S + \alpha_2 \times \Delta R_M + \alpha_3 \times \Delta NDVI \tag{2.1}$$

Where ΔHU is the number of newly developed housing units in a block from

time t_1 to time t_2, ΔR_S is the areal change of single-family land use in the block, ΔR_M is

the areal change of multi-family land use in the block, and $\Delta NDVI$ is the changes of

NDVI values in that block, and α_1, α_2, and α_3 are their coefficients respectively. After

obtaining the relationship among newly developed housing units and the variables

derived from remote sensing and GIS datasets, the total housing units for the

aggregated area (e.g. town and village of Grafton) can be re-distributed to each census

block.

2.3.2 PPH Estimation

Compared with the housing unit numbers, an accurate PPH estimate is more

essential since a minor error of PPH may result a significant error in the estimated

population. In this paper, the current method, in which the PPH is assumed to be

unchanged from the previous census, and three regression models that utilize

demographic and remote sensing and GIS variables were developed. Demographic and

economic variables include population age structures (e.g. parentage of people with 65 and over), household income, and housing values. Variables derived from remote sensing and GIS data include distances to particular land uses (e.g. commercial center, schools, and recreational areas), vegetation cover changes, and textural information generated from Landsat TM/ETM+ imagery. With these demographic and GIS/remote sensing related variables, the three regression models are described as follows.

The first model (Model A) assumes that the relationship between PPH and demographic and spatial variables is unchanged over time. Therefore, it is possible to estimate the PPH of time t_2 based on the parameters obtained from the data of time t_1. Thus, this model is an "inherit model", in which the PPH for time t_2 is estimated according to the relations obtained from the data of time t_1. The regression model is illustrated as follows (see Equation 2.2).

$$\text{Model A}: PPH_t = \alpha_0 + \sum_{i=1}^{m} \beta_i S_{i,t} + \sum_{j=1}^{n} \gamma_j D_{j,t} \tag{2.2}$$

where PPH_t is the PPH value at time t, $S_{i,t}$ indicates a spatial variable derived from remote sensing and GIS data at time t, $D_{j,t}$ represents a demographic variable at time t, m and n are the total number of spatial and demographic variables respectively, and α, β, and γ are regression coefficients.

Model A assumes that the relationship between PPH and relevant variables does not change over time. This assumption, however, may be problematic. To have a better estimation of PPH, a special survey is needed to obtain the knowledge of PPH and

demographic variables for time t_2. Therefore, the second model (Model B) attempts to estimate the PPH at time t_2 with the PPH value at time t_1, and spatial and demographic variables at time t_2 as independent variables. This model is named as an "empirical model" as the PPH at time t_1 is employed as an independent variable.

$$\text{Model B: } PPH_{t_2} = \alpha_0 + \alpha_1 PPH_{t_1} + \sum_{i=1}^{m} \beta_i S_{i,t_2} + \sum_{j=1}^{n} \gamma_j D_{j,t_2} \qquad (2.3)$$

where PPH_{t1} and PPH_{t2} are the PPH at time t_1 and time t_2 respectively, and $S_{i,t2}$ and $D_{j,t2}$ are the spatial and demographic variables at time t_2 respectively.

In addition to Model B, the third model (Model C) explores the relationship between the change of PPH and the changes of spatial and demographic variables from time t_1 to time t_2. Since this model represents the relationships between the changes of variables, it is named as a "change model". The formulation of this model is as follows (see Equation 2.4).

$$\text{Model C: } \Delta PPH = \alpha_0 + \sum_{i=1}^{m} \beta_i \Delta S_i + \sum_{j=1}^{n} \gamma_j \Delta D_j \qquad (2.4)$$

where ΔPPH is the change of PPH for a census block from time t_1 to time t_2, ΔS_i and ΔD_j are the changes of spatial and demographic variables respectively.

2.3.3 Small-area population estimation

With the HU and PPH estimates for each census block, it is feasible to derive the population estimates via the housing unit method, which can be expressed as follows (see Equation 2.5).

$$P_t = HU_t \times O_t \times PPH_t + GQ_t \tag{2.5}$$

where P_t is the estimated population for a small area at a non-census time t; HU_t is the number of housing units at time t; O_t is the occupancy rate at time t; PPH_t is the average size of household or persons per household at time t; and GQ_t is the group quarters population (e.g. persons residing in college dormitories, military barracks, nursing homes, and prisons) at time t.

With the estimated values of HU and PPH derived from sections 2.1 and 2.2, it is feasible to estimate the population for each census block with information of occupancy rate (O_t) and group quarter population (GQ_t). In this research, the occupancy rate at time t_2 is assumed to be unchanged from time t_1, and this information may also be estimated from data acquired from a special survey, if available. For an area without large group quarters facilities, the GQ population for a non-census year can be assumed to be unchanged or change proportionally to the household population (Smith and Lewis, 1980). In this research, group quarters population in Grafton at time t_2 is regarded the same as the value at time t_1. Therefore, with the estimated values of HU, PPH, O, and GQ at time t_2, the population estimate for a census block at time t_2 can be derived.

2.3.4. Accuracy assessment

To assess the estimation accuracy of housing units, *PPH*, and population, a spatially random sampling method was utilized to divide all census blocks into two groups: 50% of data was utilized as training dataset for modeling, and the other 50% of

data serves as testing dataset to assess estimation accuracy. Several error measurements, including the mean absolute error (*MAE*) (see Equation 2.6), mean absolute percentage error (*MAPE*) (see Equation 2.7), and mean algebraic percentage error (*MALPE*) (see Equation 3.8), were employed in this paper.

$$MAE = \frac{1}{n} \sum_{i=1}^{n} |\hat{A}_i - A_i|$$ (2.6)

$$MAPE = 100\% \times \frac{1}{n} \sum_{i=1}^{n} \left| \frac{\hat{A}_i - A_i}{A_i} \right|$$ (2.7)

$$MALPE = 100\% \times \frac{1}{n} \sum_{i=1}^{n} \frac{\hat{A}_i - A_i}{A_i}$$ (2.8)

where $\hat{A}_i$ is the estimated value for a variable, and A_i is the actual value for that variable, and n is the total number of samples (e.g. census blocks). For these three measurements, *MAE* is popularly utilized in remote sensing and GIS studies, while *MAPE* and *MALPE* are widely employed in demographic research. Both *MAE* and *MAPE* are measures of precision, reflecting how close the estimated values to the actual values, while *MALPE* is a measure of bias, focusing on whether the total estimate shows an upward or downward tendency (Smith et al., 2002; Cai, 2007).

2.4. Results and Discussion

2.4.1 House Unit Estimation

Following the methodology described in section 2.1, the simple step-down interpolation technique and the regression-based approach were implemented in the

study area. For the step-down interpolation, the geographical area of each census block is utilized as the weight for new housing unit assignment; that is, the number of new housing units received by a block is a linear function of its geographical area. The *MAE* of the housing unit estimation with this approach is 8.70, and a comparison with the actual new housing unit distribution (see Figure 2.3a) illustrates that the housing units in a majority of census blocks are overestimated, in particular the blocks with larger geographical areas (e.g. blocks in the Village of Grafton). Comparatively, the housing units in a few blocks at the edge of Grafton Town are under-estimated. This is because recent developments of housing units were along the edge of Grafton Town, while the step-down technique simply assumes that the number of new housing units is linearly correlated to block size, which does not reflect the actual development pattern of new housing units.
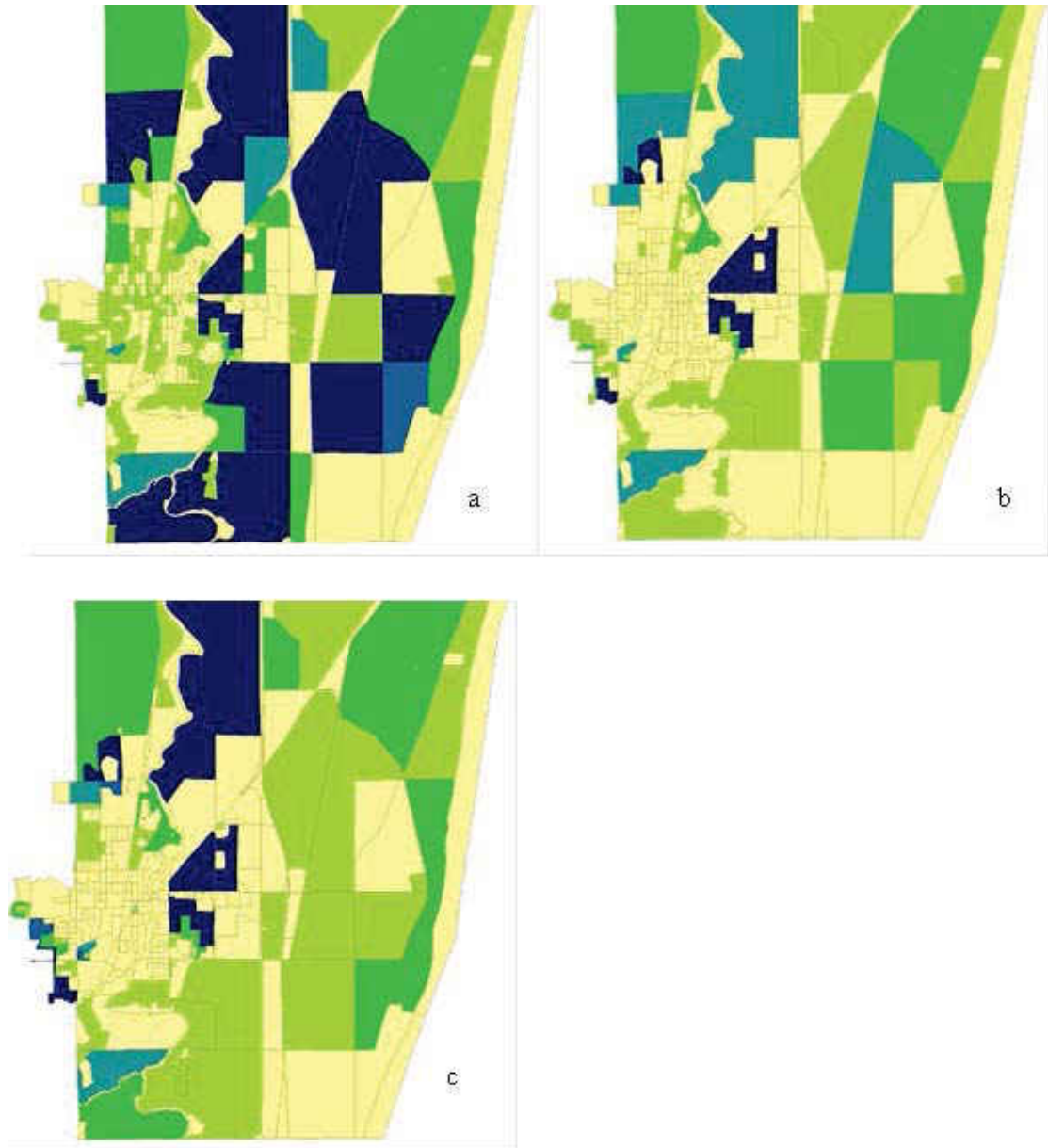
Figure 2.3 Comparison of housing unit estimates among a) estimates using simple step-down interpolation method, b) estimates using regression model, and c) actual housing unit numbers.

In addition to the simple step-down interpolation technique, the regression model with remote sensing and GIS information was also implemented. Results of this

model (see Table 2.1) indicate that the spatial pattern of new housing units can be

reasonably explained by the GIS and remote sensing variables, with the adjusted

R-square equal to 0.526. Among the three variables, the change of single family and

multi-family areas are statistically significant at the 95% confidence level, while the

change of NDVI, although negatively correlated with new housing development, does

not have significant contributions. Therefore, for the housing unit interpolation, only

single family and multi-family residential area changes were utilized.

Table 2.1 Housing unit regression model results

Coefficient	B	t	p-value
Intercept	1.411	2.027	0.047[**]
ΔNDVI	-6.744	-1.400	0.163
ΔR$_M$	18.804	9.818	0.000[**]
ΔR$_S$	1.378	6.405	0.000[**]

($ΔR_M$ is the change of multi-family land use areas, $ΔR_S$ is the change of single-family land use areas, [**] indicates statistically significant at the 95% confidence level. Adjusted R-square is 0.526)

Results show that the MAE with this regression model is 3.37, which is much

lower than that obtained from the simple step-down interpolation method (8.70).

Moreover, when compared with the actual housing unit map (see Figure 3.3b and 3.3c),

it is apparent that the spatial pattern of housing unit estimates from regression analysis

can accurately reflects the actual distribution of new housing development. In

particular, the housing unit development in the Town of Grafton has been almost

saturated, and most of the new developments are in the fringe of the Town of Grafton, with a few new developments in the Village of Grafton.

2.4.2 Persons per household (PPH) Estimation

Four methods for estimating PPH, including the current method (PPH is assumed to be unchanged from previous census) and three regression models (Model A, B, and C) were applied for the study area, and results of these three regression models are reported in Table 2.2. Table 2.2 indicates that the value of PPH can be modeled reasonably well by demographic and spatial variables. In fact, the adjusted R-squares for all these three models are over 0.60, indicating that over 60% of the variations in PPH can be explained. Four demographic variables, percentage of people with ages under 17, 18-39, 40-64, and 65 and over, were utilized for PPH estimates. Results indicate that PPH has a significant and positive relationship with the percentage of young population (people with age under 17), and a significant but negative relationship with the percentage of elder population (people with age of 65 and over). These results are not unexpected, and consistent with the findings of Smith et al. (2002). Beside demographic variables, several spatial variables, including distance to commercial centers, distance to schools, and distance to recreational areas, were calculated using GIS land use data. Results indicate that PPH is positively correlated with the distance to commercial centers, but negatively correlated with the distance to recreational areas. These results imply that households with a larger size tend to choose residential locations far away from commercial centers, and close to recreational areas.

Spatial variables derived from Landsat data, including NDVI and textural parameters, however, were insignificant in any model. Therefore, these variables were dropped from these regression models.

Table 2.2 Coefficient summary of PPH regression models

Coefficients	Model A	Model B	Model C
Intercept	1.646	1.012	-0.215
PPH_90	/	0.208	/
Age 0_17	4.334	3.391	3.681
Age 18_39	/	/	/
Age 40_64	/	/	/
Age 65above	/	/	-0.855
Dist_Commercial	0.349	0.361	/
Dist_School	/	/	/
Dist_Recreation	-0.96	/	-0.346
R square	0.627	0.718	0.698

("/" indicates the variable does not have significant contribution (at the 95% confidence level) to the regression model)

The results of PPH estimates are illustrated in Figure 2.4, with *a*, *b*, *c*, and *d* showing the estimation results of Model A, B, C, and the current method respectively, and 4e displaying the actual spatial distribution of PPH in 2000 for comparison purposes. It can be discerned that the PPH estimates from the Models A, B, and C have similar spatial patterns when compared to the actual PPH values in 2000. Comparatively, the estimates of Models A and B seem to be consistent with the spatial

patterns of the actual PPH distribution, and Model C clearly overestimates the PPH in many census blocks. For the current method, though, the spatial trend is inconsistent with the actual PPH distribution, and the PPH values in a large number of blocks are visibly overestimated, particularly in the blocks in Grafton Village. The reason of this overestimation may be that the PPH in the study area has a downward trend in the past decades as the declining birth rates and the tendency for adults to lead separate households.
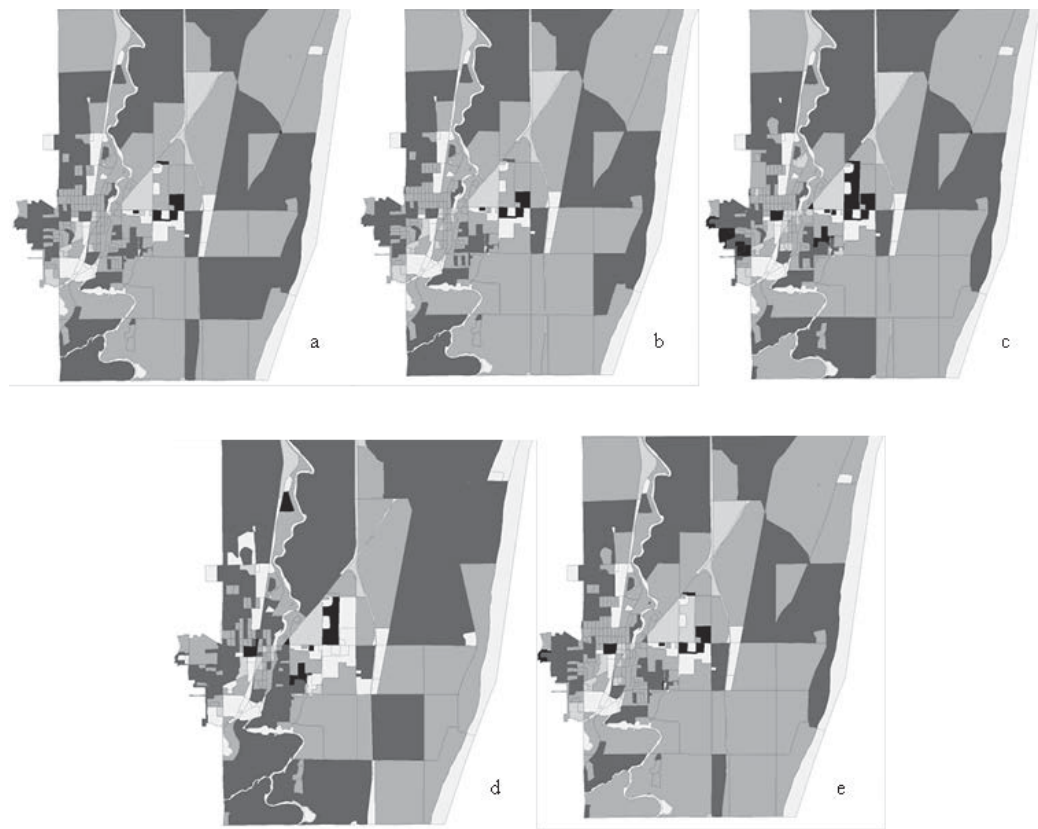
Figure 2.4 Comparison of persons per household (PPH) estimates among a) Model A, b) Model B, c) Model C, d) Current method, and e) actual PPH values.

In order to quantitatively evaluate the accuracy of the PPH estimates, the three accuracy measurements, MAPE, MALPE, and MAE, were calculated and reported in Table 2.3. Results indicate that the current method has the lowest precision, with the highest MAPE (24.19%) and MAE (0.62). Moreover, it has the largest bias, and overestimates the PPH by approximate 13%. This proves that it is inappropriate to assume that the PPH is constant over time. Comparatively, all three regression models perform better than the current method. Models A and C have slightly better precisions, but much lower bias than the current method. For example, the MALPEs of Models A and C are 4.21% and 7.77%, much lower than that of the current method (13.13%). Model B has the best overall performance. In particular, it has the highest precision, with the lowest MAPE (9.98%) and MAE (0.27), and the smallest bias (MALPE equal to 0.21). The lack of precision improvements with Models A and C may be associated with the assumptions of these two models. In particular, Model A, as an "inherit model", assumes that the relationship between PPH and relevant variables does not change overtime. Model C, as a "change model", considers that the change of PPH can be effectively explained by the changes of spatial and demographic variables, irrelevant to the previous PPH values. These assumptions, however, are problematic, as the PPH in a census block is dependent on both the previous PPH values and the changes of spatial and demographic variables. Therefore, Model B, taking both factors into account, has proven to be the most accurate model for PPH estimation.

Table 2.3 Accuracy comparison of estimation models of HU, PPH, and population at the census-block level

	Model	MAPE%	MALPE%	MAE
HU	Step-down method	41.08	19.26	8.70
	HU Regression	35.34	6.82	3.37
PPH	Current method	24.19	13.13	0.62
	Model A	22.22	4.21	0.59
	Model B	9.98	0.21	0.27
	Model C	19.19	7.77	0.50
Population	Simple demographic method	58.27	32.68	30.02
	Regression model	25.56	5.52	11.68

2.4.3 Small-area Population Estimation

With the HU and PPH estimates for a non-census year, it is necessary to generate the population estimates using the housing unit method described in Section 2.3. In this paper, two approaches were developed for comparison. The first one is the simple demographic approach, which utilizes the step-down interpolation method for HU estimation, and assumes that PPH is as same as that obtained from the previous census. The second approach involves a sequence of regression analyses with demographic and spatial data. In particular, the HU estimates were achieved from the

regression model using detailed land use datasets (as described in Section 3.1) and the PPH estimates were generated using the Model B, in which demographic and spatial variables were utilized (as detailed in Section 2.2).

Results of population estimates with these two approaches, together with the actual population count from 2000 Census, are displayed in Figure 2.5. In particular, Figure 2.5*a* shows the results obtained from the simple demographic approach, and 5*b* illustrates the estimates from the regression models. In addition, detailed accuracy assessments of these population estimates are reported in Table 2.3. Analysis of results indicates that the estimates from the simple demographic method are not acceptable. In general, it overestimates the population for the whole study area by over 30%, largely due to the overestimates of the PPH values. Moreover, the relative errors are also very large, as the MAPE is approximate 58% and MAE is about 30. On the contrary, the regression-based approach only slightly overestimates the overall population (5.5%), and is much more precise that the simple demographic approach. In fact, the MAPE (25.56%) and MAE (11.68) indicate that the regression models with demographic and spatial variables can derive small-area population estimates reasonably well.

Besides an overall accuracy assessment, analysis of relative errors for the HU, PPH, and population estimates (see figure 2.6) illustrates the patterns of error propagation. Figure 2.6*a* shows that the HU values in seven blocks (out of 313) have been highly overestimated (with relative errors higher than 15%). Within these seven blocks, six have highly overestimated population counts (see figure 2.6*c*). In addition,

the HU values in nineteen blocks are highly underestimated (with relative errors lower than 15%), and with them, fifteen have highly underestimated population counts. These results indicate that the errors of HU estimates have significant influences on those of population estimates. When compared to the HU, the errors of PPH do not have such strong influences on the errors of population estimates. In particular, within the twelve blocks with highly overestimated PPH values, the population counts within nine of them are highly overestimated. Moreover, within the ten blocks with highly underestimated PPH values, only four of them have highly underestimated population counts.
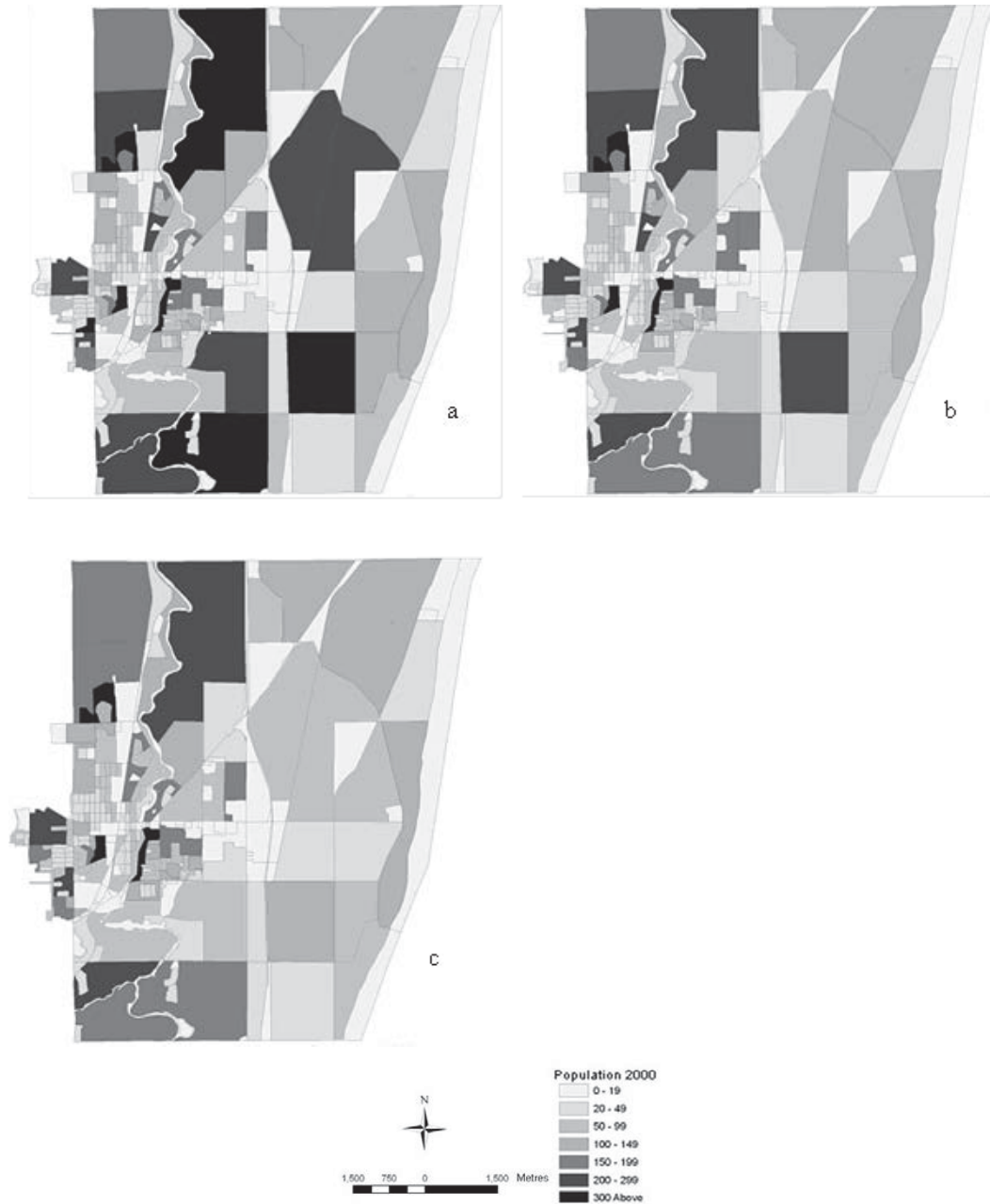
Figure 2.5 Comparison of block-level population estimates derived from a) Simple

demographic method, b) Regression analyses with demographic and remote

sensing/GIS data, and c) actual population count from 2000 Census

Figure 2.6 Comparison of relative errors at the block level for a) Estimated housing

units by the Regression method, b) Person per household by the Regression Model B,

and c) Population by the Equation 2.5 with the estimated housing units from a) and

Person per household from b)

2.5 Conclusions

In this paper, we propose to integrate GIS and remote sensing techniques into the housing unit method for generating better small-area population estimates. In particular, housing units (HU) and persons per household (PPH) at the census block level were derived using regression models with demographic and spatial variables. Then these estimates were inputted to the housing unit method for deriving block-level population estimates. The accuracy of small-area estimation with this regression-based method was compared to the current method.

Analysis of results suggests two major conclusions. First, the accuracy of small-area population estimates can be significantly improved through integrating remote sensing/GIS information. Detailed land use information has proven to be the most important GIS dataset for small-area population estimation. In particular, it can be utilized to redistribute aggregated building permit information for better HU generation, and employed to calculate spatial variables for better PPH estimation. Second, this research proves that persons per household can be effectively modeled by demographic and spatial variables. In fact, several demographic variables, including the percentage of population with age under 17, and population with age 65 and over, and several spatial variables, such as the distance to commercial centers, schools, and recreational areas can explain over 60% of PPH variations.

Although this study showed that the integration of GIS and remote sensing

information into the housing unit method can greatly improve the small-area population estimates, there are many issues for future research. One direction is for better housing unit estimation. Detailed and more accurate housing unit estimation can be achieved using high spatial resolution remote sensing imagery (such as IKONOS and QuickBird data) and Light Detection and Ranging (LiDAR) datasets. Moreover, the footprint and volume information generated from these data can help the estimation of PPH. Another direction is to explore whether demographic variables can be derived through GIS and remote sensing information. Currently, a special census, or sampling, is needed for creating demographic variables. This work, however, is always time consuming and labor intensive.

CHAPTER 3 DEVELOPMENT OF A SPECTRAL INDEX FOR REMOTE SENSING OF URBAN ENVIRONMENTS[*]

3.1 Introduction

Over the past decades, urbanization has taken place at an unprecedented rate around the world. In 1950, as an example, only 29% of the world population resided in urban areas, and this number rose to 49% by 2005. Moreover, this trend is projected to continue in the future decades (United Nations, 2006). In the process of urbanization, natural landscapes have been rapidly transformed to anthropogenic urban land uses, and biophysical compositions and characteristics of natural environments have been dramatically modified. While urbanization brings social and economic benefits (e.g. improved quality of life and economic prosperity), it also leads to a number of environmental problems (e.g. water quality degradation, air pollution, loss of biodiversity, and urban heat island effect) and social issues (e.g. excess commuting, economic and social inequality, congestion, etc.) (Xian and Crane, 2006). Due to these significant impacts, understanding urban environments and their spatio-temporal changes is essential for regional and local planning and environmental management. Remote sensing techniques provide an important means for understanding urban environments. With a synoptic view and repetitive coverage of a large geographic area,

---

[*] Portions of this chapter have been published in *Remote Sensing of Environment*, coauthored with Dr. Changshan Wu.

remotely sensed data have been applied extensively to analyze urban environments. Traditionally, remote sensing imagery has been employed to derive multi-temporal land use land cover (LULC) maps with numerous spectral, spatial, and con-textural analytical algorithms (Yuan and Bauer, 2007). In particular, the United States Geological Survey (USGS) has developed multi-temporal national land use land cover (NLCD) datasets with the help of Landsat Thematic Mapper (TM)/Enhanced Thematic Mapper Plus (ETM+) imagery (Yang et al., 2001). In addition to traditional land use land cover classification approaches, sub-pixel analysis has been developed following the vegetation – impervious surface – soil (V–I–S) model proposed by Ridd (1995). According to this conceptual framework, all land cover types (other than water) in an urban environment can be regarded as a combination of three basic biophysical components, namely vegetation, impervious surfaces, and soil. On this basis, two major categories of methods were developed to quantify biophysical compositions in an urban area. The first category is machine learning methods, including artificial neural network (ANN) (Flanagan and Civco, 2001; Mohapatra and Wu, 2007; Pu et al., 2008; Hu and Weng, 2009), regression/decision tree method (Yang et al., 2003a; Yang et al., 2003b; Xian and Crane, 2005; Yuan et al., 2008; Lu and Weng, 2009; Mohapatra and Wu, 2010), and regression modeling (Yang and Liu, 2005; Yang, 2006; Wu and Yuan, 2007; Mohapatra and Wu, 2010). With these machine learning methods, biophysical composition information is derived by establishing an empirical relationship with various spectral and spatial characteristics extracted from remote sensing imagery. The second category is spectral unmixing

techniques (Roberts et al., 1998; Small, 2001, 2005; Phinn et al., 2002; Rashed et al., 2003; Wu and Murray, 2003; Wu, 2004; Lu and Weng, 2004; Powell et al., 2007; Powell et al., 2008; Wu, 2009; Weng, 2012). Under the assumption that the spectrum of a pixel is a combination of the spectra of several typical homogeneous ground components, named endmembers (Adams et al., 1995; Roberts et al., 1998), the areal fractional coverage of each ground component can be derived from the spectral mixture analysis (SMA) approach.

Although both per-pixel and sub-pixel analyses have been employed for analyzing urban environments with different degrees of success, these methods are always considered as complicated, computationally intensive, and sometime subjective, especially when applied to a large geographic area (Plaza et al., 2004; Somers et al., 2011). Taking the sub-pixel analysis as an example, the success of machine learning algorithms relies heavily on the quality of training and testing data, and the selection of which might be relatively subjective during the process of model building and validation (Yang et al., 2003a). Further, although the SMA algorithms are physically based approaches and able to acquire sub-pixel endmember fractions effectively (Powell et al., 2007; Franke et al., 2009; Roberts et al., 2012), it is extremely difficult for practical users because of its complicated implementation process. Such difficulties lie mainly in technical problems including endmember selection and intra-class variability quantification, etc (Wu, 2009; Somers et al. 2011). One exception is the multiple endmember spectral mixture analysis (MESMA) method developed by Roberts and his colleagues (Powell et al., 2007; Franke et al., 2009; Roberts et al.,

2012), although it is also considered to be computationally intensive. When compared with per-pixel and sub-pixel image analyses, spectral indices have apparent advantages due to their easy implementation and convenience in practical applications. A number of indices, including normalized difference vegetation index (NDVI; Rouse et al., 1974), soil adjusted vegetation index (SAVI; Huete, 1988), normalized difference built-up index (NDBI; Zha et al., 2003), and normalized difference impervious surface index (NDISI; Xu, 2010), have been developed to quantify biophysical characteristics of the earth's surfaces (Jackson and Huete, 1991). Although these indices have shown effectiveness to some degree, when applied to urban environments, several problems still exist. The first problem is that most spectral indices are designed to highlight only one land cover type (e.g. vegetation and built-up area, etc.), and confusions among other land cover types, in particular impervious surfaces and bare soil, have not been successfully addressed. For instance, NDVI is designed for the signal enhancement of vegetation abundance, with which, however, impervious surfaces are always confused with bare soil. Moreover, although NDBI is intended to highlight built-up area, it cannot effectively differentiate built-up materials from barren soil (He et al., 2010). The second problem of spectral indices is associated with the limited applicability in remote sensing imagery at different spatial and spectral resolutions. Other than vegetation indices (i.e. NDVI and SAVI), all the aforementioned indices are unavailable for most high spatial resolution remote sensing imagery due to their dependence on shortwave infrared (SWIR) bands, which are not always included in high spatial resolution remotely sensed data (one exception is WorldView-2 imagery). Therefore, the

objectives of this paper consist of (1) proposing a biophysical composition index (BCI) for simple and convenient derivation of urban biophysical compositions for practical applications by enhancing contrast and separability among different biophysical compositions, and (2) exploring the potential of the applicability of BCI in various remotely sensed imagery at different spatial resolutions.

The remainder of this article is organized as follows. Section 3.2 introduces the study areas and data. Section 3.3 presents the methodology of the BCI development, including a reexamination of Tasseled Cap components and their representations in urban environment, the formulation of BCI index, and the assessment of BCI's ability of representing urban biophysical compositions. Results of applying the BCI with Landsat ETM+, IKONOS, and MODIS imagery are reported in Section 3.4, and comparative studies with other three indices, namely NDVI, NDBI, and NDISI, are detailed in Section 3.5. Further, discussions are provided in Section 3.6, and finally, this paper concludes in Section 3.7.

3.2 Study area and data

In this research, we selected two study areas, the town and village of Grafton, Wisconsin and the state of Wisconsin, USA, to analyze urban environments at different spatial resolutions. As an important constituent of the Midwest region in the United States, Wisconsin covers an area of 169,639 square km and has a population about 5.7 million. Dominant land use types of Wisconsin include agricultural, forest, grassland,

wetland, and urban land uses (Reese et al., 2002). Major cities in Wisconsin include Eau Claire and Superior in the northwest, Appleton, Green Bay and Oshkosh in the northeast, La Crosse and Madison in the southwest, and Milwaukee, Kenosha, Racine and Waukesha in the southeast. Among all regions, Southeast Wisconsin is the most populous region and important economic center of the state, where total employment, civilian labor force, population, number of households have increased around 10% to 20% per decade since 1980s (SEWRPC, 2004b; U.S. Census Bureau, 2010). It is also anticipated that this trend will continue in future decades (SEWRPC, 2004a, 2004b). Located at the northern suburb of the Milwaukee metropolitan area in Southeast Wisconsin, Grafton is an exurbia city and composed of the town and village of Grafton. According to the detailed land use data of Grafton in 2000, Grafton Town is mainly occupied by high- and medium-density residential, commercial, civic (government services, hospital and educational institutes) and industrial lands, while low-density residential, agricultural, and open lands dominate Grafton Village.
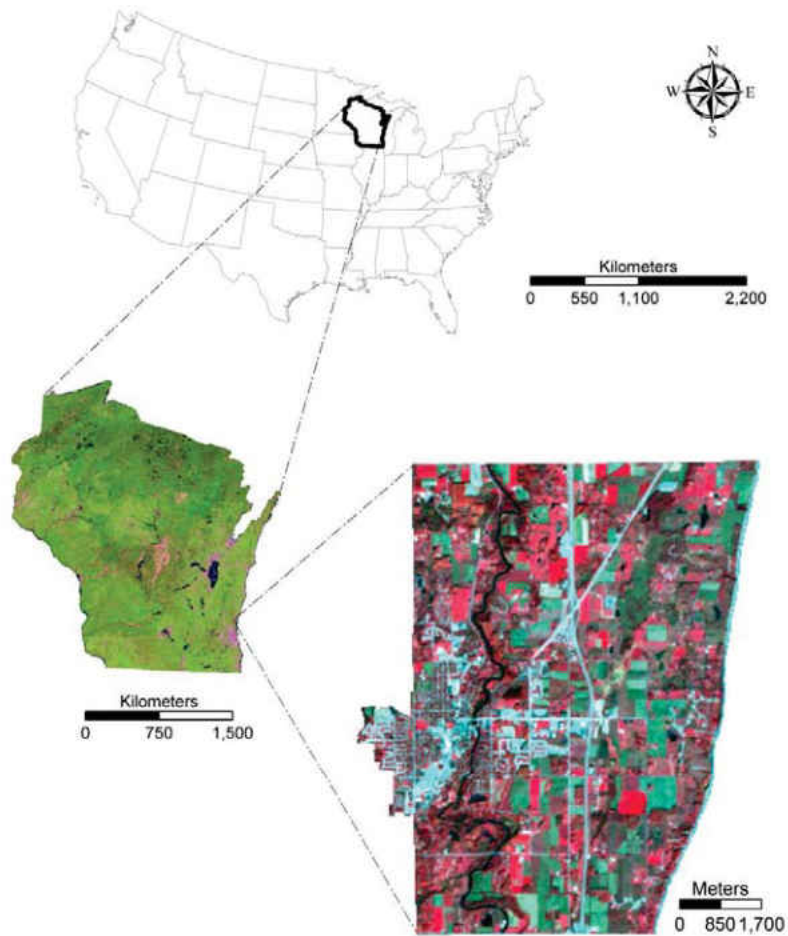
Figure 3.1 Study areas, Town and Village of Grafton and the state of Wisconsin, USA, illustrated in a false-color Landsat ETM+ image on Oct 16, 2002 and a true MODIS image, respectively.

In this research, we employed three categories of remote sensing imagery with different spatial and spectral resolutions, including a Landsat Enhanced Thematic Mapper Plus (ETM+) image with a spatial resolution of 30 meters, an IKONOS image with a resolution of 4 meters and a Moderate Resolution Imaging Spectroradiometer (MODIS) Nadir Bidirectional-reflectance-distribution-function (BRDF) Adjusted

surface Reflectance (NBAR) image with a resolution of 1 kilometer. The Landsat

ETM+ image was taken on Oct 16, 2002, and the IKONOS image was acquired on Sept

3, 2002.   No atmospheric correction was carried out for either image due to its small

geographical extent and the cloud-free atmospheric condition. The digital numbers

(DNs) of both images were converted to at-satellite reflectance according to sensor's

characteristics respectively (Markham and Barker, 1986; Irish, 2000; Taylor, 2009). In

addition, a MODIS NBAR image taken on August 21, 2001 was utilized (Schaaf et al.,

2002; Zhang et al., 2002; Zhang et al., 2003; Lobser and Cohen, 2007). For examining

the performance of the developed indices with the Landsat ETM+ and IKONOS

images, we obtained a Digital Orthophoto Quarter Quadrangle (DOQQ) image for the

Grafton area. This DOQQ was acquired in November, 2002 and has a spatial resolution

of 0.61 meter. Further, to assess the index performance applied to the MODIS imagery,

we obtained the 2001 National Land Cover Dataset (NLCD) land cover and

imperviousness percentage data. NLCD dataset has a spatial resolution of 30 meters, as

they were derived from Landsat TM/ETM+ images. Details of the 2001 NLCD data can

be referred to the works of Yang et al. (2003a), Yang et al. (2001) and Homer et al.

(2004). A Universal Transverse Mercator (UTM) projection with zone 16 and WGS84

datum was applied to all the remotely sensed data.

3.3 Methodology

3.3.1 Biophysical Composition Index (BCI): principle and development

In order to effectively represent major biophysical compositions in an urban environment, the BCI was designed to follow the mechanism of Ridd's conceptual V-I-S triangle model (see Figure 3.2). With the BCI, impervious surfaces are expected to have positive and relatively high values; vegetation is expected to be differentiated from other land covers through its negative and low values; and bare soil is expected to have a value of near zero, and can be separable from impervious surfaces. To reach this objective, we first conducted a reexamination of Tasseled Cap (TC) transformation and evaluated whether the BCI can be derived using TC components.
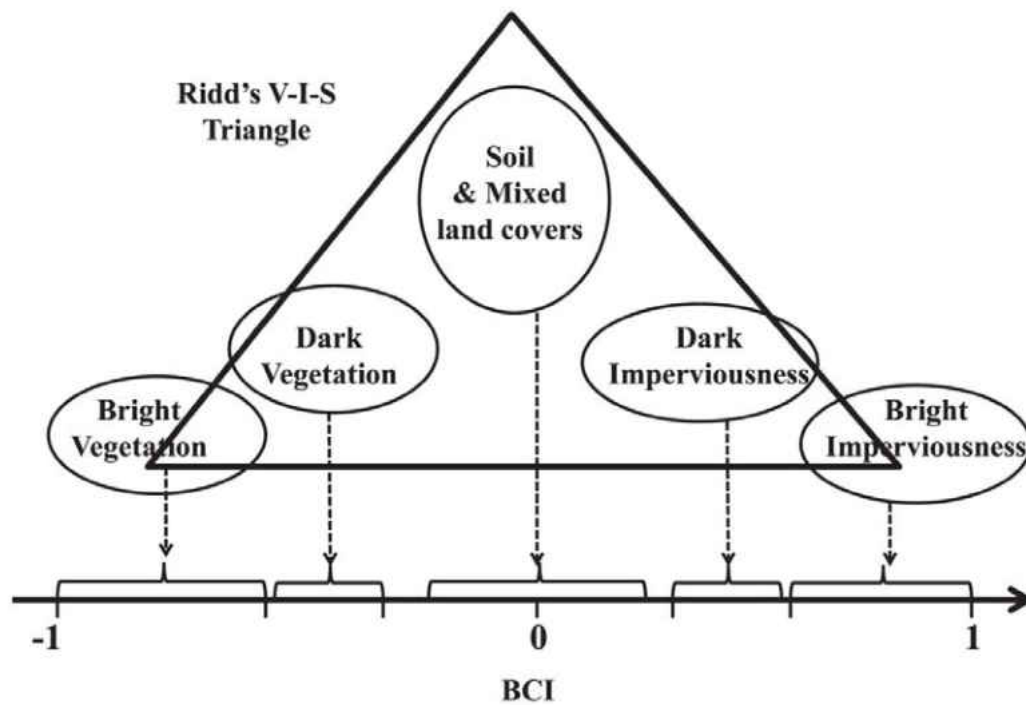
Figure 3.2 The scheme of BCI following Ridd's conceptual V-I-S triangle model.

Originally, TC transformation was developed by Kauth and Thomas (1976) to identify agricultural crop developments. Crist and Cicone (1984a; 1984b) pointed out that TC transformation was able to (1) quantify the inter-band relationships for interested land covers, (2) compress spectral information from multiple bands into fewer feature space scenes resembling principal component analysis, and (3) highlight spectral characteristics of different land cover types. Since then, TC transformation has been widely accepted and applied for forest management (Cohen et al., 1995; Helmer et al., 2000) and forest disturbance and recovery detection (Healey et al., 2005; Masek et al., 2008), etc. In urban remote sensing, TC components have been utilized as independent variables in various machine learning methods (e.g. regression model, regression tree, and ANN, etc.) for automatic imperviousness estimation (Bauer et al., 2004; Yang and Liu, 2005; Yang, 2006; Mohapatra and Wu, 2010). However, the TC transformation has rarely been applied for analyzing spectral signatures of biophysical compositions in an urban environment since its development. Therefore, in this paper, we attempted to examine the relationship between TC components and land cover types in an urban environment. More specifically, taking the most popular Landsat ETM+ imagery as an example, we performed a reexamination of spectral features of various typical urban biophysical compositions (e.g. water, vegetation, dark and bright impervious surfaces, and soil). For an objective comparison, all three TC components were normalized to the range of 0 to 1. Then, feature space scatterplots were generated using the first three TC components. In addition, samples of each typical biophysical

composition were selected and plotted in three feature space images, respectively (see

Figure 3.3).
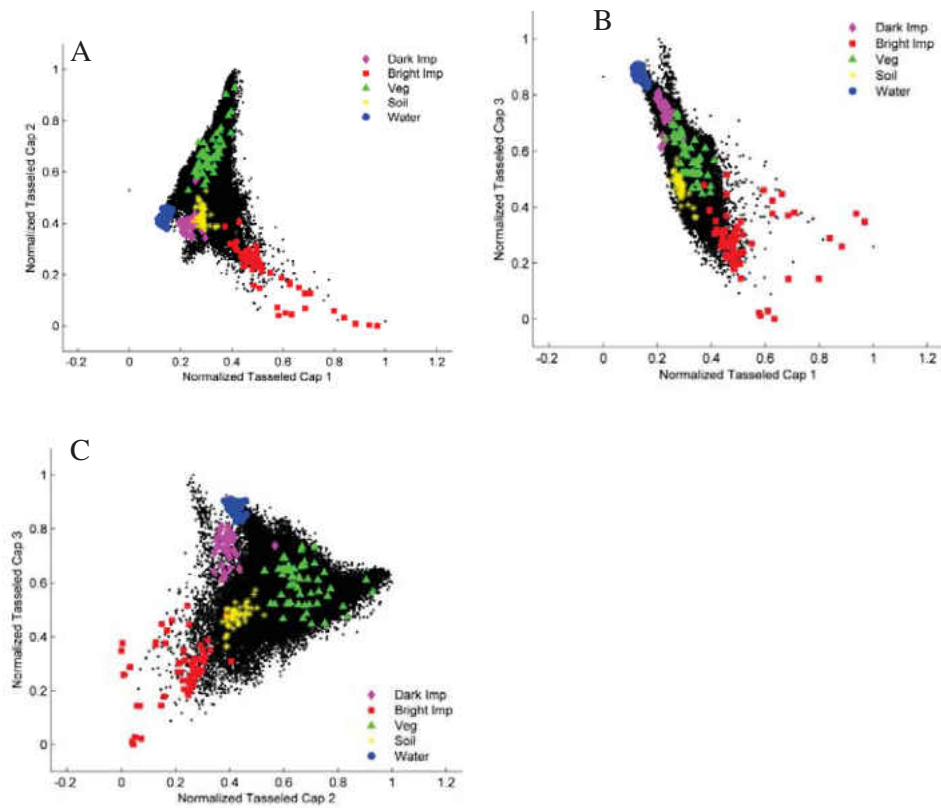
Figure 3.3 Feature space scatterplots of the first three normalized Tasseled Cap

components with typical urban biophysical compositions.

In the feature space of TC1 and TC2 (Figure 3.3A), vegetation, bright

imperviousness, and water and dark imperviousness occupies three vertices of the

spectral feature triangle respectively, while soil is clustered between bright and dark

imperviousness and is somewhat mixed with dark impervious surfaces. As shown in the

feature space scatterplot of TC1 and TC3 (Figure 3.3B), there exists an elongated strip

in which one end is occupied by bright imperviousness, the other by water and dark imperviousness, and vegetation and soil are located in the middle of the strip. In the feature space scatterplot of TC2 and TC3 (Figure 3.3C), the vertices of the spectral feature triangle are held respectively by vegetation, bright imperviousness, and water and dark imperviousness. Two noteworthy observations can be identified from these feature space scatterplots. First, TC1 and TC3 display a strong negative linear relationship by the elongated strip. To validate this observation, we also conducted a correlation analysis and found that a statistically significant and negative relationship exists between these two components, with a Pearson's R of -0.908. Second, a higher value of TC3 (generally termed "wetness") does not always correspond to higher water concentration as illustrated in Figure 3.3B. In rural areas, TC3 may be responsive to moist soil, vegetation or open water because there are very few manmade materials in natural environments. In contrast, in heterogeneous urban environments, high values in TC3 are also associated with low albedo impervious surfaces (e.g. asphalt in parking lots, roads, and roofs) and shadows. This confusion lies mainly in the spectral similarity between water and low-albedo materials (Small, 2001; Wu and Murray, 2003; Lu and Weng, 2004, 2006). Therefore, we suggest alternative terms to more appropriately capture the physical characteristics of TC components in an urban environment: TC1 as "high albedo", TC2 as "vegetation", and TC3 as "low albedo". Through this spectral analysis, TC1 and TC3 were proven closely related to impervious surfaces in an urban environment, and thus can be employed to assist in developing a biophysical composition index for delineating various urban biophysical compositions.

Two steps were performed in the pre-processing step of the BCI calculation. First, water pixels were identified and masked out using an unsupervised ISODATA classification. Second, after carrying out the TC transformation, each derived TC component was linearly normalized within the range of 0 and 1. For demonstration purpose, the Landsat ETM+ image for Grafton area was employed to derive normalized TC components of typical urban biophysical compositions as illustrated in Figure 3.4. With these normalized TC components, it is observed that bright impervious surfaces have a relatively high value in TC1; dark impervious surfaces are with a high value of TC3; and vegetation is associated with a high value of TC2. Moreover, when we observe the shape of the TC components 1-3, it appears that, for vegetation, the value of TC2 is much higher than the average value of TC1 and TC3, and forms a "peak". On the contrary, for both dark and bright impervious surfaces, the value of TC2 is much lower than the average value of TC1 and TC3, and therefore forms a "valley". In terms of soil, there is neither an evident "peak" nor "valley" as its value of TC2 is nearly equal to the average value of TC1 and TC3. Therefore, following the principles of designing the BCI, we developed the BCI using Eq. (3.1).

$$\text{BCI} = \frac{(H+L)/2 - V}{(H+L)/2 + V} \qquad (3.1)$$

where H is "high albedo", the normalized TC1; L is "low albedo", the normalized TC3; and V is "vegetation", the normalized TC2. These three factors can be given by following formula:

$$H = \frac{TC1 - TC1_{min}}{TC1_{max} - TC1_{min}} \qquad (3.2)$$

$$V = \frac{TC2 - TC2_{min}}{TC2_{max} - TC2_{min}} \tag{3.3}$$

$$L = \frac{TC3 - TC3_{min}}{TC3_{max} - TC3_{min}} \tag{3.4}$$

where TCi (i=1, 2, and 3) are the first three TC components; TCi_{min} and TCi_{max} are the minimum and maximum values of the i_{th} TC component, respectively.

Although originally developed for Landsat 5 MSS imagery (Kauth and Thomas, 1976), different forms of TC transformation have been proposed for a series of remote sensing sensors with various spatial and spectral resolutions, such as Landsat 7 ETM+, IKONOS and MODIS, etc. With respect to Landsat ETM+ images, TC components can be derived according to the coefficients suggested in the research of Huang et al. (2002) on the basis of principal component analysis (PCA). Similarly, based on the principle of linear affine transformation, specific coefficients for TC components for IKONOS and MODIS NBAR imagery were provided in the work of Horne (2003) and the studies of Zhang et al. (2002) and Zhang et al. (2003), respectively. Because TC transformation is available for remote sensing imagery at different spatial resolutions, BCI is therefore anticipated to be applied to imagery from various remote sensors with multiple resolutions.
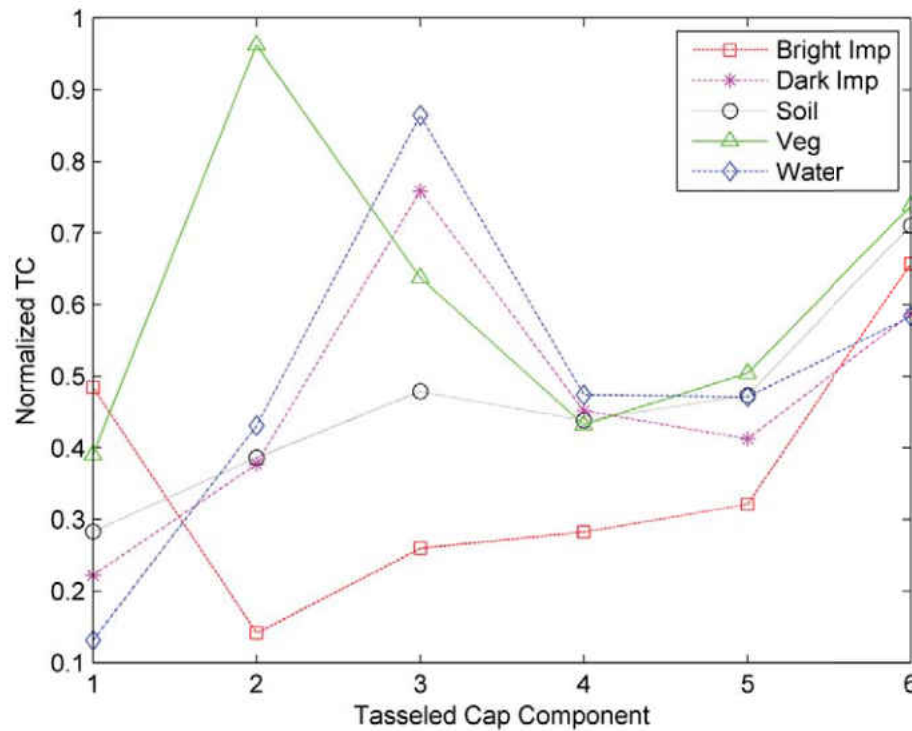
Figure 3.4 Normalized Tasseled Cap reflectance spectra of different urban biophysical compositions.

3.3.2. Examining the performance of BCI at different spatial resolutions

To assess the performance of BCI in representing various urban land covers in remote sensing imagery at different resolutions, correlation analyses were conducted to quantify the association between the proposed index and ground truth information (e.g. abundances of impervious surface and vegetation) with random sampling sets (see Table 3.1).

Table 3.1. Availability of indices for assessing impervious surface and vegetation abundance applied to remote sensing imagery at different spatial resolutions ("√": available, "×": unavailable or not applicable)

	Impervious surface fraction (%)			Vegetation fraction (%)		
	Landsat ETM+	IKONOS	MODIS	Landsat ETM+	IKONOS	MODIS
BCI	√	√	√	√	√	√
NDVI	√	√	√	√	√	√
NDBI	√	×	√	×	×	×
NDISI	√	×	√	×	×	×

3.3.2.1. Correlation analysis with impervious surfaces abundance

With remote sensing imagery at each spatial resolution, correlation analyses were first performed to examine the relationship between BCI and impervious surface abundance for sample pixels. For the Landsat ETM+ and IKONOS images, the DOQQ image was applied for deriving ground references. In order to guarantee enough samples containing impervious surfaces, a stratified random sampling method was applied to derive samples for urban and non-urban areas (Cochran, 1977; Stehman, 1996). Ground truth information of every sample was then obtained through visual interpretation and manual digitization from the DOQQ image. For the MODIS imagery, the stratified random sampling method was adopted as well. Due to its relatively large pixel size, it is extremely time consuming and labor intensive for

interpreting and digitizing land covers from the DOQQ image. Instead, the 2001 NLCD impervious surfaces product was employed as the ground reference.

3.3.2.2. Correlation analysis with vegetation abundance

Similarly, for each spatial scale, a correlation analysis was performed to explore the relationship between the BCI and vegetation abundance for sampling pixels. Note that the sampling method for actual impervious surface fraction cannot be utilized directly for vegetation due to apparent land cover changes in the one-month time lag between the Landsat ETM+ and IKONOS images and the DOQQ image. Careful visual examinations reveal that, during this time difference, major land cover changes in our study areas include changes from vegetation (e.g. various species of crops) to bare soil in cultivated land due to harvest, and also from bare soil to soil mixed with sparse vegetation in pasture land. Comparatively, land covers in urban area and other natural areas appear much more stable. Therefore, without including agricultural lands in the study areas, we generated all samples in non-agricultural lands to reduce the anthropogenic impacts on land cover changes. For the Landsat ETM+ and IKONOS images, subpixel ground-truth vegetation abundance was derived by manually digitizing the DOQQ image. In terms of the MODIS image, at first all land covers in the 2001 NLCD data were reclassified into three general categories, i.e. water, vegetated and non-vegetated lands, then the vegetation fraction in a MODIS pixel was calculated as the number of vegetated NLCD pixels divided by the total number of NLCD pixels falling within that MODIS sample pixel.

3.3.2.3. Separability between bare soil and impervious surfaces

Due to seasonal land cover changes and its inherent mixture with vegetation, bare soil cannot be accurately quantified from an aerial photograph (Wu, 2004). Thus, in this research we did not test the correlation between BCI value and bare soil abundance at the sub-pixel level. Alternatively, we investigated the separability between pure pixels of bare soil and impervious surfaces by visually examining their histograms and quantifying their separability using three measurements, the spectral discrimination index (SDI; Kaufman and Remer, 1994; Pereira, 1999), the Jeffries-Matusita distance (J-M distance; Swain and Davis, 1978) and the transformed divergence (TD; Swain and Davis, 1978; Mausel et al., 1990). SDI measures the degree of separation between the histograms of two land covers, especially emphasizing on the relative locations and spreads of two histograms. More specifically, the degree of separability between two classes depends on two factors, between-group variance and within-group variance. SDI can be calculated using Eq. (3.5).

$$SDI_{INDEX} = \frac{|\mu_i - \mu_s|}{\sigma_i + \sigma_s} \qquad (3.5)$$

where SDI_{INDEX} is the SDI value for a certain index, μ_i and μ_s are average index values of two classes (e.g. impervious surfaces and soil), σ_i and σ_s are standard deviations of a certain index for the two classes. For a particular index, SDI with a value greater than one indicates good separability between the two classes, while values less than one denote poor separability due to large overlaps. In addition to the SDI, the J-M Distance and TD are metrics measuring the ability of discriminating two

groups as well (Swain, 1978; Scott, 1997; Thomas et al., 1987). Specifically, the J-M

distance indicates the separability between two classes, with a value less than 1.00

indicating that the two classes are poorly separable. Further, if the J-M distance is

larger than 1.38, it indicates a high degree of separability, and if its value is between

1.00 and 1.38, it means the two classes are moderately separable (PCI, 1997; Thomas

et al., 1987). Similarly, a TD value greater than 1,900 indicates a high degree of

separation between two classes. With a TD value lying between 1,700 and 1,900, a

moderate separation is present. When it is less than 1,700, the two classes are

overlapped with each other and it indicates a poor separation (Jensen, 2005).

3.3.2.4 Comparative analysis with other indices

To evaluate the performance of BCI for delineating major biophysical

compositions in an urban environment, three other spectral indices, NDVI, NDBI and

NDISI, were employed for comparisons. Note that unlike BCI and NDVI, NDBI is only

available for remote sensing images with SWIR bands, and NDISI requires both SWIR

and thermal infrared (TIR) bands. These spectral indices were calculated according to

Eqs. (3.6), (3.7) and (3.8), respectively.

$$NDVI = \frac{NIR - RED}{NIR + RED} \tag{3.6}$$

$$NDBI = \frac{SWIR - NIR}{SWIR + NIR} \tag{3.7}$$

$$NDISI = \frac{TIR - (MNDWI + NIR + SWIR)/3}{TIR + (MNDWI + NIR + SWIR)/3} \tag{3.8}$$

with

$$MNDWI = \frac{GREEN - SWIR}{GREEN + SWIR} \tag{3.9}$$

where GREEN, RED, NIR, SWIR and TIR are the reflectance of green, red, near-infrared, shortwave infrared and thermal infrared spectral bands, respectively; and MNDWI is the modified normalized water index proposed by Xu (2006).

3.4 Results

With the Landsat ETM+ and IKONOS images for Grafton WI and the MODIS image for the State of Wisconsin, the resultant BCI images (see Figures 3.5, 3.6, and 3.7) were derived using Eq. (3.1). With these images, the relationships between BCI and impervious surfaces and vegetation abundances were examined using correlation analysis. In addition to the correlation coefficient (R), histograms and separability measurements were also employed to quantify the degree of separation between bare soil and impervious surfaces for Landsat ETM+ and IKONOS images. For the MODIS image, separation analysis was not performed due to the difficulty of identifying pure impervious surface pixels at the 1 km resolution.

3.4.1. Landsat ETM+BCI

With the Landsat ETM+ image, a Tasseled Cap transformation was conducted following the method of Huang et al. (2002), and then the BCI image was derived through applying Eq. (3.1). As illustrated in Fig. 3.5A, the resultant Landsat ETM+ BCI image indicates that bright impervious surfaces, including concrete roads and bright roofs (e.g. glass, metal, and plastic), have the highest and positive values, and are characterized as a white tone. Dark impervious surfaces, including asphalt roads,

parking lots, and dark roofs, have the second highest and positive values, and are indicated as a light grey tone. Further, soils and mixed land covers (including mixtures among vegetation and soil, vegetation and imperviousness, and all three major components) have a BCI value near to zero, and are shown with a tone of medium grey. Dark and bright vegetation, e.g. trees, senescent grasses and developing green grasses, etc., has the lowest and negative values (less than around -0.1), and is displayed as dark grey and black. To examine the overall trends of BCI quantitatively, a correlation analysis was performed, and a strong positive correlation between BCI values and impervious surface fractions was found (R = 0.757, $p \leq 0.01$) (see Table 3.2). Moreover, a significant and negative correlation (R = -0.842, $p \leq 0.01$) between BCI and vegetation fraction was also discerned. These results of correlation tests indicate that, with Landsat ETM+ imagery, the BCI can effectively extract both impervious surfaces and vegetation abundance information. Further, through visually examining the histograms of impervious surfaces and soil (Fig. 3.8A), we found that, with the BCI, the histogram of soil has a peak approximately -0.07, while the histogram of impervious surfaces has three small peaks for dark, medium, and bright impervious surfaces with BCI values of approximately 0.06, 0.11 and 0.19 respectively. Finally, all the three separation measures indicate that, among these four indices, impervious surfaces and bare soil can be moderately separated with BCI, as supported by high values of SDI (1.226, greater than 1), J-M Distance (1.090 out of 1.414), and TD (1,889 out of 2,000) (see Table 3.3).
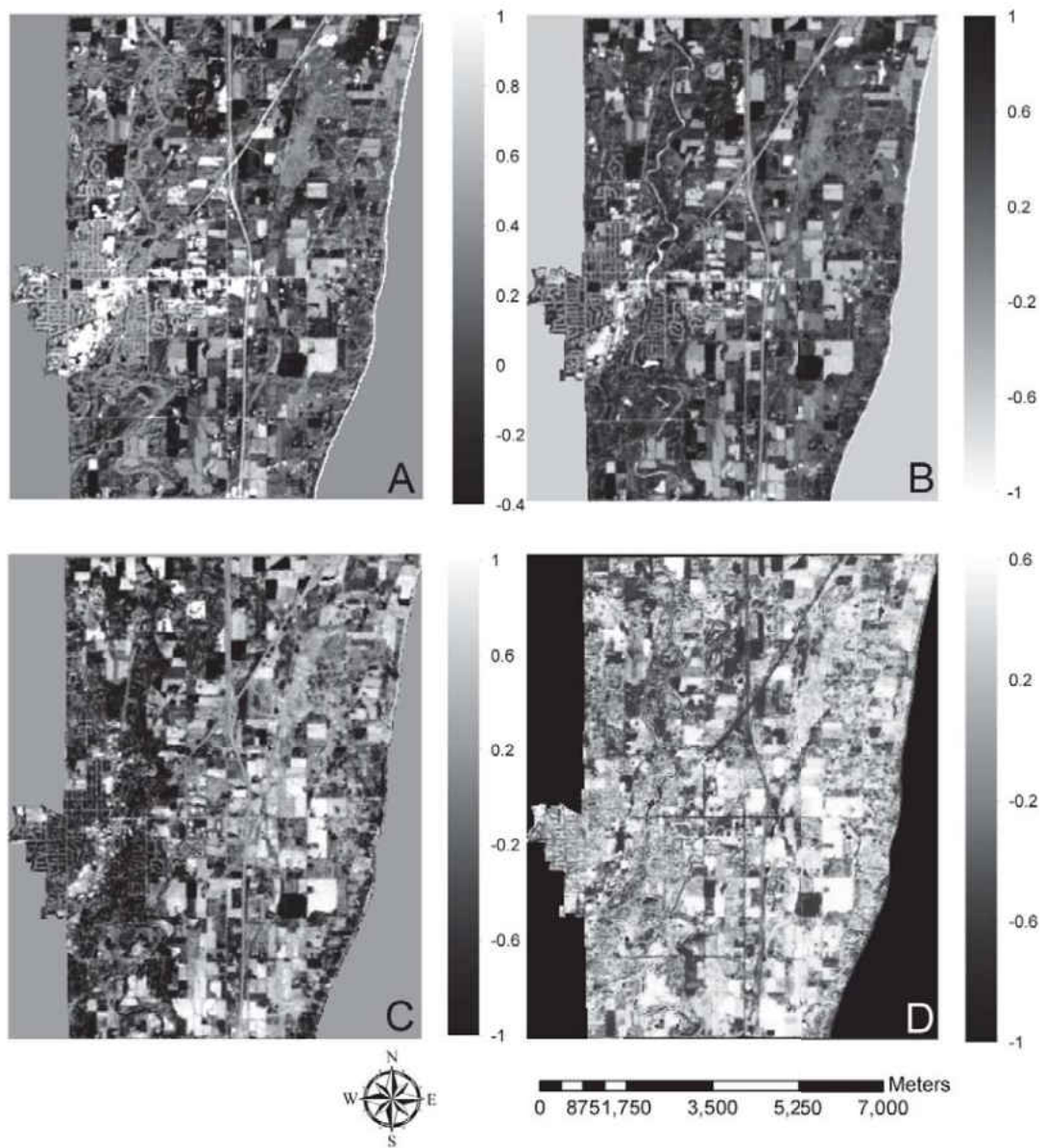
Figure 3.5 Comparisons of Landsat ETM+ indices: A) BCI, B) NDVI, C) NDBI, and D) NDISI.

76
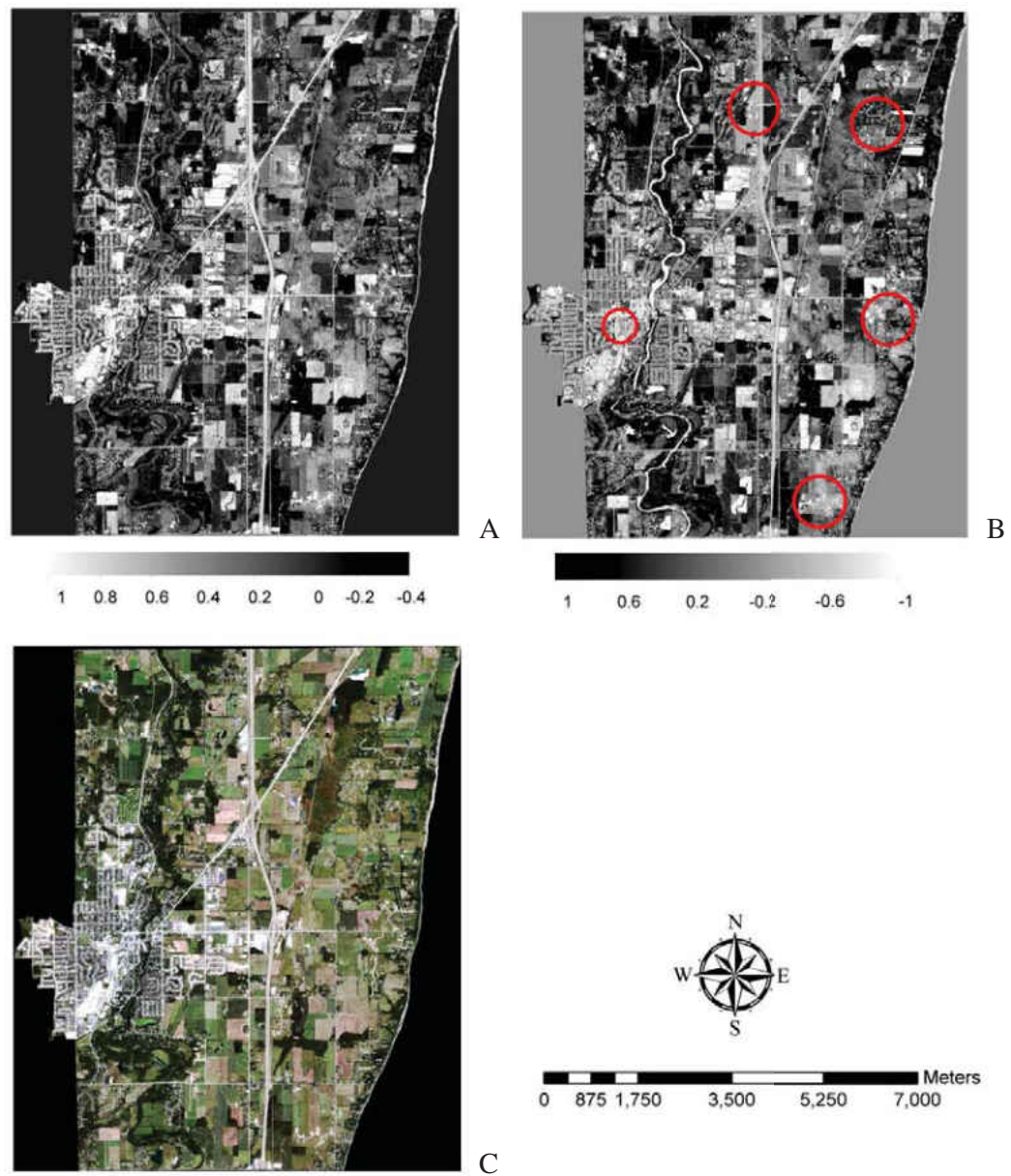
Figure 3.6 Comparisons of IKONOS indices: A) BCI, B) NDVI, and C) true-color

IKONOS image. Red circles indicate a few impervious surfaces visually confused

with soils when NDVI is applied.
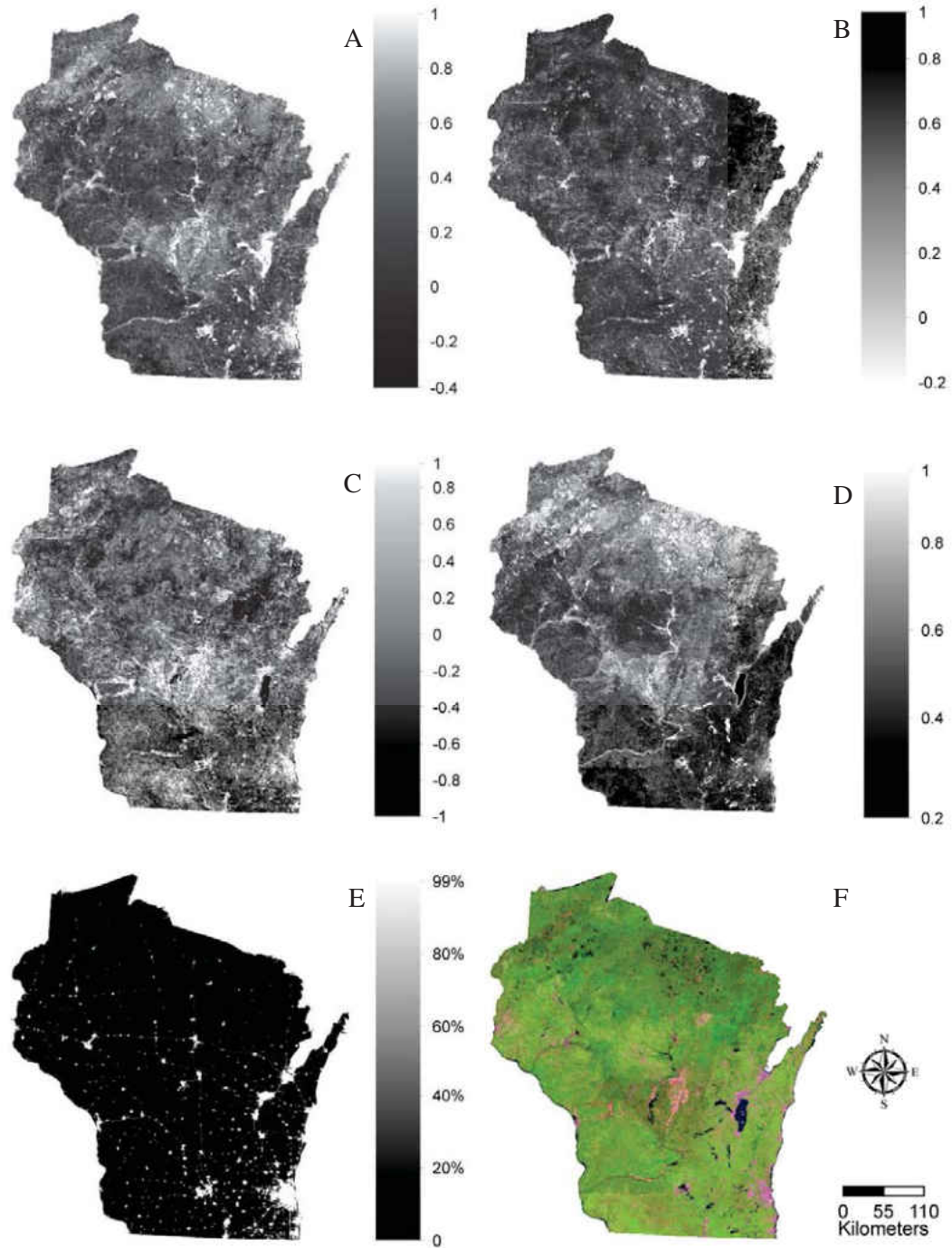
Figure 3.7 Comparisons of MODIS indices: A) BCI, B) NDVI, C) NDBI, D) NDISI, and E) the aggregated 2001 NLCD impervious surface image, F) true-color MODIS image.

Table 3.2. Correlation coefficients between different indices and impervious surfaces and vegetation abundance with remote sensing imagery at different spatial resolutions

	Landsat ETM+		IKONOS		MODIS	
	Imp (%)	Veg (%)	Imp (%)	Veg (%)	Imp (%)	Veg (%)
BCI	0.757**	-0.842**	0.848**	-0.889**	0.845**	-0.861**
NDVI	-0.682**	0.863**	-0.695**	0.816**	-0.853**	0.884**
NDBI	0.024	NA	NA	NA	0.745**	NA
NDISI	-0.419**	NA	NA	NA	0.451**	NA

** Correlation is significant at the 0.01 level

Table 3.3. Separability measures between impervious surfaces and soil with different indices

	Landsat ETM+			IKONOS		
	SDI	J-M Distance	Transformed Divergence	SDI	J-M Distance	Transformed Divergence
BCI	1.226*	1.090*	1889*	1.266*	1.051*	1140
NDVI	0.880	0.809	661	0.066	0.172	30
NDBI	0.500	0.573	397	NA	NA	NA
NDISI	0.721	0.883	1399	NA	NA	NA

*: moderate separability

3.4.2. IKONOS BCI

With the IKONOS image, a TC transformation was achieved following the method of Horne (2003), and the resultant BCI image was obtained (see Fig 3.6A). Similar to the results from the Landsat ETM+ image, bright and dark impervious surfaces are displayed as white tones, soil as light grey, mixed land covers as dark grey, and vegetation as black. Statistically significant correlations were found between BCI and impervious surface fraction ($R = 0.848$, $p \leq 0.01$) and between BCI and vegetation fraction ($R = -0.889$, $p \leq 0.01$). These results suggest that although more intra-class variation appears in the high resolution IKONOS image, BCI is very effective in identifying the physical characteristics of impervious surfaces and vegetation. Further, to examine the degree of separation, histograms of both bare soil and impervious surfaces were derived and separability measurements were calculated. As shown in Fig. 8B, the histograms of impervious surfaces and soil are separable, as indicated by small overlaps between their histograms. Moreover, high SDI value (1.266) and J-M Distance (1.051) indicate that impervious surfaces and bare soil are moderately separable. The TD measure (1,140), however, indicates these two land covers cannot be separated completely.

3.4.3. MODIS BCI

For the MODIS image, at first a TC transformation was carried out based on the methods of Zhang et al. (2002) and Zhang et al. (2003). In contrast to the Landsat ETM+ and IKONOS images, the 1 km by 1km pixel size of the MODIS image can hardly contain any pure pixels of impervious surfaces. The large amount of mixed land

covers in MODIS pixels makes it more difficult to represent and differentiate biophysical compositions than in any other higher resolution images. Therefore, only correlation analysis was performed for the MODIS image. The resultant MODIS BCI (see Figure 3.7A) indicates that major urban areas of Wisconsin are effectively highlighted in bright tones; bare soil and mixed land covers are represented by light and dark grey tones; and vegetation is displayed as dark tones. Further analysis indicates a statistically significant positive correlation between BCI and impervious surface fraction ($R = 0.845, p \leq 0.01$) and a statistically significant negative correlation between BCI and vegetation fraction ($R = -0.861, p \leq 0.01$) (see Table 3.3). Due to the difficulty of identifying pure impervious surface and bare soil pixels, we did not conduct a confusion analysis between these two compositions with the MODIS image.

3.5 Comparative analyses with other indices

With the purpose of examining the performance of the BCI index, comparative analyses with three other indices, including NDVI, NDBI, and NDISI indices, were performed at the three spatial resolutions (see Tables 3.1 and Figures 3.5, 3.6, and 3.7). Note that NDBI and NDISI cannot be calculated for the IKONOS image due to the absence of SWIR and TIR bands. Therefore, only NDVI was applied to the IKONOS image for comparison. Correlation analyses between index values and the ground-truthing fractional covers of two major biophysical compositions (i.e. impervious surface and vegetation) were performed and reported in Tables 3.2.

Besides, to evaluate the ability of different indices in separating impervious surfaces with bare soil, the histograms of these indices for both soil and impervious surfaces were plotted (see Figure 3.8). In addition, three separability measurements, i.e. SDI, the J-M Distance and TD, were employed to quantify the levels of separability between bare soil and impervious surfaces, and the results are reported in Table 3.3.

3.5.1. Comparisons with NDVI

NDVI images derived from the Landsat ETM+, IKONOS, and MODIS images are displayed in figures 3.5B, 3.6B, and 3.7B respectively. Note that due to the numerical range differences between NDVI and other three indices, a reverse color ramp was adopted for the NDVI maps in order to conduct consistent visual examinations and comparisons with other index maps. Analyses of the NDVI images indicate that there is a close relationship between NDVI and impervious surface fractions. With the derived NDVI images (Figures 3.5B, 3.6B, and 3.7B), impervious surfaces are displayed as bright tones (e.g. low values); bare soil and mixed land covers are illustrated as grey tones; and vegetation is shown as dark tones (e.g. high values). Moreover, correlation analyses indicate NDVI values are significantly and negatively correlated with impervious surface fractions, supported by a correlation coefficient of -0.682 for Landsat ETM+ image, -0.695 for IKONOS image, and -0.853 for MODIS image. This relation, however, is not as strong as the correlation between BCI and fractional impervious surface, in particular when applied to Landsat ETM+ and

IKONOS images. Similar correlation coefficients were found with the MODIS images, though.

A detailed analysis of the correlation between NDVI and impervious surface distribution indicates that the poorer performance is mostly due to the confusion between impervious surfaces and bare soil, especially for the Landsat ETM+ and IKONOS images. For example, with the IKONOS NDVI image (see Figure 3.6B), obvious spectral confusions between bare soil and impervious surfaces can be discerned when compared to the true-color IKONOS image. For example, tones of several soil patches are displayed much brighter than those of bright impervious surfaces, indicating that they possess lower NDVI values than imperviousness, and thus may be easily mis-classified as impervious surfaces. Moreover, a few impervious surfaces highlighted with the circles in Fig. 3.6B, e.g. some bright building roofs and concrete roads, are characterized at the gray tone and therefore visually confused with soil. On the contrary, these confusions cannot be discerned in the IKONOS BCI map (see Fig. 3.6A). As a further analysis, the NDVI histograms of impervious surfaces and bare soil (See Fig 3.8C and 3.8D) indicate that, unlike the BCI index, significant confusion exists between these two land cover types. Especially, the NDVI values for impervious surfaces and bare soil are similar, and their histograms have a wider range when compared to the BCI. This observation is supported by lower values of SDI (0.880 for Landsat ETM+ and 0.066 for IKONOS), J-M Distance (0.809 for Landsat ETM+ and 0.172 for IKONOS), and TD (661 for Landsat ETM+ and 30 for IKONOS). As a summary, NDVI image cannot effectively separate impervious surfaces and bare

soil with both the Landsat ETM+ and IKONOS images, and a much worse performance was observed when applied to the IKONOS image. This is probably due to small between-group variances for both classes and relatively large within-group variances with the IKONOS image. With the MODIS NDVI image, the confusions between bare soil and impervious surfaces are displayed in the central Wisconsin (with a great number of bare soil patches) and the north Wisconsin (bare soil mixed with wetlands) (see Figure 3.8B). Some of these confusion problems, however, are reduced due to the large pixel sizes of the MODIS image.

For vegetation, for all the three images, significant and negative correlations were found in BCI (see Table 3.2). In particular, for the Landsat ETM+ and MODIS images, the performances of BCI are slightly poorer than those of NDVI in identifying vegetation information. For the IKONOS image, though, the correlation coefficient between NDVI and vegetation abundance ($R = 0.816$, $p \leq 0.01$) is slightly lower than that (with absolute value) between BCI and vegetation fraction ($R = -0.889$, $p \leq 0.01$). As a summary, the performances of NDVI and BCI in identifying vegetation information are comparable at all three spatial scales.

3.5.2. *Comparisons with NDBI*

The NDBI images at two different spatial resolutions (e.g. Landsat ETM+ and MODIS) are illustrated in figures 3.5C and 3.5D respectively. With the Landsat ETM+ NDBI image, it is observed that there exists severe confusions between bare soil and impervious surfaces, as both of these two land covers are highlighted with bright tones.

Moreover, when the correlation analysis was conducted between NDBI and impervious surface fraction, it is found that NDBI has the lowest and statistically insignificant correlation coefficient ($R = 0.024$, $p = 0.76$), indicating NDBI cannot be employed to represent impervious surface information in the study area. This may be due to the severe spectral confusion between imperviousness and soil in the NDBI map. This assumption was supported by the histogram analyses of impervious surfaces and bare soil (see Figure 3.8E) and separability measures (see Table 3.3). Especially, visual comparisons of the NDBI histograms between impervious surfaces and soil reveal apparent overlaps (see Figure 3.8E). This observation is also confirmed by very low scores of SDI (0.500), J-M Distances (0.573), and TDs (397), falling far behind the values of BCI and NDVI.

With the MODIS NDBI image, we found that, although urban impervious surfaces can be identified with white tones, severe confusions between bare soil and imperviousness exist: light grey tone appeared in many parts of the state and bright tones shown in the central Wisconsin, where few urbanized areas can be found. Nevertheless, a significant and positive correlation between MODIS NDBI image and impervious surface fraction was found with a relatively lower correlation coefficient ($R = 0.745$) when compared to those of the BCI and NDVI.

3.5.3. *Comparisons with NDISI*

NDISI images at two different spatial resolutions (e.g. Landsat ETM+ and MODIS) are illustrated in figure 3.5D and 3.7D respectively. Similar to NDBI, the

Landsat ETM+ NDISI map does not reflect the proportion and distribution of impervious surfaces appropriately in the study area, and unexpectedly displays a negative correlation with impervious surfaces as shown in Table 3.2 (R = -0.419, p = 0.76). The major reason might be that NDISI is highly dependent on the temperature information derived from the TIR band, and there is no evident urban heat island (UHI) effect in such a lakefront area with small geographical extent. Moreover, breeze and vapors from Lake Michigan and the relatively dense vegetation coverage in Grafton area might also mitigate the impacts of temperature, thus offsetting the temperature impacts in the study area. Further, the severe confusion between bare soil and impervious surfaces is proven by the histogram analysis (see Figure 3.8F) and the separability measures (see Table 3.3). In particular, the NDISI has low SDI (0.721), J-M Distance (0.883), and TD (1399) values, indicating the confusion between bare soil and impervious surfaces. Such findings are not surprising, as it is consistent with the results reported by He et al. (2010).

Further, the performance of NDISI is unsatisfactorily when applied to the MODIS image. The confusion between bare soil and urban impervious surfaces is still a severe problem, as large soil patches in the Northern and Central Wisconsin have relatively high values of NDISI. As illustrated in Table 3.2, correlation analysis also supports these observations, as the correlation coefficient between NDISI and impervious surface fraction (R = 0.451) is much less than those of BCI and NDVI at the 0.01 significance level (BCI_R = 0.845 and NDVI_R = -0.853), indicating that NDISI

performs worse in identifying impervious surface information when compared to the BCI and NDVI.

3.6 Discussion

The major objective of developing the BCI index is to derive a simple and convenient spectral enhancement approach that can enhance the contrasts among three major urban biophysical compositions, namely vegetation, impervious surfaces, and soil, following Ridd's conceptual V–I–S model (Ridd, 1995). Analysis of results suggests that BCI has a significant and positive correlation with urban imperviousness, and a significant but negative association with vegetation fraction at various resolutions. More importantly, BCI showed promise in discriminating bare soil from impervious surfaces, which has proven to be a difficult problem (Powell et al., 2007; Roberts et al., 2012). Another advantage of BCI is that it can be applied to various remote sensing images at different spectral and spatial resolutions, as the derivation of BCI does not depend heavily on any specific waveband as other spectral indices (e.g. NDVI, and NDISI, etc).

On the other hand, although the separability metrics suggest that BCI can moderately separate soil from impervious surfaces, we admittedly notice the lack of a rigorous validation of soil abundance due to the difficulty of deriving "ground truth" soil fractions in the study area. Further research on examining the power of BCI on differentiating soil from impervious surfaces is necessary. Moreover, although BCI performs slightly better when compared to a number of similar indices (e.g. NDVI,

NDBI, and NDISI), its correlation with "ground truth" imperviousness is likely to be lower when compared to the results reported in other SMA studies (Powell et al., 2007; Weng and Hu, 2008; Weng et al., 2008; Hu and Weng, 2009; Roberts et al., 2012). In particular, Powell et al. (2007) reported much higher r^2 values for imperviousness (0.849) and vegetation fraction (0.850), although with a larger sample size. Roberts et al. (2012) also reported higher r^2 values for imperviousness (0.718) and vegetation fraction (0.808) at 60-meter resolution, and for imperviousness (0.53) and vegetation fraction (0.82) at 15-meter resolution with the MESMA method, respectively. The relatively poorer performance of BCI is not unexpected when compared with physically SMA methods, as it is a spectral enhancement approach without *a priori* knowledge of the study area. Moreover, unlike the comparisons between reference and estimated abundances of imperviousness reported in other studies, BCI does not have a one-to-one correspondence to the impervious surface fraction, as the value of BCI ranges from -1 to +1, which is different from the abundances of dark and bright impervious surfaces derived from MESMA (with range between 0 and 1). Therefore, BCI may serve as a convenient spectral enhancement method, rather than an approach to the estimation of fractional imperviousness or vegetation.

The development of BCI is mainly dependent on spectral signatures of the normalized TC spectra, the idea of which is similar to another forestry index, the normalized difference fraction index (NDFI), for the enhancement of deforestation detection (Souza et al., 2005). With respect to NDFI, three fractional ground components obtained from MESMA, i.e. shade-normalized green vegetation (GV),

nonphotosynthetic vegetation (NPV) and soil (although with different direction and weights when compared with BCI), were taken into consideration. Both indices have proven to characterize land covers effectively: detection of deforestation levels with NDFI, and urban land cover compositions with BCI. Specifically, higher values of NDFI indicate higher level of vegetation preservation, whereas lower ones highlight degraded forests. Comparatively, BCI values from low to high represent vegetation (negative values), bare soil (near zero), and impervious surfaces (positive values) respectively, with transitional/mixed land covers in between.

3.7 Conclusions

Biophysical composition information is critical to delineate urban ecological morphology for sustainable public planning and environmental management and modeling. However, traditional methods to acquire biophysical composition information, such as land use land cover classification approach and spectral unmixing technique, were either dependent on subjective training and testing datasets, or too complicated to carry out (Plaza et al., 2004). Therefore, this study proposes a new BCI index for simple and convenient derivation of urban biophysical compositions following Ridd's conceptual V-I-S triangle model.

As the first step of BCI development, we performed a reexamination of TC transformation to explore the change of spectral feature space due to the composition change in an urban environment. Through spectral analysis, it is found that, in a heterogeneous urban environment, high values of TC3 are associated not only with

water content and soil moisture but also with low-albedo impervious surfaces and shades, probably due to their inherent spectral similarity. This observation is also confirmed by a statistically significant negative linear relationship between TC1 and TC3, where TC1 is generally utilized to characterize the "brightness" of land covers. Accordingly, alternative terms are suggested to capture the physical characteristics of urban land covers with TC components more appropriately: the original "brightness", "greeness" and "wetness" replaced by "high albedo", "vegetation", and "low albedo" respectively. Thus, TC1 and TC3 are believed to contain abundant imperviousness information in an urban environment, and can be utilized for developing the BCI index. With the observed spectral relationships and features from the reexaminations, we developed a new spectral index named BCI to identify different urban biophysical compositions and improve the separation between impervious surface and bare soil.

Analyses of the BCI images at three different spatial resolutions (e.g. Landsat ETM+, IKONOS, and MODIS) suggest three major conclusions. First, results of correlation analysis indicate that, when compared to other widely used indices (e.g. NDVI, NDBI, and NDISI), BCI has the closest relationship with impervious surface abundance, with statistically significant and highest correlation coefficients at all three spatial resolutions. Specifically, NDVI has slightly lower correlation coefficients, and NDBI and NDISI have the poorest performances in identifying urban impervious surfaces. Further, the performances of BCI in quantifying vegetation abundance are comparable with NDVI at all three spatial scales. Finally, with much higher values of

separability metrics than any other index, BCI was shown to be the most effective index

of the four evaluated for separating impervious surfaces and bare soil.

CHAPTER 4 IMPROVING SMALL-AREA POPULATION ESTIMATION: AN INTEGRATED GEOGRAPHIC AND DEMOGRAPHIC APPROACH[*]

4.1. Introduction

Knowledge of detailed and accurate population information is important to understand many socio-economic, political, and environmental problems, and to support necessary planning practices for both public agencies and private sectors (Rees, Norman and Brown, 2004). As an example, accurate population estimates are critical for deriving diagnostic indicators, such as mortality rate, morbidity rate, unemployment rate, etc, which play essential roles in the decision making process for state and local governments (Smith et al., 2002). Moreover, population information has served as an important input in socio-economic studies and planning practices (Plane and Rogerson, 1994), including location and allocation analyses of critical facilities (Sathe and Miller-Hooks, 2005; Horner and Downs, 2010; Widener and Horner, 2011; Maliszewski et al., 2012), health-care planning and analysis (Martin and William 1992; Bikker and de Vos, 1992; Birkin et al., 1996), natural resource management and assessment (Keeley et al., 1999; Underwood et al., 2008; Kwak et al., 2011), risk assessment in public health (Kwan-Gett et al., 2009; Reid et al. 2009;

---

[*] Portions of this chapter have been published in *Annals of the American Association of Geographers*, coauthored with Dr. Changshan Wu.

Wilhelmi and Hayden, 2010), environment inequality analysis (Mennis, 2002; Fielding, 2007; Maantay and Maroko, 2009; Mennis, 2011), disaster response and relief management (Bouwer et al., 2007; Stone et al., 2007), urban expansion modeling (Wu and Martin, 2002; Yeh and Li, 2002), election analysis (Norman et al., 2007), and public transit service planning (Murray et al., 1998; Horner and Murray, 2004; Wu and Murray, 2005). For private sectors, detailed and timely updated population information is vital for delineating the external environment of a marketplace, determining trade area, evaluating retail trading performances (such as trade area analysis, market loss assessment, site evaluation, etc.), selecting potential store locations, predicting retail sales per capita, assessing market shares, and forecasting potential customer groups, etc. (Epstein, 1984; Mercurio, 1984; Simmons, 1984; Wilson, 1984; Ghosh and McLafferty, 1987; England, 2000; Church and Murray, 2009). Therefore, it is essential to derive accurate and timely population information to satisfy the apparent needs from public agencies and private sectors.

Although detailed population information is important in a number of planning applications, such data are generally available only (in the U.S.) once for every decade through the National Census. Obsolete population data, however, cannot satisfy the needs of urban and regional planning and business analyses, especially for rapidly growing areas. For planning practices, the utilization of inaccurate census data could result in an imbalanced distribution of public resources. Similarly, for private sectors, investment loss may be partly due to the usage of obsolete population information for market delineation, prediction, assessment, and decision making.

Recognizing the importance of timely population information, researchers have proposed many techniques to derive population estimates for non-census years, and these techniques can be divided into two major groups: demographic and geographic techniques.

Major demographic techniques include Component II (CM-II), Administrative Records (AR), Ratio Correlation (RC), and Housing Unit (HU) methods (Ghosh and Rao, 1994). The CM-II method estimates the change of population count based on major demographic changes. The population count for a particular year is calculated by adding the total births and net migration at all ages, and subtracting the estimated number of deaths to the population totals at the base year (Smith and Mandell, 1984). Similarly to CM-II method, the AR method estimates the net migration of population under 65 years old using the federal income tax form, and the population aged 65 and above using the federal Medicare enrollment information (Plane and Rogerson, 1994). The RC method builds the relationship between a change share and different types of symptomatic variables (i.e. representing school enrollment, auto registration, and ratio of resident births/death, etc), and utilizes this relationship to adjust the population estimates (Martin and Serow, 1978). Instead of detecting population change by various demographic variable changes, the HU method estimates the population for a spatial unit by multiplying the number of housing units, estimated from electric or water bills or building permits, by the persons per household (PPH), estimated from census data or by demographic modeling, then adding up their product with the group quarters population (e.g. persons residing in college dormitories, military barracks,

nursing homes, and prisons). Unlike CM-II, AR and RC methods, the HU method has been accepted by the U.S. Census Bureau for last two decades as its only method to yield small-area population estimation. Moreover, it is considered to be the most commonly used, and one of the most accurate and cost-effective methods, for small-area population estimation (Smith and Mandell, 1984; U.S. Census Bureau, 1998, 2005, 2010; Smith and Cody, 2004).

Besides demographic approaches, geographic techniques have also been applied since the 1950s for deriving population estimates. In particular, not only by demographers, the HU method was also adopted by remote sensing specialists to estimate population information with housing unit counts produced manually from aerial photographs (Hsu, 1971, 1973; Lo and Chan, 1980; Watkins, 1984; Watkins and Morrow-Jones, 1985; Lo, 1986a, 1986b). Then the total population in an area is derived as the product of housing unit counts and the average PPH obtained through a special survey. While this method is relatively accurate, such an approach is time consuming and labor intensive, therefore rarely used for large urban areas. To address the problems associated with manual enumeration of individual housing units, automatic approaches with the help of remote sensing and geographic information system (GIS) techniques have been developed (Hsu, 1971; Lo, 1995, 2003). Remote sensing information employed for generating housing unit and population estimates includes spectral radiance/reflectance, land use/cover classification, urban impervious surface and vegetation distribution, light radiance, etc. (Collins and El-Beik, 1971; Dueker and Horton, 1971; Kraus et al., 1974; Lo, 1995; Chen, 2002; Harvey, 2002a;

Lo 2003; Wu and Murray, 2007; Deng et al., 2010; Sutton et al. 1997). In addition, geographic information, such as transportation network density (Qiu et al., 2003), point-based postal data (Mesev, 2005, 2007), etc., has been applied to represent built environment and population distribution. With remote sensing and geographic information, regression-based techniques have been typically applied to estimate population information (Harvey, 2002b; Lo, 2003; Wu and Murray, 2007).

Although both demographic and geographic approaches have been developed for small-area population estimation, the resultant estimates of both methods were still unable to satisfy the demand for detailed and accurate population estimation. With the demographic approaches, only population at aggregated scales, such as county, city, etc., can be obtained due to data constraints and privacy concerns. Although several simple interpolation and step-down techniques have been employed to derive population estimates at the census block or block group levels, the resultant estimates, however, are unreliable and imprecise (Deng et al., 2010). With remote sensing based approaches, parameters extracted from images only have an indirect linkage to the built environment, and the spatial resolutions of remote sensing images are often too coarse to reveal information of individual housing units. As a result, the estimated population counts for small areas are always inaccurate, and cannot be utilized to estimate inter-census population information.

Although both demographic and geographical approaches have their respective limitations in estimating small-area population, a synthesis of these two

methods may provide a viable solution. A potential solution may resort to the HU method, which provides a linkage between demographic and geographic methods. In particular, the recent rapid development of GIS and remote sensing technologies, such as detailed land use and parcel dataset, and very high resolution remote sensing imagery with a meter-level resolution, provides an opportunity to improve the estimation accuracy of the number of housing units, one of the major components of the HU method. Estimation of the other primary component of the HU method, persons per household (PPH), may be benefited by remote sensing/GIS techniques as well. Currently, PPH was only estimated through simplified methods, such as the usage of PPH from the most recent census, the simple mathematic extrapolation (i.e. linear and exponential extrapolation and proportional change rate) (Starsinic and Zitter, 1968; Smith and Lewis, 1980; Smith 1986; Swanson and Hough, 2012), or regression analysis (Smith et al. 2002; Kimpel and Lowe 2007; Deng, Wu and Wang 2010). The difficulty of obtaining an accurate PPH estimation may be associated with the small sample sizes (Ghosh and Rao, 1994). Moreover, as a demographic parameter and an "invisible" factor on images, it is difficult to attract the attention and interest of remote sensing specialists and geographers, whose major focus is on "visible" dwelling unit counts from remotely sensed imagery. PPH estimation has rarely been conducted by any geography-related means because there is a lack of an effective connection between PPH and geographic measurements. Factors affecting PPH include age structure (Smith et al., 2002), living arrangements (Kobrin, 1976), housing stock characteristics (Myers and Doyle, 1990), and marital status (Gober,

1990). Among these factors, from a geographical perspective, distance to certain activities may indirectly reflect behavioral preferences and demographic specialization of different households' marital and income status. For example, singles and married couples without children may emphasize entertainment and cultural activities, while married couples with children may prefer family-centered activities, etc. Therefore, it is very necessary to improve the PPH estimation with a combination of remote sensing/GIS techniques and demographic approaches.

To implement small-area population estimation with the HU method, we developed an automated technique for counting dwelling units through combining high resolution impervious surface information, parcel data, and land use data. Further, the persons per household (PPH) was estimated through modeling the relationship between PPH and housing structural information and household socio-economic status. With the estimated HU numbers, PPH and population, we examined the estimation accuracy with three measurementsindices: mean absolute error (MAE), mean absolute percentage error (MAPE), and mean algebraic percentage error (MALPE), and compared this integrated approach with other widely applied methods. Further, we also performed sensitivity analyses to evaluate the respective contributions of HU and PPH estimation errors to the small-area population estimation errors.

The remainder of this article is organized as follows. The study area and data are introduced in Section 4.2. Section 4.3 describes the proposed methods for

estimating dwelling units and PPH respectively. Section 4.4 presents the results of estimation and estimation accuracy. Section 4.5 details the comparisons between different techniques for HU, PPH, and population estimation. Sensitivity analyses are reported in the sixth section, and finally the last section concludes this article.

4.2 Study Area and Data

The Town and Village of Grafton, Wisconsin, USA were chosen as the study area for this research (see Figure 4.1). Located about 30 kilometers north to the Milwaukee City, Wisconsin, Grafton is an exurban area in the Milwaukee metropolitan area. The Town of Grafton is located at the western side of the study area, and its land use types are dominated by residential, commercial, civic (hospital, government services and educational institutes), and industrial lands. Grafton Village occupies the rest of Grafton area, and its land uses are dominated by agricultural, residential and other natural lands. According to the US Census Bureau, population and housing unit (HU) numbers in Grafton have increased steadily, with the total population growing from 13,330 in 1990 to 14,444 in 2000, and the number of housing units rising from 4,827 in 1990 to 5,773 in 2000. This is likely due to the emigration from the Milwaukee County during the past decades. Such a growth trend has been projected to continue in the coming decades (Southeast Wisconsin Regional Planning Commission 2004). Therefore, an accurate estimation of small-area population is of great importance for planning practices in both the Ozaukee County and Southeast Wisconsin.
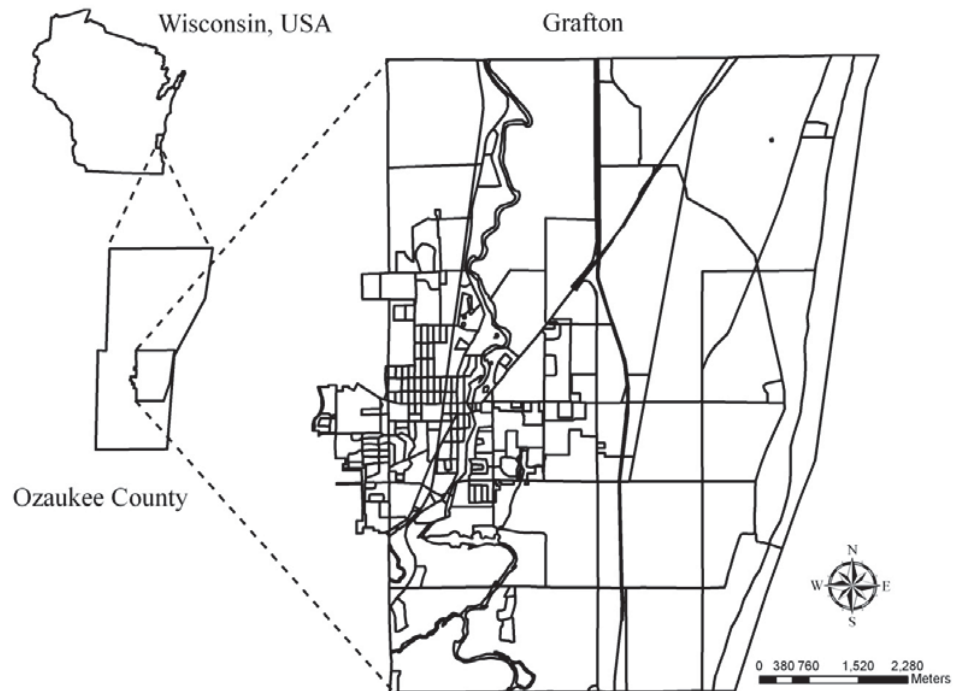
Figure 4.1 Town and Village of Grafton, Wisconsin, USA.

For model calibration and validation, population data in 2000 at the census block level were extracted from the American FactFinder provided by the U.S. Census Bureau. For each census block, housing unit counts, population and demographic information (e.g. age structure, racial composition, median income, gender, etc.) were provided. In addition to population data, parcel data (with 6,378 individual parcels) in 1998 was obtained from the Ozaukee County Land Information Office (see Figure 4.2A). Further, detailed land use data in 2000 (see Figure 4.2B) were acquired from the

Southeast Wisconsin Regional Planning Commission. In particular, detailed land use

information was classified based on the Anderson classification system (Anderson et

al., 1976). Besides GIS datasets, an IKONOS image taken on 3 September 2002 was

requested from the American geographical society library (AGSL) at the University of

Wisconsin-Milwaukee. Digital number of each pixel in IKONOS image was converted

to per pixel reflectance according to the IKONOS technical document (Taylor, 2009).

For accuracy assessment of impervious surface estimation, a Digital Orthophoto

Quarter Quadrangle (DOQQ) image acquired in November 2002 was obtained from the

AGSL as well. All these images were re-projected to the Universal Transverse

Mercator projection with zone 16 and WGS84 datum. In order to mitigate the impacts

of time differences between land use data and remotely sensed image, the newly-built

housing units after 2000 were not taken into account, therefore impervious surfaces

located outside the residential land use of the 2000 SEWRPC data were ignored.

4.3. Methodology

4.3.1 Housing unit estimation

We developed an automatic approach to estimate the number of housing units

through integrating detailed remotely sensed and geographic information. In this

integrated HU method, three major steps were carried out. First, detailed remote

sensing information and GIS datasets were processed based on the raw datasets.

Secondly, residential land use parcels, including single-, two-, and multi-family

residential types, were derived through integrating the parcel data, land use data, and high-resolution remotely sensed imagery. Finally, the numbers of single- and two-family housing units were enumerated automatically, and the number of multi-family housing units was estimated using a dasymetric mapping approach. The total number of housing units in a census block was then calculated as the summation of single-, two-, and multi-family housing units.

4.3.1.1 Data process of detailed remotely sensed and GIS datasets

One important parameter derived from the high-resolution remotely sensed imagery is the impervious surface distribution. Impervious surfaces refer to any materials that water cannot penetrate. In urban areas, most impervious surfaces are associated with urban infrastructure, such as rooftops, driveways, parking lots, road networks, and bridges, etc. (Schueler, 1994; Bauer et al., 2004). Urban impervious surface information, therefore, may help in identifying housing units in a land parcel. In this research, we extracted urban impervious surface information from IKONOS imagery using a constrained spectral mixture analysis (SMA) method developed by Wu (2009). SMA has been widely used for impervious surface estimation (Phinn et al., 2002; Rashed et al., 2001; Small, 2001; Wu and Murray 2003; Wu, 2004). As a physically based method, SMA assumes that reflectance of each pixel is a linear combination of several homogeneous land cover types (also called endmembers), which can be described as follows.

$$R_b = \sum_{i=1}^{N} f_i R_{i,b} + e_b \qquad (4.1)$$

where $\sum_{i=1}^{n} f_i = 1 \; and \; f_i \geq 0$; n is the number of endmembers; R_b is the reflectance

for each band b of the remotely sensed image; N is the total number of endmembers; f_i is

the fraction of endmember i; $R_{i,b}$ is the reflectance of endmember i in band b; and e_b is

residual of model.

In this study, impervious surface fraction for each pixel was derived with the

following steps. First, spectral normalization was applied to the IKONOS image to

reduce the shadow effect and spectral variations. Second, three endmembers, including

vegetation, soil, and impervious surfaces, were selected according to the scatterplots of

the minimum noise fraction (MNF) components. Finally, a fully constrained SMA was

applied to obtain the fraction of each endmember. The result of impervious surface

fraction for the study area is shown in Figure 2C. Accuracy assessments were carried

out by digitizing the DOQ image as the reference. The accuracy of impervious surface

estimation for the entire study area is relatively high, with a small systematic error

(2.66%) and mean absolute error (9.2%). For more details of this method, readers can

refer to the work of Wu (2009).
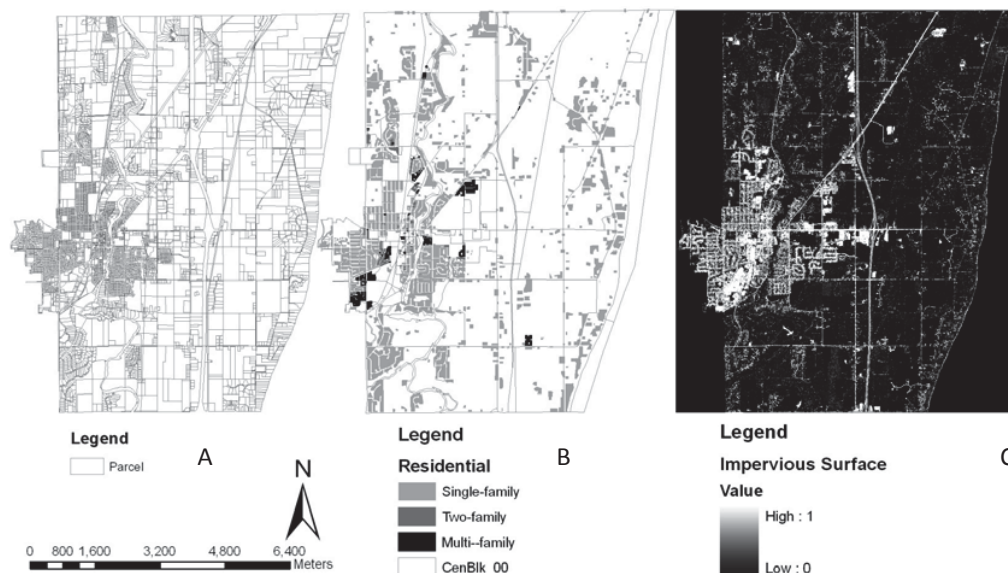
Figure 4.2 Detailed remote sensing and GIS datasets in study area: A) parcel map; B)

residential land use map; and C) impervious surface fraction map. "CenBlk_00"

stands for census block in 2000.

In addition to the high resolution impervious surface fraction data, detailed residential land use data was derived from the land use data in 2000 provided by SEWRPC. Three residential land use types, single-family, two-family, and multi-family residential, were identified and extracted for further analysis (see Figure 4.2B). For parcel data, the perimeter and area of each parcel were calculated, and employed as the inputs to the housing unit estimation models.

4.3.1.2 Generation of residential parcel data

For deriving the number of housing units, at first we overlaid the parcel layer with the land use map to generate residential parcels. These residential parcels, however, have two problems. The first problem is associated with the land use data. In

a few cases, although a parcel is designated as the residential land use type, it is essentially occupied by vacant lands and the actual construction project may start up to several years later. One example is displayed in Figure 4.3. The other problem is associated with spatial data overlay method. Many very small polygons (e.g. slivers) were present along shared boundary lines of the parcel and land use maps. This problem is likely due to digitizing and data interpretation errors. To address these problems, we developed a classification tree approach to remove these mis-classified parcels using MATLAB^{TM} (The MathWorks, Inc.). The classification tree model constructs the relationships between a categorical dependent variable (e.g. whether a parcel is classified as the residential land use type) and a number of independent variables (e.g. impervious surface fraction, parcel perimeter, parcel area). It grows a categorical tree by splitting the data repeatedly according to the interactions between the dependent variable and independent variables (Breiman et al., 1984). For each time of splitting, the data is categorized into more homogeneous groups through uncovering the structure of the underlying problems. As a non-parametric approach, classification tree does not require the assumptions of normality and independence.

Figure 4.3 Overlay of residential parcels with impervious surface fraction map

(parcels within green boxes are those with low impervious surface coverage, and

should be re-classified as non-residential).

In this study, around 20 percent of the parcels were employed as training samples for the classification tree approach. Independent variables include the derived impervious surface fraction within each parcel, and parcel areas and perimeters. It is assumed that a parcel with a higher percentage of impervious surfaces is likely to be considered as residential land uses. Parcels with a relatively low impervious surface fraction may not have been fully developed, and should be removed from the residential class. Moreover, parcels with abnormal perimeters or geographical areas may be created during the process of data overlay, and should also be excluded. To derive an accurate residential parcel map, we implemented the classification tree model with urban impervious surface fraction, parcel perimeter, and parcel area as inputs.

4.1.2.3 Housing units estimation

With the derived residential parcels, we can effectively estimate the number of housing units for single-, two-, and multi-family parcels. In particular, for single-family residential parcels, we simply assumed that there is only one housing unit in each parcel. Therefore, the number of single-family housing units was regarded as same as single-family residential parcel numbers. Similarly, for two-family residential parcels, the number of housing units was calculated as two times the numbers of parcels.

Multi-family residential parcels generally contain buildings with a large number of housing units (e.g. three- or four-family HU, condominiums, apartment complex, etc.), ranging from three to hundreds. To address this problem, a dasymetric-mapping method was employed to model the relationship between number

of HU and the areal extent of multi-family land use in each census block. An ordinary

least square (OLS) regression analysis was utilized to calibrate the weight of

geographical area of these residential parcels. Thus, the number of HUs for

multi-family can be estimated as follows (see Equations 4.2 and 4.3).

$$HU_{m,i} = \alpha + \beta A_{m,i} + \varepsilon_{m,i} \tag{4.2}$$

$$A_{m,i} = \sum_{j=1}^{n} A_{m,i,j} \tag{4.3}$$

where $HU_{m,i}$ and $A_{m,i}$ are the numbers of HU for multi-family and the aggregated

geographical area of the multi-family residential parcels in block i, respectively; $A_{m,i,j}$

is the geographical area of the jth multi-family residential parcel in census block I; α

and β are regression coefficients; and $\varepsilon_{m,i}$ is an error term.

After finishing the calculations of single-, two- and multi-family housing units

respectively, the total number of housing units in a census block can be calculated as

the summation of all these three types of housing units. The formula can be expressed

as follows (see Equation 4.4).

$$HU_i = HU_{s,i} + HU_{t,i} + HU_{m,i} \tag{4.4}$$

where HU_i is the total number of housing units in census block i, $HU_{s,i}$ is refers the

number of single-family housing units, $HU_{t,i}$ is the number of two-family housing

units, and $HU_{m,i}$ is the number of multi-family housing units.

4.3.2 Persons per household (PPH) estimation

In addition to the housing unit estimation, we also proposed a regression-based PPH estimation method with the help of geographic, demographic, and housing characteristic information. Geographic variables include the distances to different land uses, such as recreation centers, schools, and commercial centers, *etc*, reflecting behavioral preferences and demographic characteristics of different households. Demographic variables take into account age structure, such as percentages of youth, people at middle age, and people with age 65 and over, etc. Housing characteristic variables include house value, the number of bedrooms, and house age, etc. An ordinary least squared (OLS) regression model for PPH estimation was proposed as follows.

$$PPH_t = \alpha_0 + \sum_{i=1}^{m} \beta_i S_{i,t} + \sum_{j=1}^{n} \gamma_j D_{j,t} + \sum_{k=1}^{r} \delta_k E_{k,t} + \varepsilon_t \qquad (4.5)$$

where PPH_t is the PPH value at time t; $S_{i,t}$ indicates spatial variables derived from remote sensing and GIS data at time t, $D_{j,t}$ represents demographic variables at time t; $E_{k,t}$ stands for housing characteristic variables at time t; m, n and r are the total numbers of spatial, demographic and housing characteristic variables respectively; α_0, β_i, γ_j and δ_k are regression coefficients; and ε_t is an error term.

After estimating HUs and PPH respectively, the formula of this integrated HU method could be expressed as follows.

$$P_t = HU_t \times r_t \times PPH_t + G_t \qquad (4.6)$$

where P_t is the estimated population for a small area at a non-census time t; HU_t is the

enumerated HU number at time t, estimated by Equation (4.4); r_t is the occupancy rate at time t; PPH_t is the estimated persons per household at time t, estimated by Equation (4.5); and G_t is the group quarters population at time t. Occupancy rate r_t and group quarters population G_t were both regarded the same as the most recent census (Smith and Lewis 1980). In order to evaluate accuracy of the proposed estimation model, we carried out small-area population estimation in 2000 and compared the results to the 2000 Census data. The employment of the 2000 Census data is due to the unavailability of inter-censal population data in the study area for model validation. For validating inter-censal HU, PPH, and population estimates, updated demographic information obtained from the American community survey (ACS) could be a viable solution (Swanson and Hough, 2012).

4.3.3 Accuracy assessment and comparison

The accuracies of the developed models, including Equations (4.4), (4.5) and (4.6), were all assessed at the census block level, with half of the blocks of 2000 Census data served as training samples for model calibration and the other half serving as testing samples for model validation, each containing 121 blocks. Three indices were employed to measure population estimation accuracy: mean absolute error (*MAE*), mean absolute percentage error (*MAPE*), and mean algebraic percentage error (*MALPE*). *MAE* measures the numeric variation between the predicted value and the 'true' value, and has been widely utilized by remote sensing and GIS specialists. On the other hand, *MAPE* and *MALPE* are commonly adopted by demographers. As a measure of precision, *MAPE* measures the percentage of the absolute error to each actual value.

In contrast, being a measure of bias, *MALPE* cancels out negative and positive errors and reflects an overall upward or downward estimation tendency (Smith et al., 2002; Cai, 2007). The formulas are illustrated as follows.

$$MAE = \frac{1}{n}\sum_{i=1}^{n} |\hat{y}_i - y_i|$$

(4.7)

$$MAPE = 100\% \times \frac{1}{n}\sum_{i=1}^{n} \left| \frac{\hat{y}_i - y_i}{y_i} \right|$$

(4.8)

$$MALPE = 100\% \times \frac{1}{n}\sum_{i=1}^{n} \frac{\hat{y}_i - y_i}{y_i}$$

(4.9)

Where $\hat{y}_i$ is the estimated population count in block i; y_i is the actual population count in block i; and n is the total number of census blocks.

4.3. Results

4.3.1 Housing Unit Estimation

With the derived high-resolution remotely sensed and GIS datasets, especially the impervious surface information, parcel data, and residential land use datasets, a classification tree algorithm was developed to generate residential parcel data. The rules of the classification tree algorithm are illustrated in Table 4.1, and its classification accuracy is reported as a confusion matrix in Table 4.2. Results indicate that, for residential parcels, the user's and producer's accuracy measures are over 90 percent, suggesting that the classification tree method can effectively identify wrongly

labeled residential parcels. Especially, parcels with low impervious surface coverage (i.e. less than approximate 8 percent of the parcel area) were identified and subsequently removed from the residential parcel dataset (see Figure 4.3). Moreover, the slivers produced in the process of map overlay were also identified and eliminated. For example, parcels with abnormal perimeters (e.g. larger than 6,695 meter) or irregular shapes (e.g. elongated polygons) were eliminated according to the classification tree rules.

Table 4.1 Rules derived from Classification Tree

Impervious Surface

Fraction (percent)	Perimeter	Area	Type
<1.11			Non-residential parcel
>=1.11	>=6694.87		Non-residential parcel
>=1.11 and <7.88	<6694.87	<795.86	Non-residential parcel
>=1.11 and <7.88	<6694.87	>=795.86	Residential parcel
>7.88	>1676.63		Residential parcel
>7.88	<=1676.63	>=651.36	Residential parcel
>7.88	<151.77	<651.36	Residential parcel
>7.88	>151.77	<651.36	Non-residential parcel

Table 4.2 Confusion matrix of residential parcel classification

	Categories	Classified data		Producer's Accuracy (percent)
		Residential	Non-residential	
Reference data	Residential	280	14	95.24
	Non-residential	6	20	76.92
User's Accuracy (%)		97.90	58.82	93.75

Kappa index equals to 0.6329.

With the derived residential parcels, the number of housing units in a census block was calculated as the number of single-family residential parcels, plus two times the number of two-family residential parcels, plus an estimated housing unit count for multi-family residential parcels derived using the regression model detailed in Equations (4.2) and (4.3). Results of the regression modeling (see Table 4.3) indicated that the number of multi-family housing units has a statistically significant ($p<0.05$) and positive relationship with the geographical area of multi-family residential parcels. The model can explain about 40.6 percent of the variation between census blocks in the number of HUs in multi-family residential parcels.

Table 4.3 Results of regression model for estimating the number of housing units in multi-family residential parcels within a census block.

Coefficient	B	t-Stat	p-value
Intercept	1.305	1.659	0.110
Area_Multi_LU	0.002	4.331	0.000[**]

Notes: *Area_Multi_LU is the area of multi-family land use in a census block*, [**] indicates

statistically significant at the 95 percent confidence level. Adjusted R-square is 0.406.

With the housing unit counts for single-, two-, and multi-family residential parcels, the total number of housing unit for a census block was calculated as a summation of different categories of housing units. To compare with the 'true' values of housing units, a scatterplot was drawn to visually examine the accuracy of the estimates (see Figure 4.4). It could be observed that most points clustered around the 45-degree reference line, especially those with lower values. It reflects that the estimated HU numbers in the census blocks with a small number of HUs, especially those only containing single-family HUs, are very close to the actual HU numbers. Most of the outliers contain multi-family HUs, which is a major reason of inaccurate estimations. A comparison of the estimates by the proposed method and the actual HU number is demonstrated in Figure 4.5A and 4.5B. Through a visual examination, an

overall good agreement can be found between these two maps. Moreover, an accuracy assessment was performed, and results indicated that the errors associated with this method is relatively small (MAE = 3.27 HUs; MALPE = 2.78 percent).
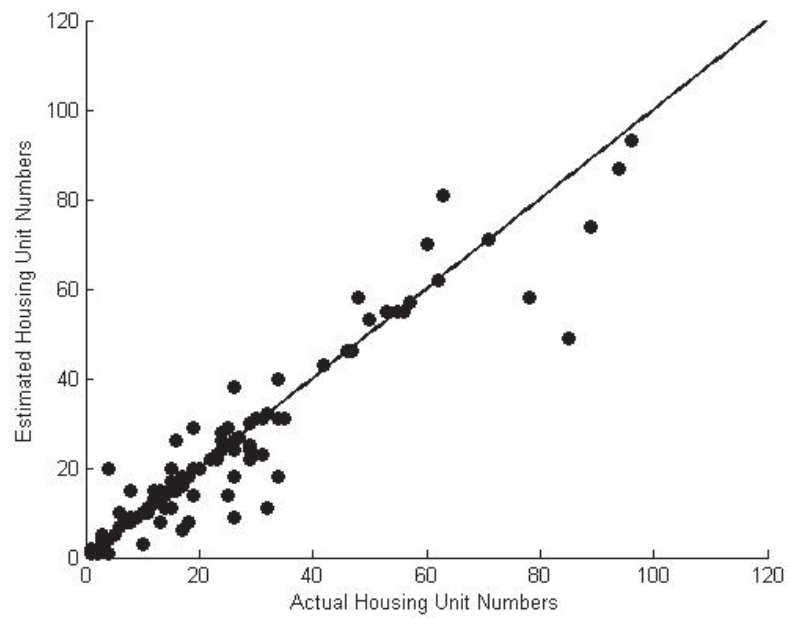
Figure 4.4 Scatterplot of the HU numbers estimated using the proposed method versus the "true" HU numbers at the census block level.
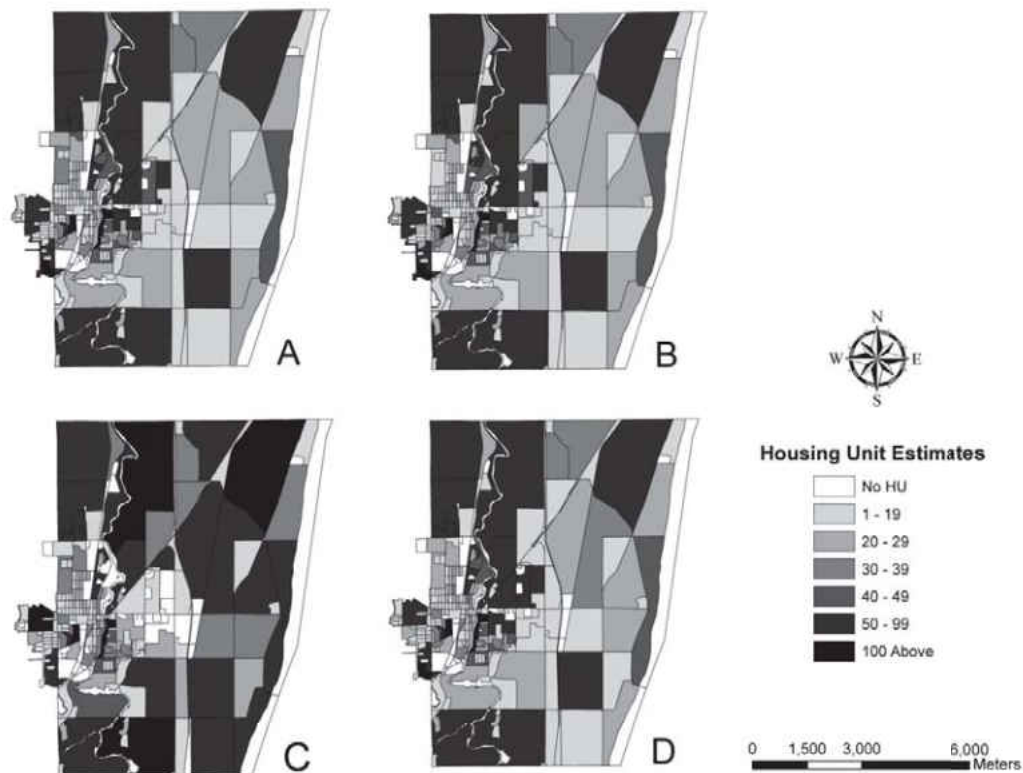
Figure 4.5 Comparisons of the block-level housing unit (HU) numbers derived from

(A) 2000 Census, (B) the proposed integrated method, (C) the step-down interpolation

method, and (D) the newly-built HU disaggregation method.

4.3.2 PPH Estimation

The other important component, PPH for each census block, was estimated using

the stepwise regression model (Equation (4.5)) with various geographic, demographic,

and housing structural variables as inputs. In particular, the employed variables include

distances to different activities (schools, recreation centers, commercial centers, etc.),

the percentage of vegetation coverage (represented by the normalized difference

vegetation index (NDVI)), percentages of the population age under 17, 18 to 39, 40 to 64, and 65 and above, etc. Results indicate that percentages of the youth with age under 17, distance to commercial land use, and PPH from the most recent census (see Table 4.4) are the only significant variables, and about 71.8 percent of the variations of the PPH can be explained by these variables. A scatterplot was constructed to visually examine the relationship between the estimated and actual PPH numbers (see Figure 4.6), and it shows that the PPH estimates matched the 'true' PPH values well, especially for the blocks with lower values of PPH (e.g. less than 4.0). On the other hand, large estimation errors occur in the blocks with only one single-family household or with an extremely large household size. Comparisons of the PPH estimates and the actual PPH number (see Figures 4.7A and 4.7B) indicate that the spatial patterns of the regression-based estimates match that of the actual PPH values reasonably well. There were hardly any apparent differences between the estimates and the observed numbers, as supported by relatively small errors (see Table 4.5).

Table 4.4 Results of stepwise regression model for PPH

Independent Variables	Coefficients
Intercept	1.012
PPH_90	0.208
Percent Age Under 17	3.391
Percent Age 18 to 39	/
Percent Age 40 to 64	/
Percent Age 65and above	/
NDVI	/
DIS_Commerical	0.361
DIS_School	/
DIS_Recreation	/
Adjusted R^2	0.718

Table 4.5 Accuracy comparisons of total housing unit and PPH estimates among different methods

	Model	MAE	MAPE (percent)	MALPE (percent)
	Proposed Integrated Method	3.27 HUs	18.49	2.78
Housing Unit	Step-down Method	8.7 HUs	41.08	19.26
	Newly-built HU Regression Method	3.37 HUs	22.91	6.82
PPH	PPH Regression Model	0.27 persons	9.98	0.21
	PPH_90 Method	0.62 persons	24.19	13.13
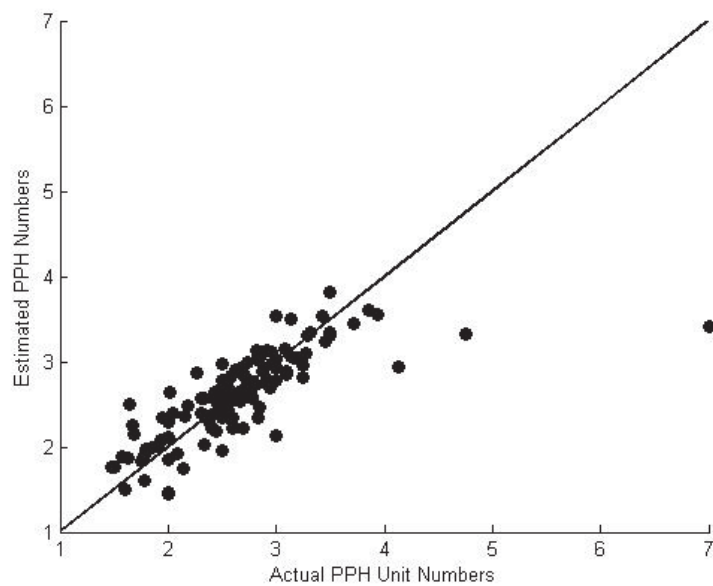
Figure 4.6 Scatterplot of the PPHs estimated by the regression model versus the "true"

PPH values at the census block level.
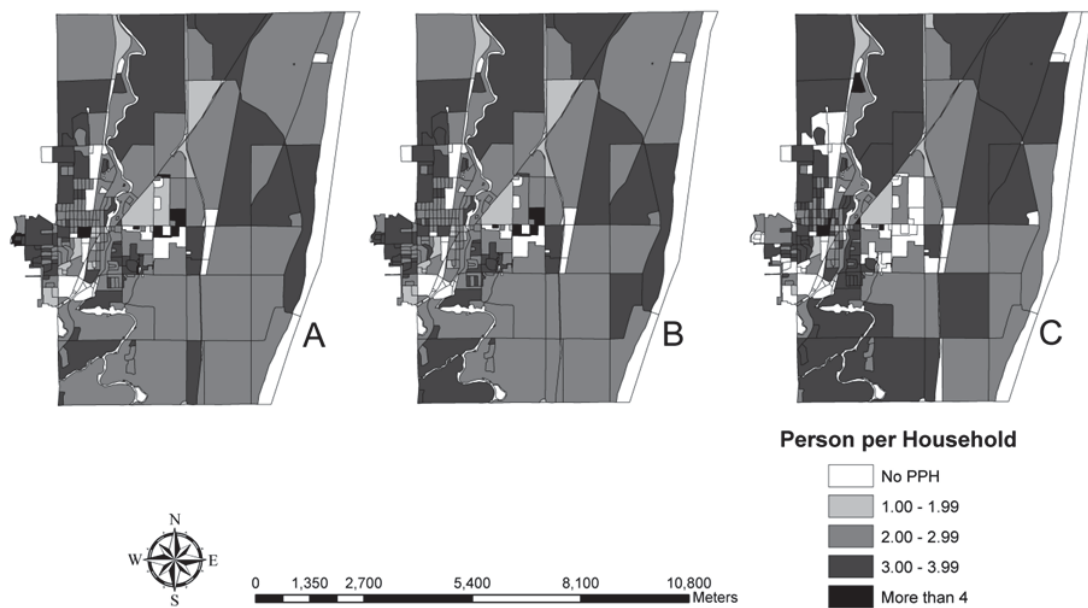
Figure 4.7 Comparisons of block-level PPH values derived from (A) 2000 Census, (B)

PPH regression-based model, and (C) PPH_90 method.

4.3.3 Small-area Population Estimation

With the estimated HU and PPH, population numbers were then estimated using

Equation (4.6), and compared with the observed population counts in Census 2000

data. A scatterplot of the estimated and actual population counts (see Figure 4.8) shows

that most points are along the 45-reference line, indicating a good overall match.

Further, through a visual examination of the distribution map (see Figure 4.9), it is

observed that most overestimations appear in the blocks with more multi-family HUs,

while most underestimations take place in the fast-developing blocks with more

newly-built HUs. The underestimation of some blocks is probably due to the usage of

the parcel data in 1998 to estimate population in 2000. Some new parcels for residential

land uses may be created during these two year lags, thus the usage of the parcel data in

1998 may cause less residential parcel numbers/HUs to be estimated in some blocks

when compared to the actual data in 2000. The HU estimation errors originating from

such mismatch of acquisition time would propagate to population estimation, leading to

underestimation in these blocks. The overall satisfactory performance of the proposed

integrated method is also verified by the accuracy assessment results (see Table 4.6).
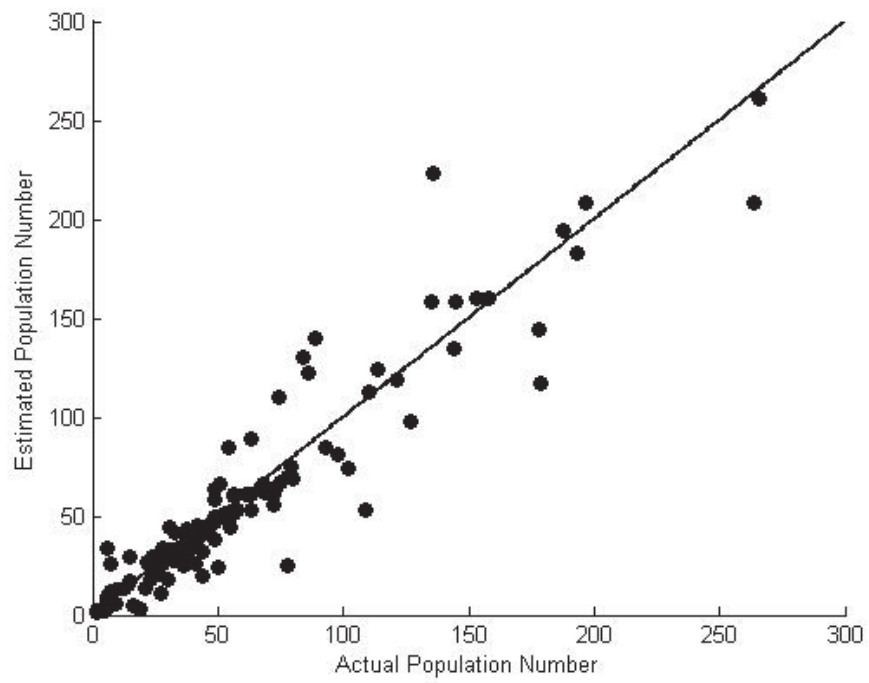
Figure 4.8 Scatterplot of the population estimated by the integrated method versus the

"true" population count at the census block level.

123
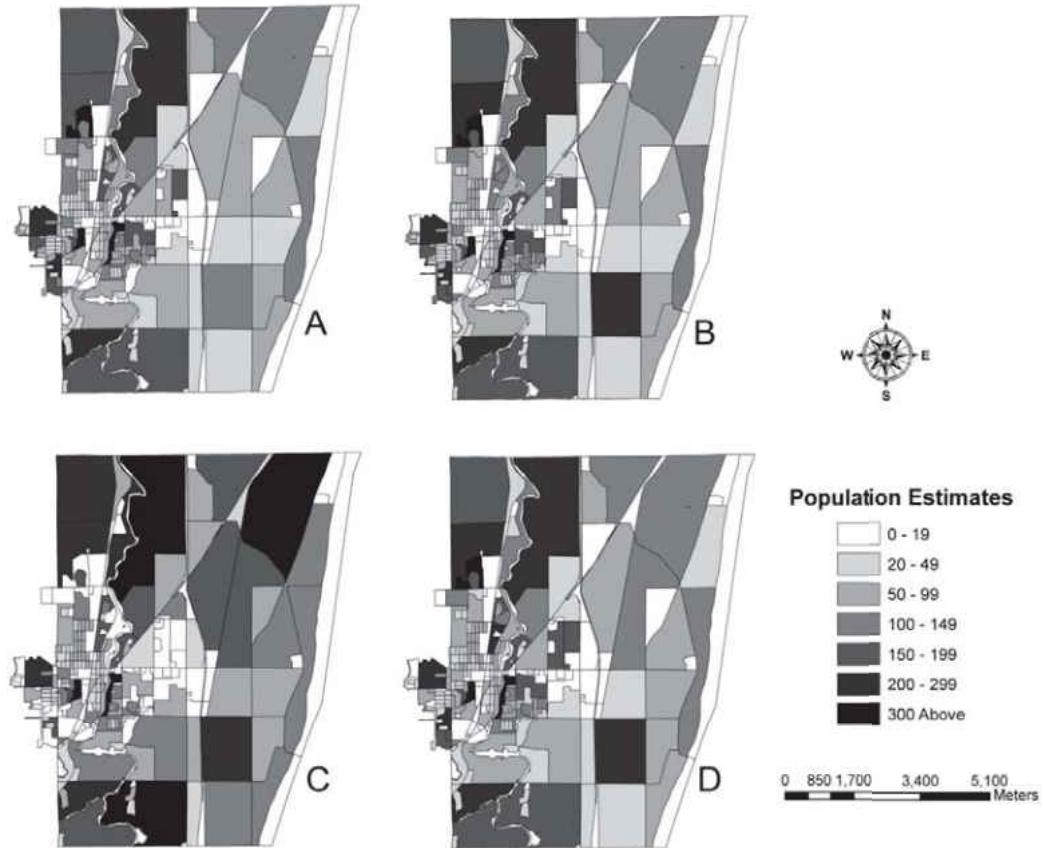
Figure 4.9 Comparisons of block-level population counts derived from (A) 2000

Census, (B) estimation Model 1, (C) estimation Model 2, and (D) estimation Model 3.

4.4. Comparative analysis

In order to evaluate the performance of the proposed integrated method, we

compared the resultant HU, PPH, and population estimates with those estimated from

other corresponding approaches. For estimating the HU numbers, the proposed method

was compared to another two representative "top-down" approaches, i.e. the step-down

method and the newly-built HU regression method developed. These two top-down approaches redistribute the total number of housing units into each block instead of actually enumerating individual housing units within them. The step-down interpolation method, developed by Perry and Voss (1994), assumes that the newly-built HU numbers in each block since the last census are linearly correlated with the geographic area of that census block (Perry and Voss, 1994). Alternatively, the newly-built HU regression method developed by Deng, Wu and Wang (2010) redistributes aggregated newly-built HUs according to the changes of residential land use areas in each block.

For PPH estimation, the proposed regression-based method was compared to the traditional approach which employs PPH values from the most recent census. Finally, the population estimates with the proposed HU and PPH estimation methods ("bottom-up" approach) were compared with the other two top-down approaches. Results of these comparative analyses were reported as follows.

4.4.1 Comparisons of HU models

Comparisons of the HU estimation maps indicate that the step-down interpolation method (see Figure 4.5C) performs poorly with clear over-estimations in large blocks. This is likely due to the assumption that a block with larger geographical area contains more newly-built HUs. In fact, blocks with lager geographical areas may not contain more new HUs, because such blocks may have less vacant lands for new development, or been planned for other types of land uses rather than residential.

Comparatively, the spatial distributions of HU estimates from the proposed integrated method (see Figure 4.5B) and the newly-built HU regression method (see Figure 4.5D) match the actual HU distribution reasonably well (see Figure 4.5A).

In addition to the visual comparisons, quantitative accuracy assessments were also performed and reported in Table 4.5. It shows that the step-down method has the lowest accuracy among these three methods, with the largest errors (approximate 9 HUs for MAE, 41 percent for MAPE and 19 percent for MALPE). This is probably because the newly-built dwelling units are distributed according to the geographical area of a block, while ignoring any detailed land use changes inside a block. On the contrary, both the newly-built HU redistribution regression method and the proposed integrated method have considerably better accuracy. Specifically, compared to the newly-built HU regression method, the proposed method provides slightly better accuracy with lower values of MAE and MAPE, and smaller upward bias.

4.4.2 Comparisons of PPH models

The proposed regression-based PPH estimation method was compared to the traditional approach, in which the PPH values from the most recent census were utilized. With this approach, it is assumed that the PPH remains unchanged since the latest censual year. For this research, the PPH values from 1990 Census were employed directly and interpolated to the 2000 Census block boundaries, and this method is named "PPH_90 method".

Results (see Figure 4.7C) indicate that the spatial patterns of PPH estimates derived from the PPH_90 method differ greatly when compared to that of the actual PPH values. At the census block level, PPH values change significantly from 1990 to 2000. They increase rapidly in the blocks with new residential developments, and decline in many other blocks because of the separation of young adults from their parents. In contrast, the regression-based PPH estimates (see Figure 4.7B) closely resembled the actual PPH values. The reason may be that the regression model considers not only the constitution of different age groups, but also the spatial distances to different land uses, which reflects behavior preferences of people with diverse marital and economic status. The accuracy comparisons for PPH estimates were also quantified in the bottom panel of Table 4.5. All three assessment measures show that the regression-based model is much more accurate than the PPH_90 method, as indicated by considerably lower values of MAE, MAPE, and MALPE.

4.4.3 Comparisons of population estimation by different techniques

With the respective methods for HU and PPH estimation, we compared the developed population estimation method (Model 1) to two top-down approaches to examine their performances of small-area population estimation. The first top-down method (Model 2) utilized the simple step-down interpolation method for HU estimation and the PPH_90 method for PPH estimation. The second top-down method (Model 3) utilized the newly-built HU regression method for HU estimation and a regression-based model for PPH estimation (see Table 4.6).

Table 4.6 Accuracy comparisons among three different small-area population estimation models

	Model Type	HU Submodel	PPH Submodel	MAE (persons)	MAPE (percent)	MALPE (percent)
Model 1	Bottom-up	Proposed Integrated Method	PPH Regression Model	11.07	26.62	7.10
Model 2	Top-down	Step-Down Method	PPH_90 Method	30.02	58.27	32.68
Model 3	Top-down	Newly-built HU Regression Method	PPH Regression Model	12.29	27.28	9.17

Results of the model comparisons (see Figure 4.9 and Table 4.6) indicate that Model 2, the classic approach for small-area population estimation, has the worst estimation accuracy. In fact, the spatial distributions of population estimates by this approach (see Figure 4.9C) are remarkably different from those of the actual population information. Moreover, the population estimates derived from this method have the largest errors, as measured by the MAE (30.02 persons), MAPE (58.27 percent), and MALPE (32.68 percent). This result is likely due to the poor assumptions in both HU and PPH estimations. On the contrary, the spatial patterns of population estimates from Models 1 (see Figure 4.9B) and 3 (see Figure 4.9D) are very close to those of the actual population information (see Figure 4.9A). A detailed accuracy assessment shows that the performance of Model 1 is slightly better than Model 3, and much better than Model

2. The better performance of Model 1 is likely due to the usage of high resolution remotely sensed imagery, parcel data, and detailed land use data. Moreover, an advantage of this method is that it is unnecessary to perform a regional estimate of total numbers of housing unit. Instead, they can be enumerated automatically from each residential parcel to each census block. These results are consistent with the findings in Smith and Cody's research (1994, 2004, 2011), although the unit of analysis in this research (census block) is much finer than theirs (county and subcounty level).

4.5. Sensitivity analysis

In addition to the comparative analyses, we also performed sensitivity analyses to evaluate which component, the HU or PPH, is more important to the small-area population estimates. The basic idea of sensitivity analyses is: under the assumption that one major component of the HU method is estimated perfectly, all the errors of population estimates can be attribute to estimation error of the other component, and thus the impacts of this component can be measured accordingly. To compare and evaluate the impacts of HU and PPH estimates at the census block level, five scenarios for small-area population estimation were investigated: three utilizing "true" 2000 Census data for PPH, and two utilizing "true" 2000 SEWRPC data for HU (see Table 4.7). For a fair comparison, these scenarios were divided into two categories: classic demographic models (without the help of GIS/remotely sensed data) and integrated demographic and geographic models. For each scenario, accuracy measurements,

MAE, MAPE, and MALPE were calculated and compared.

Table 4.7 Sensitivity analyses of the HU method at the census block level

Model Type	HU Submodel	PPH Submodel	MAE (persons)	MAPE (percent)	MALPE (percent)
Classic demographic models	Step-Down Method	"True" PPH data	22.39	41.83	18.90
	"True" HU data	PPH_90 method	12.83	25.97	12.87
Integrated demographic and geographic models	Newly-built HU Regression	"True" PPH data	9.07	24.17	6.80
	Integrated Method	"True" PPH data	9.04	21.86	2.54
	"True" HU data	Regression method	6.45	14.08	0.37

Results of the sensitivity analyses (see Table 4.7) indicate that for both classic demographic models and integrated demographic and geographic models, the HU estimation errors have higher contributions to the population estimation error than those of the PPH estimation. Especially, with the classic demographic models, when the PPH values are assumed to be estimated perfectly, the error of small-area population estimates is much higher when compared to the scenario in which the "true" (or perfectly estimated) HU data is employed. Similarly, with the integrated demographic and geographic models, the accuracy of population estimates is more

sensitive to the HU estimates. As a summary, the results of this error propagation analyses indicate that the error from the estimation of HUs contributes more to the small-area population estimation error, and the PPH estimates only play a minor role. This finding is consistent with the results from Smith and Cody's studies (1994, 2004, 2011), although their results are based on a larger geographical scale (i.e. county/subcounty).

4.6. Conclusion

Small-area population estimation is a challenging task due to data unavailability and privacy concerns. Traditionally, demographic methods and geographic techniques have been applied respectively for estimating detailed population information. The resultant population estimates, however, are unsatisfactory due to the limitations of each field. The recent advance of geographic techniques, in particular high-resolution remotely sensed and GIS information, provides a great opportunity for a better estimation of detailed population information. Therefore, through integrating the demographic and geographic methods, we developed a bottom-up approach to estimate the HU, PPH, and population information at the census block level, and the comparisons with other methods have been conducted.

Analysis of results suggests two major conclusions. First, the integration of demographic and geographic approaches has significantly improved the estimation accuracy of HU, PPH, and population counts at the census block level. In particular, the

proposed HU method performs the best with the lowest values of MAE (3.27 HUs), MAPE (18.49 percent), and MALPE (2.78 percent). Similarly, when compared to the real PPH values, PPH estimates have the smaller errors (e.g. MAE: 0.27 persons, MAPE: 9.98 percent, and MALPE: 0.21 percent). Also, the results of small-area population estimation are the best when compared to other widely applied methods. Secondly, results of sensitivity analyses show that, with the classic demographic approaches and the integrated methods, the error of HU number estimates contributes more to the population estimation errors than that of PPH. This result is consistent with the findings of Smith and Cody (1994, 2004, 2011), and proves that necessary of integrating high-resolution geographic information for better HU estimation.

CHAPTER 5 CONCLUSIONS

5.1 Summary

Timely, detailed and accurate population information is essential to analyze and address a wide variety of socio-economic, political, and environmental issues and to support the planning practices required by both public agencies and the private sector. However, these important data are generally only available once every decade in the form of the national census. Moreover, populations in certain rapidly-developing areas may increase quickly, such that this ten-year frequency does not meet the needs of these areas. Therefore, a cost-effective population estimation method is necessary. To address this issue, this research integrated geographic, sociological and demographic theories and exploited remote sensing imagery and geographic information system (GIS) datasets to derive improved population estimates at the census block level, the finest level in the national census. Specifically, three new approaches have been proposed to improve small-area population estimation accuracy, a longstanding technical issue in the acquisition of population data. In particular, on the one hand, remotely sensed and GIS data have been effectively employed to estimate two major components of a demographic model: redistributing newly built dwelling units from a more aggregated geographic level to the census block level and improved PPH estimation at such a fine scale. On the other hand, detailed urban environmental information was extracted from high-resolution

remote sensing images and GIS data and employed to automatically enumerate individual housing units. In particular, to derive impervious surface information, a desirable environmental parameter that is difficult to directly derive from remote sensing imagery, a new spectral index has been proposed to assist in the automated identification of dwelling units in the demographic model.

5.2 Contributions

Small-area population estimates in non-census years are essential for supporting a wide variety of socio-economic analyses. Currently, a number of demographic or geographic information based models have been developed to generate small-area population estimates. Few studies, however, have attempted to integrate these two types of models to obtain improved estimates. Therefore, the first contribution of this research is our exploration of the feasibility of incorporating GIS, remote sensing (RS), and demographic data into the housing unit method, a popular demographic model, to estimate the small-area population of Grafton, WI. In particular, two major components of the housing unit method, housing unit (HU) counts and PPH, were obtained by modeling their relationships with demographic and geographic factors using a sequence of ordinary least squares (OLS) regression models. The analysis of results indicates that spatial factors derived from remote sensing and GIS datasets, together with demographic information, can significantly improve the accuracy of small-area population estimates. Moreover, the use of spatial

and demographic variables derived from remotely sensed, GIS and socio-economic data was also found to significantly improve PPH estimates.

Second, remotely sensed data have been extensively applied to facilitate the monitoring and analysis urban environments in support of various planning practices because of their synoptic view and repetitive coverage of a large geographic area. Compared to traditional per-pixel and sub-pixel image analyses, spectral indices have clear advantages due to their easy implementation in practical applications. However, most spectral indices are designed to only highlight only one type of land cover, and the misidentification of land cover types, in particular confusing impervious surfaces and bare soil, has not been successfully addressed. Therefore, the second contribution of this study is that we proposed a biophysical composition index (BCI) for the simple and convenient identification of urban biophysical compositions in practical applications following Ridd's conceptual Vegetation – Impervious surface – Soil triangle model by a reexamining the TC transformation. Further, this research explores the applicability of BCI to various remotely sensed images at different spatial resolutions. The results indicate that BCI is more correlated with impervious surface abundance than the normalized difference vegetation index (NDVI), normalized difference built-up index (NDBI) and normalized difference impervious surface index (NDISI), with correlation coefficients of approximately 0.8 at various resolutions. Moreover, BCI's performance in quantifying vegetation abundance is comparable with that of NDVI at all three spatial scales. Additionally, as it exhibits much higher values of separability metrics than any other index, this study confirms

that BCI is the most effective index in distinguishing between impervious surfaces and bare soil.

Finally, in addition to the presented top-down method, the third contribution of this research is that it proposed a new bottom-up method for population estimation at the census block level by combining high-resolution remotely sensed imagery/geographic information system (GIS) data and a demographic housing unit (HU) model. The number of housing units and persons per household (PPH), two primary factors in the HU method, were estimated using detailed urban environmental information extracted from high-resolution remotely sensed imagery and GIS data. Further, population counts for each census block were generated by applying the HU model. The analysis of the results suggests that the proposed integrated method performs reasonably well, as indicated by relatively small estimation errors. To obtain an improved assessment, the estimation accuracies of the HU, PPH, and population counts were compared with other widely applied techniques, and the results indicated that this method significantly improved estimation accuracy. Finally, sensitivity analyses were conducted to evaluate the sources of errors in the population estimates. The results indicate that, when compared to PPH estimates, the error associated with HU count estimates is a major source of small-area population estimation errors.

5.3 Future research

Future research attempting to introduce remotely sensed and GIS data into

demographic theory to obtain population estimates, should focus on two aspects. First, attention could be directed to estimating multi-family HU numbers at the census block level. Although remote sensing techniques have provided additional building information for HU identification, such information is only helpful in improving single-family HU identification and not the identification of multi-family HUs. Recently developed Light Detection and Ranging (LiDAR) technology provides three-dimensional information that is more detailed than traditional methods (Silván-Cárdenas et al. 2010; Lu et al. 2011). It may be possible to combine such high-resolution, remotely sensed information and demographic theory to improve multi-family HU identification. Second, more multi-source datasets can be considered and integrated to improve the "invisible" PPH estimation at the census block level. Datasets from different sources, such as more detailed socio-economic data and information from remotely sensed images, could be explored and linked to existing geographic, sociological and demographic theories for the estimating PPH at a finer level.

REFERENCES

Adams, J. B., Sabol, D. E., Kapos, V., Almeida Filho, R., Roberts, D. A., and Smith, M. O. (1995). Classification of multispectral images based on fractions of endmembers: Application to land-cover change in the Brazilian Amazon. *Remote Sensing of Environment*, *52*, 137−154.

Anderson, J. R., Hardy, E. E., Roach, J. T., and Witmer, R. E. (1976). A land use and land cover classification system for use with remote sensor data. *U.S. Geological Survey Professional Paper, No. 964*. USGS, Washington, D.C.

Bauer, M. E., Heinert, N. J., Doyle, J. K., and Yuan, F. (2004). Impervious surface mapping and change monitoring using Landsat remote sensing. *Proceedings of the American Society of Photogrammetry and Remote Sensing Annual Conference*, May 24-28, Denver, CO. unpaginated CD ROM, 10.

Bikker, J. A., and de Vos, A. F. (1992). A regional supply and demand model for inpatient hospital care. *Environment and Planning A*, 24(8), 1097–1116.

Birkin, M., Clarke, G., Clarke, M., and Wilson, A. (1996). *Intelligent GIS: Location decisions and strategic planning*. Cambridge, UK: GeoInformation International.

Bongaarts, J. (2001). Household size and complexity in the developing world in the 1990s. *Population Studies*, 55, 263-79.

Breiman, L., Friedman, J., Olshen, R., and Stone, C. (1984). *Classification and regression trees*. Belmont, CA: Wadsworth International Group.

Cai, Q. (2007). New techniques in small area population estimates by demographic characteristics. *Population Research and Policy Review*, 26(2), 203-218.

Chen, K. (2002). An Approach to Linking Remotely Sensed Data and Areal Census Data. *International Journal of Remote Sensing*, 23, 37–48.

Church, R. L., and Murray, A. T. (2009). *Business site selection, location analysis and GIS*. New York: Wiley.

Cochran, W. G. (1977). *Sampling Techniques*. (3rd ed.). New York: John Wiley and Sons.

Cohen, W. B., Spies, T. A., and Fiorella, M. (1995). Estimating the age and structure of forests in a multi-ownership landscape of western Oregon, U.S.A. *International Journal of Remote Sensing*, *16*(4), 721–746.

Collins, W. G., and El-Beik, A. H. A. (1971). Population census with the aid of aerial photographs: An Experiment in the city of Leeds. *Photogrammetric Record,* 7, 16–26.

Crist, E. P., and Cicone, R. C. (1984a). Application of the tasseled cap concept to simulated Thematic Mapper data. *Photogrammetric Engineering and Remote Sensing*, *50*, 343–352.

Crist, E. P., and Cicone, R. C. (1984b). A physically-based transformation of Thematic Mapper data—the TM tasseled cap. *IEEE Transactions of Geosciences and Remote Sensing*, *22*(3), 256–263.

Deng, C., Wu, C. and Wang, L. (2010). Improving housing unit method for small area population estimation using remote sensing and GIS Information. *International Journal of Remote Sensing*, *31*(21), 5673–88.

Dueker, K., and Horton, F. (1971). Toward geographic urban change detection systems with remote sensing inputs. *Proceedings of the American Society of Photogrammetry 37th Annual Meeting*, 204–218.

England, J. (2000). *Retail impact assessment: A guide to best practice*. London and New York: Routledge.

Epstein, B. J. (1984). Market appraisals. In *Store location and store assessment research*, ed. R. L. Davies and D. S. Rogers. New York: John Willey and Sons.

Fielding, J. (2007). Environmental injustice or just the lie of the land: An investigation of the socio-economic class of those at risk from flooding in England and Wales. *Sociological Research Online* 12.

Flanagan, M., and Civco, D. L. (2001). Subpixel impervious surface mapping. *Proceedings of 2001 ASPRS annual convention, April 23–27, St. Louis, MO*.

Franke, J., Roberts, D. A., Halligan, K., and Menz, G. (2009). Hierarchical Multiple Endmember Spectral Mixture Analysis (MESMA) of hyperspectral imagery for urban environments. *Remote Sensing of Environment*, *113*, 1712−1723.

Gober, P. (1990). The urban demographic landscape: A geographic perspective. In *Housing demography: Linking demographic structure and housing markets*, ed. D. Myers, 109-130. Madison, WI: University of Wisconsin Press.

Ghosh, M. and Rao, J. N. K. (1994). Small area estimation: an appraisal. *Statistical Science,* 9(1), 55-76.

Ghosh, A., and McLafferty, S. L. (1987). *Location strategies for retail and service firms*. Lexington, Massachusetts: Lexington Books.

Goodchild, M. F. and Lam, N. N-S (1980). Areal interpolation: a variant of the traditional spatial problem. *Geo-Processing*, 1, 297-312.

Harvey, J. T. (2002a). Estimating Census District Populations from Satellite Imagery:

Some Approaches and Limitations. *International Journal of Remote Sensing*, 23(10), 2071–2095.

Harvey, J. T. (2002b). Population Estimation Models Based on Individual TM Pixels. *Photogrammetric Engineering and Remote Sensing*, *68*(11), 1181–92.

He, C., Shi, P., Xie, D., Zhao,Y. (2010). Improving the normalized difference built-up index to map urban built-up areas using a semiautomatic segmentation approach. *Remote Sensing Letters*, *1*(4), 213–221.

Healey, S. P., Cohen, W. B., Yang, Z., and Krankina, O. N. (2005). Comparison of tasseled cap-based Landsat data structures for use in forest disturbance detection. *Remote Sensing Environment*, *97*(3), 301–310.

Helmer, E. H., Brown, S., and Cohen, W. B. (2000). Mapping montane tropical successional stage and land use with multi-date Landsat imagery. *International Journal of Remote Sensing*, *21*(11), 2163–2183.

Homer, C., Huang, C., Yang, L., Wylie, B., and Coan, M. (2004). Development of a 2001 National Land Cover Database for the United States. *Photogrammetric Engineering and Remote Sensing*, *70*(7), 829–840.

Horne, J. H., (2003). A Tasseled Cap Transformation for IKONOS Images. *ASPRS Annual Conference Proceedings*. Alaska, USA.

Horner, M. W., and A. T. Murray. (2004). Spatial representation and scale impacts in transit service assessment. *Environment and Planning B: Planning and Design*, 31, 785–797.

Horner, M. W., and Downs, J. A. (2010). Optimizing hurricane disaster relief goods distribution: Model development and applications with respect to planning strategies. *Disasters* 34(3), 821–844.

Hsu, S. Y. (1971). Population estimation. *Photogrammetric Engineering* 37, 449–54.

Hsu, S. Y., 1973. Population estimation from ERTS imagery: Methodology and evaluation. *Proceedings of the American Society of Photogrammetry 39th Annual Meeting* 583–591.

Hu, X., and Weng, Q. (2009). Estimating impervious surface from medium spatial resolution imagery using the self-organizing map and multi-layer perceptron neural networks. *Remote Sensing of Environment*, *113*, 2089−2102.

Huang, C., Wylie, B., Yang, L., Homer, C., and Zylstra, G. (2002). Derivation of a tasseled cap transformation based on Landsat 7 at-satellite reflectance. *International Journal of Remote Sensing*, *23*(8), 1741–1748.

Huete, A. R. (1988). A soil-adjusted vegetation index (SAVI). *Remote Sensing of Environment*, *25*, 295–309.

Irish, R. R. (2000). Landsat 7 science data users handbook, Report 430-15-01-003-0. National Aeronautics and Space Administration.

http://landsathandbook.gsfc.nasa.gov/pdfs/Landsat7_Handbook.pdf

Jackson, R. D., and Huete, A. R. (1991). Interpreting vegetation indices. *Preventive Veterinary Medicine*, *11*, 185–200.

Jensen, J. R. (2005). *Introductory Digital Image Processing: A Remote Sensing Perspective.* (3rd ed.). Englewood Cliffs, New Jersey: Prentice–Hall.

Kaufman, Y., and Remer, L. (1994). Detection of forests using mid-IR reflectance: An application for aerosol studies. *IEEE Transaction of Geoscience and Remote Sensing*, *32*, 672–683.

Kauth, R. J., and Thomas, G. S. (1976). The Tasseled Cap—A Graphic Description of the Spectral-Temporal Development of Agricultural Crops as Seen by Landsat. *Proceedings of the Symposium on Machine Processing of Remotely Sensed Data*, 41–51.

Keeley, J. E., Fotheringham, C. J., and Morais, M. (1999). Reexamining fire suppression impacts on brushland fire regimes. *Science*, 284, 1829–1832.

Kimpel, T., and Lowe, T. (2007). Estimating household size for use in population estimates. *Population estimates and projections, Research Brief no. 47*. Olympia, WA: Washington State Office of Financial Management.

Kobrin, F. (1976). The fall in household size and the rise of the primary individual in the United States. *Demography*, 13, 127–38.

Kraus, S. P., Senger, L. W., and Ryerson, J. M. (1974). Estimating population from photographically determined residential land use types. *Remote Sensing of Environment* 3(1), 35–42.

Kwak, Y., Hasegaw, A. Inomata, H., Magome, J., Fukami, K., and Takeuchi, K. (2011). A new assessment methodology for flood risk: A case study in the Indus River basin. *Risk in water resources management (Proceedings of symposium H03, IUGG2011, Melbourne, Australia, July 2011), IAHS Publication* 347, 55–60.

Kwan-Gett, T. S., Baer, A., and Duchin, J. S. (2009). Spring 2009 H1N1 influenza outbreak in King County, Washington. *Disaster Medicine and Public Health Preparedness* 3, 109–116.

Li, G., and Weng, Q. (2005). Using Landsat ETM+ imagery to measure population

density in Indianapolis, Indiana, USA. *Photogrammetric Engineering and Remote Sensing*, 71(8), 947-958.

Lo, C. P. (1986a). Accuracy of population estimation from medium-scale aerial photography. *Photogrammetric Engineering and Remote Sensing*, 52, 1859-1869.

Lo, C. P. (Ed.) (1986b). *Applied Remote Sensing*. (London: Longman)

Lo, C. P. (1986c). *Applied Remote Sensing*. London: Longman.

Lo, C. P. (1995). Automated population and dwelling unit estimation from high-resolution satellite images—a GIS approach. *International Journal of Remote Sensing*, 16(1), 17–34.

Lo, C. P. (2003). Zone-based estimation of population and housing units from satellite-generated Land use/land cover maps. In *Remotely sensed cities*, ed. V. Mesev, 157–180. London and New York: Taylor and Francis Publications.

Lo, C. P., and Chan, H. F. (1980). Rural population estimation from aerial photographsgraphs. *Photogrammetric Engineering and Remote Sensing*, 46, 337–45.

Lo, C. P., and Welch, R. (1977). Chinese urban population estimation. *Annals of the Association of American Geographers*, 67(2), 246–53.

Lobser, S. E., and Cohen, W. B. (2007). MODIS tasseled cap: land cover characteristics expressed through transformed MODIS data. *International Journal of Remote Sensing*, *28*(22), 5079–5101.

Lu, D., and Weng, Q. (2004). Spectral mixture analysis of the urban landscapes in Indianapolis with Landsat ETM+ imagery. *Photogrammetric Engineering and Remote Sensing*, *70*, 1053–1062.

Lu, D. and Weng, Q. (2006). Use of impervious surface in urban land use classification. *Remote Sensing of Environment*, *102*, 146–160.

Lu, D., and Weng, Q. (2009). Extraction of urban impervious surface from an IKONOS image. *International Journal of Remote Sensing*, *30*, 1297–1311.

Lu, Z., Im, J., and Quackenbush, L. J. (2011). A volumetric approach to population estimation using LiDAR remote sensing. *Photogrammetric Engineering and Remote Sensing*, *77*(11), 1145–56.

Maliszewski, P. J., Kuby, M. J., and Horner, M. W. (2012). A comparison of multi-objective spatial dispersion models for managing critical assets in urban areas. *Computers, Environment and Urban Systems*, forthcoming.

Markham, B. L., and Barker, J. L. (1986). Landsat MSS and TM Post-Calibration Dynamic Ranges, Exoatmospheric Reflectances and At-Satellite Temperatures.

EOSAT Landsat Technical Notes, No. 1.

Martin, D. and Williams, H. C. W. L. (1992). Market-area analysis and accessibility to primary health-care centers. *Environment and Planning A*, 24, 1009-1019.

Martin, J. H., and W. J. Serow. 1978. Estimating demographic characteristics using the ratio correlation method, *Demography*, *15*, 223–33.

Masek, J. G., Huang, C. Q., Wolfe, R., Cohen, W., Hall, F., and Kutler, J., et al. (2008). North American forest disturbance mapped from a decadal Landsat record. *Remote Sensing of Environment*, *112*, 2914−2926.

Mausel, P. W., Kramber, W. J., and Lee, J. K. (1990). Optimum band selection for supervised classification of multispectral data. *Photogrammetric Engineering and Remote Sensing*, *56*(1), 55–60.

Mennis, J. (2002). Using geographic information systems to create and analyze statistical surfaces of population and risk for environmental justice analysis. *Social Science Quarterly* 83, 281–97.

Mennis, J. (2011). Integrating remote sensing and GIS for environmental justice research. In *Urban remote sensing: Monitoring, synthesis and modeling in the urban environment*, ed. X. Yang, 225–37.

Mennis, J. (2003). Generating surface models of population using dasymetric mapping. *The Professional Geographer*, 55(1), 31-42.

Mennis, J. and Hultgen, T. (2006). Intelligent dasymetric mapping and its application to areal interpolation, *Cartography and Geographic Information Science*, 33(3), 179-194.

Mercurio, J. (1984). Store location strategies. In *Store location and store assessment research*, ed. R. L. Davies and D. S. Rogers. New York: John Willey and Sons.

Mesev, V. (2005). Identification and characterization of urban building patterns using IKONOS imagery and point-based postal data. *Computers, Environment and Urban Systems*, *29*, 541–57.

Mesev, V. (2007). Fusion of point-based urban data with IKONOS imagery for locating urban neighborhood features and patterns. *Information Fusion*, *8*, 157–67.

Mohapatra, R. P., and Wu, C. (2007). Sub-pixel imperviousness estimation with IKONOS image: An artificial neural network approach. In Q. Weng (Ed), *Remote Sensing of Impervious Surfaces* (pp. 21–38). New York: CRC Press, Taylor and Francis Group.

Mohapatra, R. P., and Wu, C. (2010). High Resolution Impervious Surface Estimation:

an Integration of IKONOS and Landsat-7 ETM+ Imagery. *Photogrammetric Engineering and Remote Sensing*, *76*, 1329–1341.

Myers, D., and Doyle, A. (1990). Age-specific population–per-household ratios: Linking population age structure with housing characteristics. In *Housing demography: Linking demographic structure and housing markets*, ed. D. Myers, 109-30. Madison, WI: University of Wisconsin Press.

Murray, A. T., R. Davis, R. J. Stimson, and L. Ferreira. 1998. Public transportation access. *Transportation Research D* 3, 319–28.

Norman, P., Purdam, K., Tajar, A., and Simpson, L. (2007). Representation and local democracy: Geographical variations in elector to councillor ratios. *Political Geography*, 26(1), 57–77.

PCI Geomatica. (1997). *Using PCI software*. Canada: Ottawa, Ontario.

Pereira, J. M. C. (1999). A comparative evaluation of NOAA/AVHRR vegetation indexes for burned surface detection and mapping. *IEEE Transaction of Geoscience and Remote Sensing*, *37*, 217–226.

Perry, M. and Voss, P. (1996). Using geo-demographic methods for improving small area estimates. CDE (Centre for Demography and Ecology at the University of Wisconsin-Madison) Working Paper No. 96-15.

Phinn, S., Stanford, M., Scarth, P., Murray, A. T. and Shyy, P. T. (2002). Monitoring the composition of urban environments based on the vegetation-impervious surface-soil (VIS) model by subpixel analysis techniques. *International Journal of Remote Sensing*, *23*(20), 4131 – 4153.

Plane, D. A. and Rogerson, P. A. (Ed.) (1994) *The geographical analysis of population with applications to business and planning*. (New York: John Wiley).

Plaza, A., Martinez, P., Perez, R., and Plaza, J. (2004). A quantitative and comparative analysis of endmember extraction algorithms from hyperspectral data. *IEEE Transactions on Geoscience and Remote Sensing*, *42*, 650−663.

Powell, R., Roberts, D. A., Hess, L., and Dennison, P. (2007). Sub-pixel mapping of urban land cover using multiple endmember spectral mixture analysis: Manaus, Brazil. *Remote Sensing of Environment*, *106* (2), 253–267.

Powell, S. L., Cohen, W. B., Yang, Z., Pierce, J.D., and Alberti, M. (2008). Quantification of impervious surface in the Snohomish Water Resources Inventory Area of Western Washington from 1972–2006. *Remote Sensing of Environment*, *112*, 1895–1908.

Pu, R., Gong, P., Michishita, R., and Sasagawa, T. (2008). Spectral mixture analysis

for mapping abundance of urban surface components from the Terra/ASTER data. *Remote Sensing of Environment*, *112*(3), 939–954.

Qiu, F., Woller, K. L. and Briggs, R. (2003). Modelling Urban Population Growth from Remotely Sensed Imagery and TIGER GIS Road Data. *Photogrammetric Engineering and Remote Sensing*, 69(9), 1031–42.

Rashed, T., Weeks, J.R., Roberts, D., Rogan, J. and Powell, R. (2003). Measuring the physical composition of urban morphology using multiple endmember spectral mixture models. *Photogrammetric Engineering and Remote Sensing*, *69*, 1011–1020.

Rees, P., Norman, P. and Brown, D. G. (2004). A framework for progressively improving small area population estimates. *Journal of the Royal Statistical Society Series A*, 167(1), 5-36.

Reid, C. E., O'Neill, M. S., Gronlund, C. J., Brines, S. J., Brown, D. G., Diez-Roux, A. V., and Schwartz, J. (2009). Mapping community determinants of heat vulnerability. *Environmental Health Perspectives*, 117, 1730–36.

Reese, H. M., Lillesand, T. M., Nagel, D. E., Stewart, J. N., Goldmann, R. A., Simmons, T. E., Chipman, J. W. and Tessar, P. A. (2002). Statewide land cover derived from multiseasonal Landsat TM data: a retrospective of the WISCLAND project. *Remote Sensing of Environment*, *82*, 224–237.

Richter, R. (1996a). A spatially adaptive fast atmospheric correction algorithm. *International Journal of Remote Sensing*, 17 (6), 1201-1214.

Richter, R. (1996b). Atmospheric correction of satellite data with haze removal including a haze/clear transition region. *Computers and Geosciences*, 22, 675-681.

Richter, R. (2005). Atmospheric/Topographic Correction for Satellite Imagery. *DLR report DLR-IB 565-01/05*, Wessling, Germany.

Ridd, M. (1995). Exploring a V–I–S (vegetation–impervious–surface-soil) model for urban ecosystem analysis through remote sensing: comparative anatomy for cities. *International Journal of Remote Sensing*, *16*, 2165–2185.

Roberts, D. A., Gardner, M., Church, R., Ustin, S., Scheer, G., and Green, R. O. (1998). Mapping chaparral in the Santa Monica Mountains using multiple endmember spectral mixture models. *Remote Sensing of Environment*, *65*, 267–279.

Roberts, D. A., Quattrochi, D. A., Hulley, G. C., Hook, S. J. and Green, R. O. (2012). Synergies between VSWIR and TIR data for the urban environment: An evaluation of the potential for the Hyperspectral Infrared Imager (HyspIRI) Decadal Survey mission, *Remote Sensing of Environment*, *117*, 83–101.

Roberts, G., Dunderdale, M., Doll, C., d'Entremont, R. P., Hu, B., Liang, S., and

Privette, J. L. (2002). First operational BRDF, Albedo and Nadir reflectance products from MODIS. *Remote Sensing of Environment*, *83*, 135–148.

Rouse, J. W., Jr., R. H. Haas, J. A. Schell, and D. W. Deering. (1974). Monitoring the vernal advancement and retrogradation (green wave effect) of natural vegetation. Prog. Rep. RSC 1978-1, Remote Sensing Center, Texas AandM Univ., College Station, 93p. (NTIS No. E73–106393.

Sathe, A., and Miller-Hooks, E. (2005). Optimizing location and relocation of response units in guarding critical facilities. *Transportation Research Record* 1923, 127–136.

Schaaf, C. B., Gao, F., Strahler, A. H., Lucht, W., Li, X., Tsang, T., Strugnell, N., Zhang, X. Y., Jin, Y., Muller, J. P., Lewis, P., Barnsley, M., Hobson, P., Disney, M., Roberts, G., Dunderdale, M., Doll, C., d'Entremont, R. P., Hu, B., Liang, S., & Privette, J. L. (2002). First operational BRDF, Albedo and Nadir reflectance products from MODIS. *Remote Sensing of Environment*, *83*, 135–148.

Schueler, T. (1994). The importance of imperviousness. *Watershed Protection Techniques*, 1, 100–111.

Scott, J. R. (1997). *Remote sensing: the image chain approach*. New York: Oxford University Press.

Silván-Cárdenas, J. L., Wang, L., Rogerson, P., Wu, C., Feng, T., and Kamphaus, B. D. (2010). Assessing fine-spatial-resolution remote sensing for small-area population estimation, *International Journal of Remote Sensing*, 31(21), 5605–34.

Simmons, M. (1984). Store assessment procedure. In *Store location and store assessment research*, ed. R. L. Davies and D. S. Rogers. New York: John Willey and Sons.

Small, C. (2001). Estimation of urban vegetation abundance by spectral mixture analysis. *International Journal of Remote Sensing*, *22*, 1305–1334.

Small, C. (2005). A global analysis of urban reflectance. *International Journal of Remote Sensing*, *26*, 661−681.

Smith, S. K, and Lewis, B. (1980). Some new techniques for applying the housing unit method of local population estimation. *Demography*, 17, 323-339.

Smith, S.K, and Mandell, M. (1984). A comparison of population estimation methods: housing unit versus component II, ratio correlation, and administrative records. *Journal of the American Statistical Association*, *79*, 282-289.

Smith, S. K. (1986). A Review and Evaluation of the Housing Unit Method of Population Estimation. *Journal of the American Statistical Association*, 81 (394),

287-296.

Smith, S. K., Nogle, J. and Cody, S. (2002). A Regression Approach to Estimating the Average Number of Persons Per Household. *Demography*, 39(4), 697–712.

Smith, S. K., and Cody, S. (1994). Evaluating the housing unit method: A case study of 1990 population estimates in Florida, *Journal of the American Planning Association*, 60(2), 209–21.

Smith, S.K. and Cody, S. (2004). An evaluation of population estimates in Florida: April 1, 2000. *Population Research and Policy Review*, 23, 1-24.

Smith, S. K., and S. Cody. 2011. An evaluation of population estimates in Florida: April 1, 2010. *Special Population Reports, Number 8*. http://www.bebr.ufl.edu/sites/default/files/SPR_8.pdf (last assessed 23 August 2011).

Somers, B., Asner, G.P., Tits, L., and Coppin, P. (2011). Endmember variability in Spectral Mixture Analysis: A review. *Remote Sensing of Environment*, *115*, 1603–1616.

Southeastern Wisconsin Regional Planning Commission (SEWRPC). 2000. *Land use classifications and codes: SEWRPC regional land use inventory 2000*.

Southeastern Wisconsin Regional Planning Commission (SEWRPC). (2004a). The population of southeastern Wisconsin, technical report #11, Available online at: http://www.sewrpc.org/publications/techrep/tr011_population_southeastern_wisconsin.pdf   (assessed on November 26, 2010)

Southeastern Wisconsin Regional Planning Commission. (2004b) The Economy of Southeastern Wisconsin, technical report #10, Available online at: http://www.sewrpc.org/Publications/TechRep/tr-010_economy_southeastern_wisconsin.pdf (assessed on November 26, 2010)

Souza, C. Roberts, D. A., and Cochrane, M. A. (2005). Combining Spectral and Spatial Information to Map Canopy Damages from Selective Logging and Forest Fires. *Remote Sensing of Environment*, 98, 329–343.

Starsinic, D. E. and Zitter, M. (1968). Accuracy of the housing unit method in preparing population estimates for cities. *Demography*, 5 (1), 475-484.

Stehman, S. V. (1996). Estimating the kappa coefficient and its variance under stratified random sampling, *Photogrammetric Engineering and Remote Sensing*, *62*, 401–407.

Stone, G., A. Lekht, N. Burris, and C. Williams. 2007. Data collection and communications in the public health response to a disaster: Rapid population estimate surveys and the daily dashboard in post-Katrina New Orleans. *Journal of Public*

Health Management and Practice 13(5), 453–60.

Sutton, P., Roberts, D. A., Elvidge, C., and Melj, H. 1997. A comparison of nighttime satellite imagery and population density for the continental United States. *Photogrammetric Engineering and Remote Sensing* 63, 1303–13.

Swain, P. H. (1978). Fundamentals of pattern recognition. In: P. H. Swain, and S. M. Davis, (Eds.), *Remote Sensing: The Quantitative Approach* (pp. 136–187). New York: McGraw-Hill.

Swain, P. H., and Davis, S. M. (1978). *Remote Sensing: The Quantitative Approach*. New York: McGraw-Hill.

Swanson, D. A., and Hough, G. C. (2012). An evaluation of persons per household (PPH) estimates generated by the American community survey: A demographic perspective. *Population Research and Policy Review,* forthcoming.

Taylor, M. (2009). IKONOS planetary reflectance and mean solar exoatmospheric irradiance. GeoEye Technical paper.

Thomas, I. L., Ching, N. P., Benning, V. M., and D'Aguanno, J. A. (1987). A review of multi-channel indices of class separability. *International Journal of Remote Sensing*, *8*(3), 331–350.

Underwood, E. C., Viers, J. H., Klausmeyer, K. R., Cox, R. L., and Shaw, M. R. (2009). Threats and biodiversity in the mediterranean biome. *Diversity and Distributions*, 15, 188–97.

U.S. Census Bureau. (1998). Subcounty population estimates methodology. Available online at http://www.census.gov/population/methods/e98scdoc.txt (accessed 17 May 2006).

U.S. Census Bureau. (2001). Profile of general demographic characteristics. Table DP-1 in *2000 Census of Population and Housing*. Washington, DC.

U.S. Census Bureau. 2004. Estimates and projections area documentation: Subcounty total population estimates. http://www.census.gov/popest/topics/methodology/2004_su_meth.html (last accessed 28 May 2009).

U.S. Census Bureau. (2005). Methodology: 2004 estimates and projections area documentation, subcounty total population estimates. Available online at http://www.census.gov/popest/topics/methodology/2004_su_meth.html (accessed 18 May 2006).

U.S. Census Bureau. 2010. Methodology for subcounty total resident population estimates (Vintage 2009): April 1, 2000 to July 1, 2009.

http://www.census.gov/popest/topics/methodology/2009-su-meth.pdf (last accessed 30 Novemvber 2010).

United Nations, Department of Economic and Social Affairs, Population Division. (2006). *World Urbanization Prospects: The 2005 Revision*. New York, United Nations. http://www.un.org/esa/population/publications/WUP2005/2005wup.htm (Assessed on January 15, 2011).

U.S. Census Bureau. (2010). 2010 Census, American FactFinder. Available online at: http://factfinder2.census.gov/ (Assessed on November 30, 2010).

Watkins, J. F. (1984). The effect of residential structure variation on dwelling unit enumeration from aerial photographs, *Photogrammetric Engineering and Remote Sensing*, 50(11), 1599–1607.

Watkins, J. F., and Morrow-Jones, H. A. (1985). Small area population estimates using aerial photography, *Photogrammetric Engineering and Remote Sensing* 51, 1933–35.

Webster, C. J. (1996). Population and dwelling unit estimates from space, *Third World Planning Review*, 18(2), 155-176.

Weng, Q. (2012). Remote sensing of impervious surfaces in the urban areas: requirements, methods, and trends. *Remote Sensing of Environment*, *117*(2), 34–49.

Weng, Q., and Hu, X. (2008). Medium spatial resolution satellite imagery for estimating and mapping urban impervious surfaces using LSMA and ANN. *IEEE Transaction on Geosciences and Remote Sensing*, *46*(8), 2397–2406.

Weng, Q., Hu, X. and Lu, D. (2008). Extracting impervious surface from medium spatial resolution multispectral and hyperspectral imagery: A comparison," *International Journal of Remote Sensing*, *29*, 3209–3232.

Widener, M. J., and Horner, M. W. (2011). A hierarchical approach to modeling hurricane disaster relief goods distribution. *Journal of Transport Geography* 19(4), 821–28.

Wilhelmi, O. V., and Hayden, M. H. (2010). Connecting people and place: a new framework for reducing urban vulnerability to extreme heat. *Environmental Research Letters* 5:014021.

Wilson, B. L. (1984). Modern methods of sales forecasting: Regression models. In *Store location and store assessment research*, ed. R. L. Davies and D. S. Rogers. New York: John Willey and Sons.

Wu, C. and Murray, A. T. (2005). A cokriging method for estimating population density in urban areas. *Computers, Environment and Urban Systems*, 29, 558-579.

Wu, C. and Murray, A. T. (2007). Population estimation using Landsat Enhanced Thematic Mapper Imagery. *Geographical Analysis*, 39, 26-43.

Wu, C. (2004). Normalized spectral mixture analysis for monitoring urban composition using ETM+ imagery. *Remote Sensing of Environment*, *93*, 480–492.

Wu, C. (2009). Quantifying high-resolution impervious surfaces using spectral mixture analysis. *International Journal of Remote Sensing*, *30*(11), 2915–2932.

Wu, C. and Murray, A. T. (2003). Estimating impervious surface distribution by spectral mixture analysis. *Remote Sensing of Environment*, *84*, 493–505.

Wu, C., and Yuan, F. (2008). Seasonal sensitivity analysis of impervious surface estimation with satellite imagery. *Photogrammetric Engineering and Remote Sensing*, *73* (12), 1393–1402.

Wu, C., and Murray, A.T. (2005). Optimizing public transit quality and system access: the multiple-route, maximal covering/shortest-path problem. *Environment and Planning B: Planning and Design* 32 (2), 163–178.

Wu, S. S, Qiu, X. and Wang L. (2005). Population estimation methods in GIS and remote sensing: a review. *GIScience and Remote Sensing*, 42, 80-96.

Wu, F., and Martin. D. (2002). Urban expansion simulation of Southeast England using population surface modeling and cellular automata. *Environment and Planning A*, 34, 1855–1876.

Xian, G. and Crane, M. (2005). Assessments of urban growth in Tampa Bay watershed using remote sensing data. *Remote Sensing of Environment*, *97*(2), 203–215.

Xian, G., and Crane, M. (2006). An analysis of urban thermal characteristics and associated land cover in Tampa bay and Las Vegas using satellite data. *Remote Sensing of Environment*, *104*, 147–156.

Xu, H. (2010). Analysis of impervious surface and its impact on urban heat environment using the normalized difference impervious surface index (NDISI). *Photogrammetric Engineering and Remote Sensing*, *76*(5), 557–565.

Yang, L., Huang, C., Homer, C., Wylie, B. and Coan, M. (2003a). An approach for mapping large-area impervious surface: synergistic use of Landsat 7 ETM+ and high spatial resolution imagery. *Canadian Journal of Remote Sensing*, *29*, 230–240.

Yang, L., Stehman, S. V., Smith, J. H., and Wickham, J. D. (2001). Thematic accuracy of MRLC land cover for the eastern United States. *Remote Sensing of Environment*,

76,418-422.

Yang, L., Xiang, G., Klaver, J.M. and Deal, B. (2003b). Urban land cover change detection through sub-pixel imperviousness mapping using remotely sensed data. *Photogrammetric Engineering and Remote Sensing*, *69*, 1003–1010.

Yang, X. (2006). Estimating landscape imperviousness index from satellite imagery. *IEEE Geoscience and Remote Sensing Letters*, *3*(1), 6–9.

Yang, X., and Liu Z. (2005). Use of satellite-derived landscape imperviousness index to characterize urban spatial growth. *Computers, Environment and Urban Systems*, *29*, 524–540.

Yeh, A. G., and Li. X. (2002). A cellular automata model to simulate development density for urban planning. *Environment and Planning B: Planning and Design*, *29*, 431–450.

Yuan, F. and Bauer, M. (2007). Comparison of impervious surface area and normalized difference vegetation index as indicators of surface urban heat island effects in Landsat imagery. *Remote sensing of environment*, *106* (3), 375–386.

Yuan, F., Wu, C. and Bauer, M. (2008). Comparison of spectral analysis techniques for impervious surface estimation using Landsat imagery. *Photogrammetric Engineering and Remote Sensing*, *74*, 1045–1055.

Zha, Y., Gao, Y. and Ni, S. (2003). Use of normalized difference built-up index in automatically mapping urban areas from TM imagery. *International Journal of Remote Sensin*g, *24*, 583–594.

Zhang, X., Schaaf, C., Friedl, M. A., Strahler, A., Gao, F., and Hodges, J. (2002). MODIS Tasseled Cap transformation and its utility. In, Geoscience and Remote Sensing Symposium, IGARSS '02. *IEEE International*, 1063−1065.

Zhang, X., Freidl, M. A., Schaaf, C. B., Strahler, A. H., Hodges, J. C. F., and Gao, F. (2003). Monitoring vegetation phenology using MODIS. *Remote Sensing of Environment*, *84*, 471−475.

CURRICULUM VITAE

Chengbin Deng

Education:

B.S., Remote Sensing and GIS, Sun Yat-sen University, China, June 2006

M.S., Remote Sensing and GIS, Sun Yat-sen University, China, June 2008

Ph.D., Geography, University of Wisconsin-Milwaukee, USA, May 2013

Dissertation Title:

Small-area Population Estimation: An Integration of Demographic and Geographic Techniques

Publications:

1. **Deng, C.**, and Wu, C. (2013). Improving small-area population estimation: an integrated geographic and demographic approach. *Annals of the Association of American Geographers*. DOI: 10.1080/00045608.2013.770364

2. **Deng, C.**, and Wu, C. (2013). A spatially adaptive spectral mixture analysis method for mapping subpixel urban impervious surface distribution. *Remote Sensing of Environment*, 133, 62-70.

3. **Deng, C.**, and Wu, C. (2013). Estimating very high resolution land surface temperature using a spectral unmixing and thermal mixing approach. *International Journal of Applied Earth Observation and Geoinformation*, 23, 155-164.

4. **Deng, C.**, and Wu, C. (2013). Examining the impacts of urban biophysical compositions on surface urban heat island: a spectral unmixing and thermal mixing approach. *Remote Sensing of Environment*, 131, 262-274.

5. **Deng, C.**, and Wu, C. (2012). BCI: a biophysical composition index for remote sensing of urban environments. *Remote Sensing of Environment*, 127, 247-259.

6. **Deng, C.**, Wu, C., and Wang, L. (2010). Improving housing unit method for small area population estimation using remote sensing and GIS Information. *International Journal of Remote Sensing*, 31(21), 5673-5688.